THE FRANCIS CRICK INSTITUTE

UCL

UCL RADIOCHEMISTRY

CABI
centre for advanced biomedical imaging

PNI

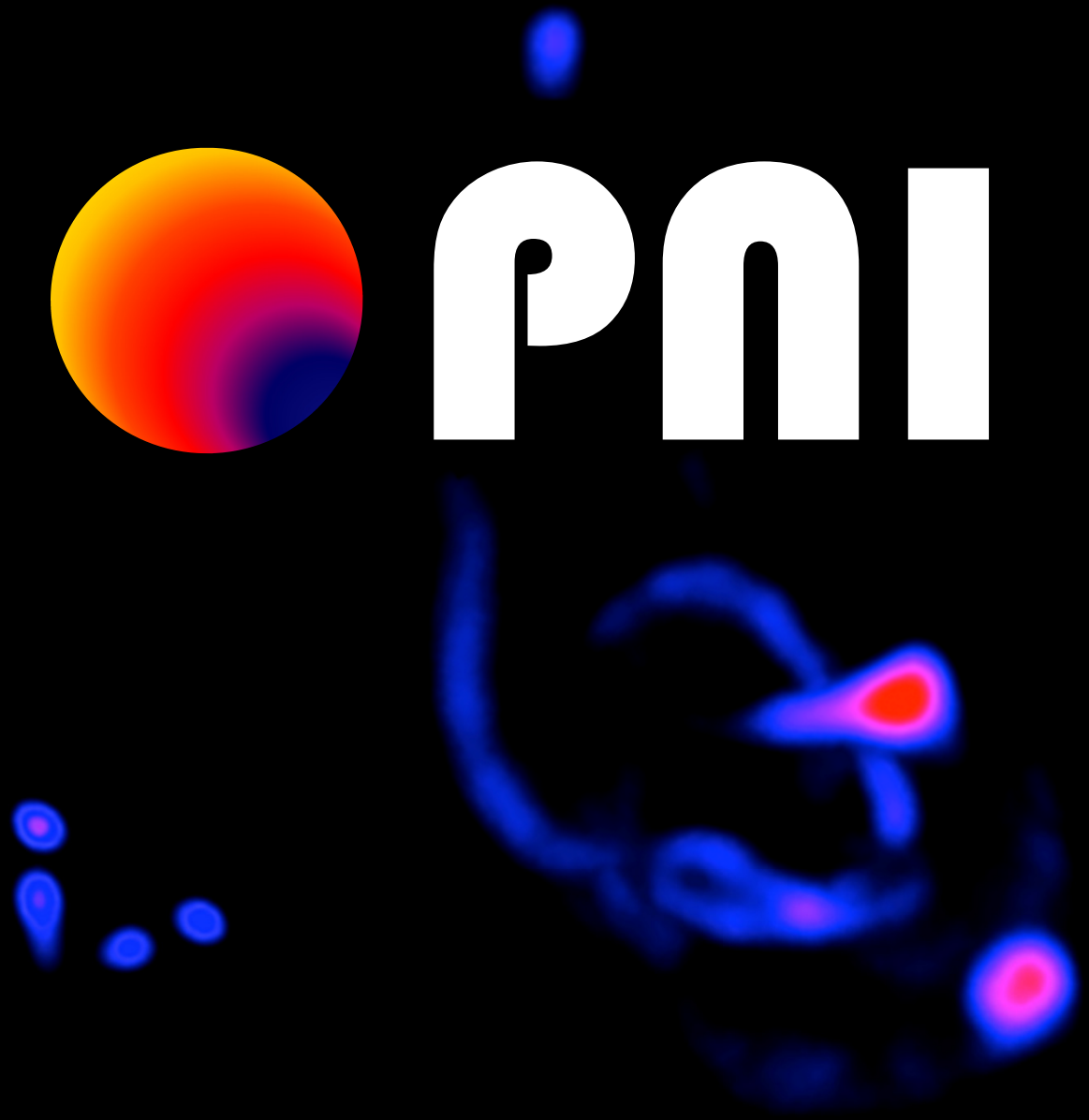

Third Symposium on Preclinical Nuclear Imaging

London – 12 November 2018

Kindly endorsed by

imaging life
esmi
European Society for Molecular Imaging

THE PNI COMMITTEE …

… are welcoming you to the Third Symposium on Preclinical Nuclear Imaging!

If you have questions during the meeting, please do not hesitate to contact one of us. We'll be happy to help!

We wish you an exciting meeting, fruitful discussions and new ideas for your science!

Kerstin Sander

Timothy Witney

Tammy Kalber

Peter Johnson

Thibault Gendron

Thomas Snoeks

Bernard Siow

TABLE OF CONTENTS

GREETINGS

DEAR COLLEAGUES AND FRIENDS

Welcome to the Third Symposium on Preclinical Nuclear Imaging (PNI)!

We are delighted that you are able to join us and contribute to an exciting day of science and collaborative exchange amongst members of the PNI community.

Three years have now passed since the last PNI meeting in 2015. – Although still growing as a scientific field, as judged by publications on pubmed, the focus of the science has changed. New exciting research avenues have been explored over the last years, spanning from the development of imaging tools for refined diagnostic applications, such as disease staging and treatment monitoring (the rapid development of dementia tracers is just one example), to new strategies for cell tracking and drug delivery, which have the potential to be advanced to tools for personalised patient care. To allow for more impactful, and therefore translatable research, preclinical imaging techniques have been refined and methods developed. For instance, tracer characterisation has sparked the development of sophisticated animal models that better reflect complex human disease mechanisms. The radiochemical space has been substantially expanded through the development of new, translatable labelling techniques, e.g. for fluorine-18. New isotopes, in particular zirconium-89, have been characterised and tested for diagnostic applications.

Today's scientific programme reflects the changing focus of our field, and we are looking forward to exciting talks and scientific discussions. We are delighted to have had an overwhelming number of abstracts submitted. With the aim to showcase the diversity of applications for PNI, and to give early career researchers a platform to present their research, we have selected outstanding abstracts for short talks as well as flash presentations.

Behind the scenes, we have worked hard towards the aim of turning the PNI into an initiative that better reflects the interests of the scientific community. To this end, we have established a scientific committee with members from institutions across the UK who were responsible to shape the scientific programme of today's meeting. Building on the feedback received following the first two PNI symposia, we have joined forces with The Crick Institute to organise a meeting that provides researchers with a platform for scientific exchange, ample opportunities to network, discuss mutual interests and share experience and expertise across the various fields of PNI.

This would not have been possible without the generous support from international imaging societies as well as our industrial partners – we would like to take this opportunity to once again thank them!

We hope you'll take this opportunity to showcase your work, gather contacts for the future, and create a sense of community via our shared experience, ideas and vision. Please enjoy this day and join us for a wind-down and drink after the meeting. Have a vibrant and fun symposium!

The PNI Organising Committee

PROGRAMME

8:30		Registration and breakfast
9:15		Opening

SESSION 1 — DISCOVER

Chairs — *S Peter Johnson, Timothy H Witney*

9:20	O1	David Y Lewis	Beatson Institute Glasgow
		Identifying rare responders in a heterogeneous mouse model of lung cancer	
9:45	O2	Christopher J Cawthorne	Katholieke Universiteit Leuven
		Evaluation of novel imaging probes for $\alpha_V\beta_6$ and CXCR4	
10:10	O3	Thibault Gendron	University College London
		Dibenzothiophene sulfonium salts as novel leaving groups for aromatic ^{18}F-fluorination	
10:25	O4	Stephen J Paisey	Cardiff University
		Biodistribution of Zr-89 anti-tenascin antibody in tumour bearing mice	
10:40		**Coffee break**	

SESSION 2 — DEVELOP

Chairs — *Thibault Gendron, Tammy L Kalber*

11:10	O5	Gabriela Kramer-Marek	Institute of Cancer Research
		Imaging of HER-mediated drug resistance towards personalised therapy in cancer	
11:35	O6	Richard Southworth	King's College London
		From perfusion bench to microPET bedside: adventures in radiotracer development	
12:00	O7	Peter J Gawne	King's College London
		In vivo PET tracking of anti-inflammatory liposomes within a rheumatoid arthritis model	
12:15	O8	Edward S O'Neill	University of Oxford
		Imaging DNA damage response to ^{177}Lu-DOTATATE radionuclide therapy	

SESSION 3 POSTER PITCHES

Chairs *Thibault Gendron, Tammy L Kalber*

12:30 Poster presenters Please see pages 23–79

13:00 **Poster session** and lunch

SESSION 4 TRANSLATE

TRASIS

Chairs *Kerstin Sander, Bernard Siow*

14:30 **O9** Wim J G Oyen — Institute of Cancer Research
ImmunoPET with Zr-89 labelled antibodies: tool for characterisation of tumours

14:55 **O10** André Müller — Life Molecular Imaging
Discovery and clinical validation of novel PET tracers for the detection of aggregated tau

15:20 **O11** David M Gorman — University of Manchester
To what extent can histology be used to qualify PET data?

15:35 **O12** P Stephen Patrick — University College London
Translational *in vivo* tracking of a cell/gene cancer therapy using ^{89}Zr-oxine and PET imaging

15:50 **Poster session** and refreshments

SESSION 5 KEYNOTE LECTURE

southern scientific EXPERIENCE & EXPERTISE LabLogic

Chair *Thomas Snoeks, Timothy H Witney*

16:20 **O13** Bertrand Tavitian — Université Paris Descartes/Inserm
Simultaneous positron emission tomography and ultrafast ultrasound for hybrid molecular, anatomical and functional imaging

17:15 Prizes for best poster presentation and best poster pitch

17:25 Closing speech

17:30 + Reception and drinks

Identifying Rare Responders in a Heterogeneous Mouse Model of Lung Cancer

D Y Lewis,[1,*] S Ros,[2] P D Santos,[2] D S Soloviev,[1] S K Lyons[3] and K M Brindle[2]

[1] CRUK – Beatson Institute, Glasgow; [2] CRUK – Cambridge Institute; [3] CSHL

* David.Lewis@cruk.cam.ac.uk

We are potentially entering a new era for some "hard-to-treat" tumours like lung cancer. Recent clinical trials have shown a proportion of patients with sustained responses to new treatments such as immunotherapy [1]. Typically only a subset of patients respond, therefore we need to develop approaches to stratify patients prior to therapy identifying rare responders from those with innate resistance.

We developed a mouse model where we could identify and isolate rare responders with single lesion resolution. To be clinically relevant a mouse model should share several features of the human disease including progression, similar genetic and phenotypic features, heterogeneity and drug resistance. To address these aims we developed two novel lentiviral vectors (LV-PGKCre-EF1SN and LV-PGKCre-EF1LS) to deliver multiple transgenic elements to somatic cells of adult mice with conditional (floxed) oncogenic Kras (LSL-KrasG12D/+) and p53fl/fl alleles (KP mice). These vectors deliver stable expression of Cre recombinase to induce tumour development and stable reporter gene expression for in vivo imaging of resultant tumours (luciferase/mStrawberry or mStrawberry/sodium iodide symporter (mNIS)).

Through the *in vivo* transduction of somatic cells we present here novel radionuclide imaging of spontaneous tumorigenesis. We exploit the tomography of radionuclide imaging to track single lesions during cancer therapy and identify inter- and intratumoral heterogeneity in drug response. These vectors comprises a new platform technology and provide a quantitative, 4D readout of cell viability, critical for monitoring therapeutic efficacy and identifying rare responders within a heterogeneous tumour.

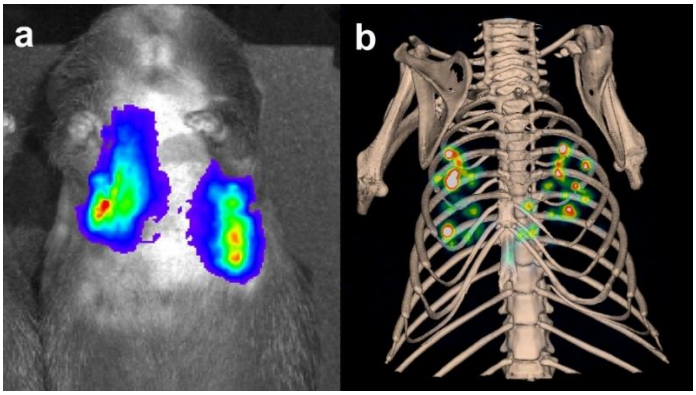

Figure 1. Imaging tumorigenesis of $KRAS^{G12D/+}$; $p53^{-/-}$ (KP) mice with **(a)** bioluminescence and **(b)** [^{99m}Tc]TcO_4^- SPECT/CT reporter genes. Optical measurements are planar and surfaced weighted but radionuclide imaging provides sensitive, 3D imaging of tumour development. Note the improved resolution for lung tumour imaging with [^{99m}Tc]TcO_4^- SPECT/CT.

[1] Borghaei *et al. Checkmate 057 trial*. N. Engl. J. Med. **2015**, *373*, 1627–1639.

O2

Evaluation of Novel Imaging Probes for $\alpha_v\beta_6$ and CXCR4

B P Burke,[1,3] J Domarkas,[1,3] C S Miranda,[3] R E Lee,[1,3] S Nigam,[3] G S Clemente,[1,3] T D'Huys,[4] T Ruest,[3] J A Thompson,[2] S Hart,[2] T J Hubin,[5] D Schols,[4] S J Archibald[1,3,*] and C J Cawthorne[3,6,*]

[1] Department of Chemistry; [2] Hull York Medical School (HYMS); [3] Positron Emission Tomography Research Centre, University of Hull, Cottingham Road, Hull, HU6 7RX, UK; [4] Rega Institute for Medical Research; [5] Department of Chemistry and Physics, Southwestern Oklahoma State University, Weatherford, OK 73096, USA; [6] Nuclear Medicine and Molecular Imaging/Molecular Small Animal Imaging Centre, KU Leuven, Leuven, Belgium

* s.j.archibald@hull.ac.uk; christopher.cawthorne@kuleuven.be

Integrin $\alpha_v\beta_6$ is an epithelial-restricted transmembrane receptor overexpressed in a range of solid malignancies. We synthesised and evaluated an $\alpha_v\beta_6$-binding cyclic peptide CRGDLASLC (RGD1) labelled with ^{68}Ga and ^{177}Lu for PET imaging and molecular radiotherapy of $\alpha_v\beta_6$. Cold and metallated peptides inhibited the anti- $\alpha_v\beta_6$ antibody binding in the sub-nanomolar range (0.09 nM). Radiolabelling resulted in non-decay corrected preparation yields of 2 to 5 % within 90 min of generator elution. No radioactive degradation products were detected by radio-HPLC in human serum after incubation for up to 3 hours. Radioligand displayed cell binding proportional to cellular $\alpha_v\beta_6$ expression in a range of cell types, for both ^{68}Ga and ^{177}Lu chelated species. Dynamic PET/CT studies showed high uptake in the gut and submandibular glands and low uptake in the lungs, commensurate with reported normal tissue $\alpha_v\beta_6$ expression levels, with uptake reduced in blocking studies demonstrating specificity to the target (Figure 1).

Expression of the chemokine receptor CXCR4 is associated with tumour dissemination and poor prognosis in a range of cancers. We developed a copper-64 labelled small molecule PET agent for imaging both human and murine CXCR4 chemokine receptors to further translational research approaches in mouse models of cancer. [^{64}Cu]CuCB-Bicyclam demonstrated high affinity for the CXCR4 receptor (IC_{50} = 10 nM). *In vitro* and *in vivo* studies demonstrated specific and selective uptake in CXCR4 expressing cells and tumours that could be reduced by > 90% using a higher affinity antagonist. There was limited uptake in non-CXCR4 expressing organs and high in vivo stability. The tracer also selectively displaced the CXCR4 antagonists AMD3100 and AMD3465 from the murine liver.

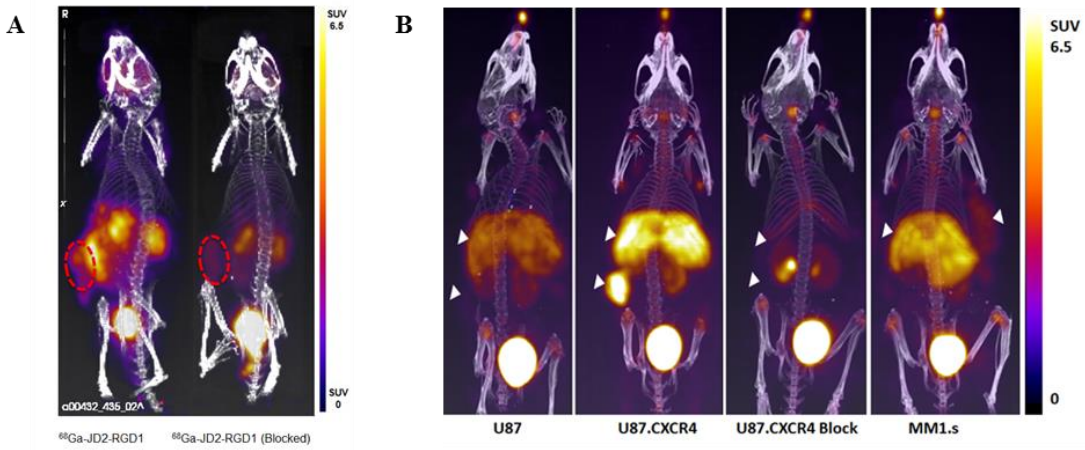

Figure 1. Uptake of ^{68}Ga-**RGD1** and [^{64}Cu]CuCB-Bicyclam in tumour models. **A)** Uptake of ^{68}Ga-**RGD1** in BxPC3 tumours ± blocking antibody. **B)** Uptake of [^{64}Cu]CuCB-Bicyclam in U87 and U87CXCR4 tumours ± blocking dose of CuCB-Bicyclam; uptake in MM1.s tumours.

Dibenzothiophene Sulfonium Salts as Novel Leaving Groups for Aromatic ^{18}F-Fluorination

T Gendron,[1,2] K Sander,[1,2] K Cybulska,[2] L Benhamou,[1,2] P K B Sin,[1,2] A Khan,[2] M Wood,[2] M J Porter[2] and E Årstad[1,2,*]

[1] Institute of Nuclear Medicine, University College London, 235 Euston Road (T-5), London NW1 2BU, United Kingdom; [2] Department of Chemistry, University College London, 20 Gordon Street, London WC1H 0AJ, United Kingdom

* e.arstad@ucl.ac.uk

Fluorine-18 is by far the most widely used positron emitter for clinical applications due to near ideal decay properties for positron emission tomography (PET). The versatile properties of aromatic C–F bonds and their widespread use in medicinal chemistry further contribute to the appeal of fluorine-18 for PET. However, direct incorporation of [^{18}F]fluoride into aromatic groups of drug-like molecules is often difficult to achieve. To overcome these limitations, we recently proposed the use of dibenzothiophene sulfonium salts as leaving group for aromatic ^{18}F-fluorination [1].

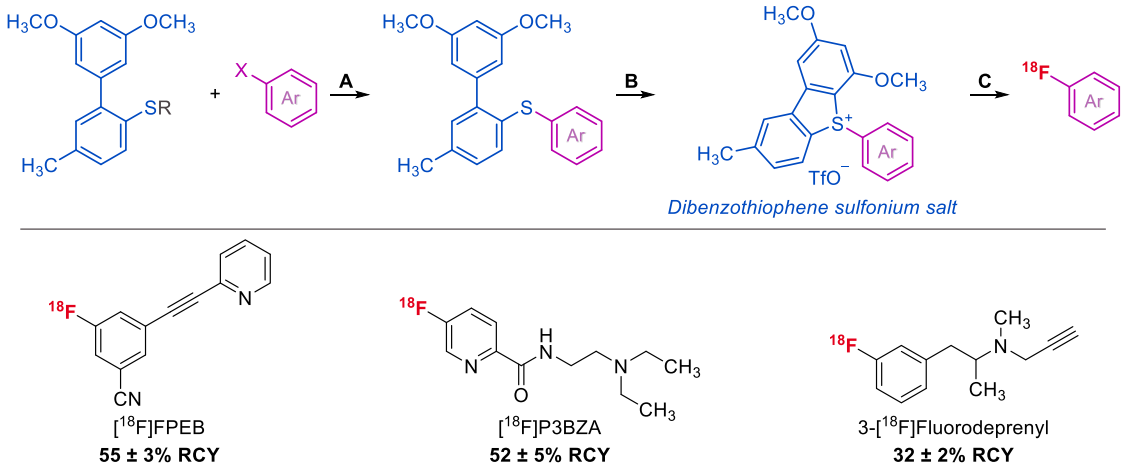

Figure 1. Top: A) Coupling of a biaryl building block with the structure of interest; B) ring-closing formation of dibenzothiophene sulfonium salt precursor; C) ^{18}F-fluorination; Bottom: example of clinically relevant tracers labelled using dibenzothiophene sulfonium salt precursor. X = Br, I; RCY: radiochemical yield.

We designed a practical synthetic methodology which provides easy access to dibenzothiophene sulfonium salts (Figure 1, top). The resulting labelling precursor are crystalline solids stable at room temperature, yet highly reactive with [^{18}F]fluoride. The strategy broadens the available radiochemical space and brings the added advantage of superior labeling efficiency for clinically relevant tracers, as exemplified by direct ^{18}F-fluorination of 3-[^{18}F]fluorodeprenyl, [^{18}F]FPEB and [^{18}F]P3BZA (Figure 1, bottom).

[1] Gendron T, Sander K, Cybulska K, Benhamou L, Sin PKB, Khan A, Wood M, Porter MJ, Årstad E. J. Am. Chem. Soc. **2018**, *140*, 11125–11132.

O4

Biodistribution of Zr-89 Anti Tenascin Antibody in Tumour Bearing Mice

S J Paisey,[1] A C Pires,[2] A M Dabkowski,[1] C Marshall[1] and A Gallimore[2,*]

[1] PETIC, School of Medicine, Cardiff University, Heath Park, Cardiff, UK; [2] Division of Infection and Immunity, School of Medicine and Systems Immunity Research Institute, Cardiff University, Heath Park, Cardiff, UK

* gallimoream@cardiff.ac.uk

Foxp3+ T lymphocytes are known as regulatory T cells (Treg) which serve to prevent autoimmunity and chronic inflammation. It is also known that these cells can suppress anti-tumour immune responses. To examine this further, we depleted Treg in mice bearing carcinogen (methylcholanthrene)-induced fibrosarcomas. We have found that of all Treg-depleted mice, around 50% respond to Treg-depletion. Responders are characterized as those where tumour growth rates decrease after treatment [1,2]. Control of tumour growth is accompanied by intratumoural development of high endothelial venules (HEV) [3] and high numbers of infiltrating anti-tumour T cells. We sought to examine why some tumours become HEV+, T cell-rich after immunotherapy whilst others remain HEV- and T cell low. Our research has shown that expression levels of the extracellular matrix protein, tenascin-C (TNC) correlate with low HEVs expression levels in tumours and so could serve as a marker for immunotherapy resistant tumours.

In this project we have radiolabelled the anti-TNC antibody with Zr-89 via previously published methods [4] and have assessed its ability to act as an imaging biomarker for development of a productive anti-tumour immune response in Treg-depleted mice by measuring TNC levels in tumours pre- and post-depletion of Treg (Figure 1).

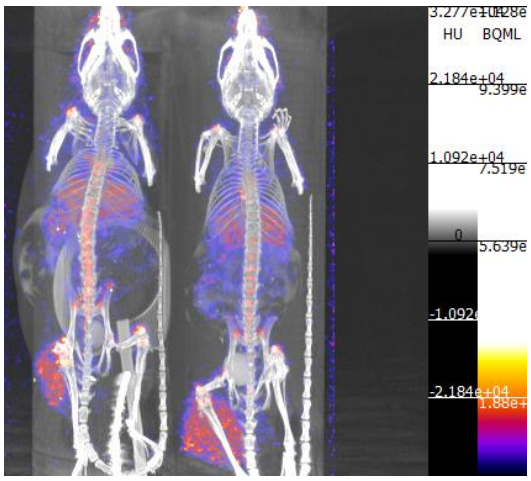

Figure 1. Zr-89-Anti-TNC antibody homing to hind limb tumour in Foxp3-DTR mice.

[1] Colbeck EJ, Jones E, Hindley JP. *Treg Depletion Licenses T Cell-Driven HEV Neogenesis and Promotes Tumor Destruction*. Cancer Immunol. Res. **2017**, *5 (11)*, 1005–1015.

[2] Drayton DL, Liao S, Mounzer RH *et al*. *Lymphoid organ development: from ontogeny to neogenesis*. Nat. Immunol. **2006**, *7 (4)*, 344–353.

[3] Hindley JP, Jones E, Smart K *et al*. *T-cell trafficking facilitated by high endothelial venules is required for tumor control after regulatory T-cell depletion*. Cancer Res. **2012**, *72 (21)*, 5473–5482.

[4] Knight JC, Paisey SJ, Dabkowski AM *et al*. *Scaling-down Antibody Radiolabeling Reactions with Zirconium-89*. Dalton Transactions **2016**, *45 (15)*, 6343–6347.

Imaging of HER-Mediated Drug Resistance Towards Personalised Therapy in Cancer

CD Martins, C Da Pieve, TA Burley, DM Ciobota, L Allott, R Smith, KJ Harrington, WJG Oyen, G Smith and G Kramer-Marek*

The Institute of Cancer Research, Division of Radiotherapy and Imaging, 123 Old Brompton Road, London SW7 3RP, UK

* Gabriela.Kramer-Marek@icr.ac.uk

The human epidermal growth factor receptors (HER) are key signalling nodes in the activation of the PI3K/AKT/mTOR pathway; promoting tumour cell survival, proliferation and metastasis. Accordingly, the development of drugs targeting the aberrantly expressed receptors and overactive signalling pathways were seen as promising treatment options for various types of cancer. However, accurately determining HER expression levels in the clinical setting to select patients for targeted therapies has been challenging, as histological analysis on isolated tissue samples can provide an unrepresentative view of heterogeneous receptor expression. Therefore, we have hypothesised that incorporating imaging with HER-specific radioligands into routine clinical practice could not only facilitate a non-invasive, real-time measurement of receptor expression levels across the patient's entire tumour burden, but also allow for dynamic monitoring of HER-mediated drug resistance providing a marker for adequate treatment dosing. To date, clinical trials with HER-specific molecular imaging probes have been frequently utilised radiolabelled mAbs. Even though they have demonstrated high tumour uptake, their large molecular size (~150 kDa) and consequential slow hepatobiliary clearance has resulted in poor contrast between tumour and normal tissues on images acquired at early time points.

Therefore, we investigated a low molecular weight targeting vectors, such as Affibody molecules as their small size (~7 kDa) enables rapid extravasation from the blood vessels and enhanced tumour penetration, providing favourable pharmacokinetics for imaging applications. Our data demonstrate that these imaging agents not only provide a global representation of tumour target expression and accessibility, but also monitor the outcome of HER-targeted treatments in xenograft models. In the future the clinical application of HER-specific Affibody-based PET agents may serve as a valuable tool in augmenting treatment personalisation.

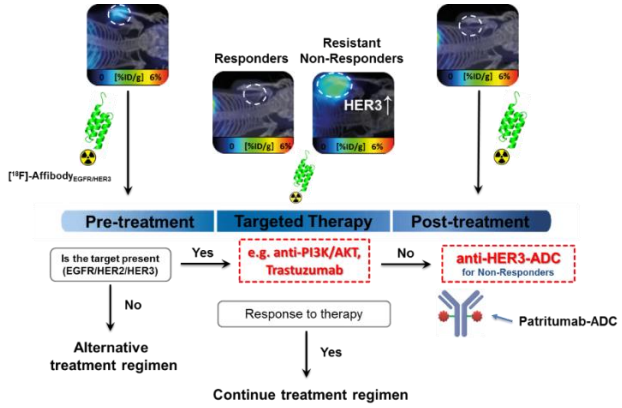

Figure 1. Experimental imaging and treatment regimen. The outcome is monitored by Affibody-based PET. Mice that develop resistance due to HER3 recovery are selected for additional treatment with anti-HER3-ADC.

O6

From Perfusion Bench to microPET Bedside: Adventures in Radiotracer Development

R Southworth

School of Biomedical Engineering and Imaging Sciences, King's College London

richard.southworth@kcl.ac.uk

The robust evaluation of novel radiotracers is crucial to their successful translation to the clinic, both in terms of validating radiotracer specificity, and providing biological context for the interpretation of the images that they provide. While cells in culture offer useful capacity in terms of high throughput radiotracer screening, they are limited in terms of physiological relevance. Conversely, small animal models may provide clinical relevance, but they are often limited in providing the experimental control required for mechanistic validation.

We therefore exploit isolated perfused organ preparations as an intermediate step which allows radiotracer screening, characterization and validation in a physiologically relevant model over which we have significant experimental control. As an illustration of their power and flexibility, I will explain how we have used such models to develop hypoxia-targeting PET imaging agents (and more recently probes targeted at mitochondrial toxicity and reactive oxygen species generation), and outline some of the considerations we believe important in selecting and validating radiotracer candidates to make them fit for clinical translation.

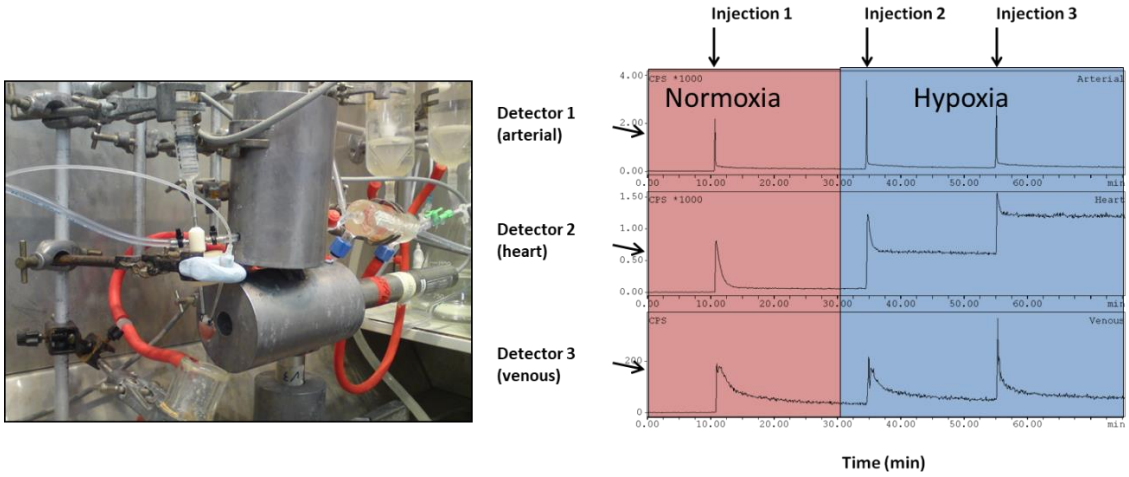

Figure 1. (left) Our custom-built triple g-detection apparatus for radiotracer screening and validation for the isolated perfused heart, and (right) representative outputs from it showing the hypoxia-dependent cardiac retention of [^{64}Cu]-CuATSM.

In Vivo PET Tracking of Anti-inflammatory Liposomes within a Rheumatoid Arthritis Model

P J Gawne,[1,*] F Clarke,[2] K Turjeman,[3] Y Barenholz,[3] S Y A Terry[1] and R T M de Rosales[1]

[1] School of Imaging Sciences & Biomedical Engineering, King's College London, St. Thomas' Hospital, London, SE1 7EH, UK; [2] Centre for Inflammation Biology and Cancer Immunology, King's College London, New Hunt's House, London, SE1 1UL, UK; [3] Department of Biochemistry and Molecular Biology, Institute for Medical Research Israel-Canada (IMRIC), The Hebrew University-Hadassah Medical School, Jerusalem.

* peter.gawne@kcl.ac.uk

To improve the treatment of rheumatoid arthritis (RA) using glucocorticoids, these drugs have been encapsulated within liposomal nanoparticles. To assess the biodistribution of one such formulation - PEGylated liposomal methylprednisolone hemisuccinate (PLMP) – was radiolabelled using [^{89}Zr]Zr-oxine [1], and tracked *in vivo* using PET imaging in a RA mouse model.

RA was induced in female C57Bl/6J mice using the K/BxN serum transfer arthritis model, whereas control groups were injected with non-arthritogenic serum or PBS. [^{89}Zr]Zr-PLMP was injected 7 days post serum/PBS injection and 48 h later, PET/CT images were obtained and biodistributions carried out.

Ex vivo biodistributions showed a clear correlation between joint swelling and [^{89}Zr]Zr-PLMP uptake. [^{89}Zr]Zr-PLMP uptake in non-target organs was similar across all groups, with high uptake in the spleen (48-59 %ID/g) and liver (29-32% %ID/g). Additionally, PET/CT images clearly showed high liposomal drug uptake at sites of inflammation (Figure 1).

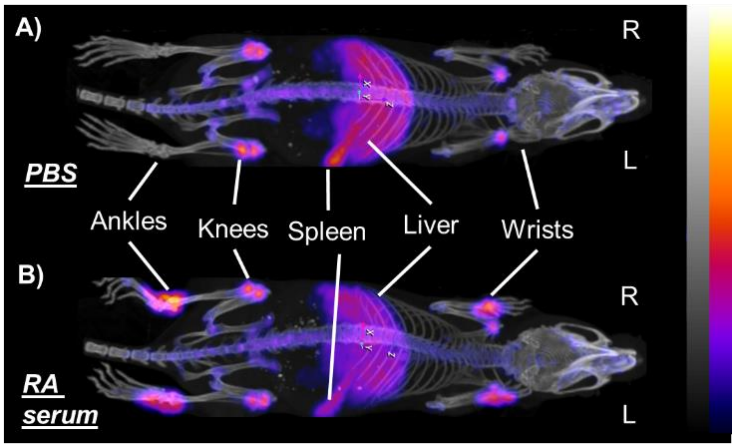

Figure 1. PET/CT maximum intensity projections of C57Bl/6J mice without **(A)** and with **(B)** serum induced rheumatoid arthritis. Swelling in the joints of the arthritic mice is clearly demonstrated by liposomal uptake in the wrists and ankles.

The uptake of liposomal medicines at RA sites has been directly imaged using PET for the first time. This technique may potentially be used as a predictor of therapeutic response to treatment with PLMP - and other nanomedicines - in inflammatory diseases.

[1] Edmonds S *et al.* ACS Nano **2016**, *10*, 10294−10307.

O8

Imaging DNA Damage Response to ^{177}Lu-DOTATATE Radionuclide Therapy

E S O'Neill,[1,*] J C Knight,[1] S Y A Terry,[2] N Falzone,[1] M H de Jong,[3] J Nonnekens,[3] K A Vallis[1] and B Cornelissen[1]

[1] Cancer Research UK and Medical Research Council Oxford Institute for Radiation Oncology, University of Oxford, UK; [2] Rayne Institute, King's College London, UK; [3] Erasmus Medical Center, Rotterdam, The Netherlands

* eric.oneill@oncology.ox.ac.uk

Peptide receptor radionuclide therapy involves the delivery of radionuclides attached to peptides targeting receptors overexpressed on tumour tissue. Lutathera (^{177}Lu-DOTATATE) received FDA approval in January for the treatment of gastroenteropancreatic neuroendocrine tumours with a standard protocol of four 7.4 GBq injected doses every 2-3 months. There is potential to improve the efficacy of this protocol using physical-dosimetry led therapies [1], and the DNA double strand break marker γH2AX has been proposed as a biodosimeter of radiation induced toxicity [2]. γH2AX foci are formed within 30 minutes of radiation-induced DNA double strand breaks, and therefore could provide a very early indicator of treatment success. We have previously demonstrated that a radiolabelled antibody-conjugate selective for these foci, ^{111}In-anti-γH2AX-TAT, allows imaging of this DNA damage response to external beam radiation by SPECT [3]. Biodosimetry of ^{177}Lu-DOTATATE therapy by ^{111}In-anti-γH2AX-TAT would therefore enable earlier evaluation of PRRT effectiveness, provide the opportunity to tailor injected dose for patients to enhance tumour toxicity whilst minimising unnecessary systemic toxicity.

CA20948 xenograft-bearing Balb/c nu/nu mice, were administered ^{177}Lu-DOTATATE (20 MBq), with subsequent injection of 111In-anti-γH2AX-TAT or non-selective ^{111}In-IgG-TAT control. There were significant increases in tumour uptake at 72 h of ^{111}In-anti-γH2AX-TAT in ^{177}Lu-DOTATATE (20 MBq) treated mice, 30 ± 15 %ID/g versus non-treatment groups, 11 ± 6 %ID/g, and 8 ± 5 %ID/g for ^{111}In-IgG-TAT with treatment ($P<0.0001$). The formation of γH2AX foci in response to ^{177}Lu-DOTATATE treatment was validated *ex vivo* by foci counting and autoradiography.

In conclusion, ^{111}In-anti-γH2AX-TAT allows *in vivo* imaging of DNA damage response following ^{177}Lu-DOTATATE peptide receptor radionuclide therapy.

[1] Garske-Román U *et al*. Eur. J. Nucl. Med. Mol. Imaging **2018**, *45*, 970–988.
[2] Denoyer D *et al*. J. Nucl. Med. **2015**, *56*, 505–511.
[3] Cornelissen, B. et al. Cancer Res. **2011**, *71*, 4539–4549.

ImmunoPET with Zr-89 Labelled Antibodies: Tool for Characterisation of Tumours

W J G Oyen

The Institute of Cancer Research Cancer Research, 123 Old Brompton Road, London SW7 3RP, UK

Wim.Oyen@icr.ac.uk

The broad application of immunotherapy has boosted the interest in radiolabelled antibodies for immunoPET to assess specific characteristics of tumour cells and tumour microenvironment. While nonspecific PET radiopharmaceuticals such as FDG are ubiquitously used for staging and restaging in oncology, this class of agents does not provide information on the expression, accessibility and heterogeneity of targets for therapeutics on tumour cells. At present, immunoPET is quite extensively used in translational cancer research, indicating potential added value in selecting patients for the most appropriate therapy and guiding optimal dosing, while avoiding futile treatment in receptor-negative patients.

While Zr-89 immunoPET provides non-invasive information on receptor expression on tumour cells, switching to a fluorescent label allows specific detection of tumours during surgery, thereby facilitating surgical procedures aimed at optimal resection of tumours.

In summary, Zr-89 labelled antibodies for immunoPET are promising tools for cancer imaging. However, immunoPET mainly remains in the domain of translational research, as systematic studies in larger patient populations, positioning immunoPET as a tool for clinical decision making, are not yet available.

Discovery and Clinical Validation of Novel PET Tracers for the Detection of Aggregated Tau

A Müller

Life Molecular Imaging GmbH, Berlin, Germany

a.mueller@life-mi.com

Misfolding of proteins is generally recognized as a causal of neurodegenerative diseases. In fact, presence of insoluble proteins like beta-amyloid (Aβ) plaques, Tau neurofibrillary tangles or α-synuclein Lewis bodies were found in the post mortem brains of Alzheimer's disease and Parkinson's disease patients.

The application of new diagnostic tools like PET imaging using tracers targeting the pathological protein aggregates in the brain may allow to identify individuals at high risk to develop clinical symptoms, track progression of the disease, and evaluate response to disease-modifying treatments. Today, PET allows already the longitudinal detection, characterization and quantification of pathological patterns of Aβ deposition in vivo during the disease progression and ideally before the onset of cognitive decline.

Aggregated Tau represent a critical pathology in AD and other forms of dementia. The distribution of Tau neurofibrillary tangles across defined brain regions appears to correspond better to the observed level of cognitive decline in AD compared to Aβ plaques. PET has been successfully used for the detection of Aβ aggregates in the brain and is currently explored for the detection of Tau aggregates in AD and other tauopathies. Several tracers targeting Tau have been discovered and tested in humans so far. However, limitations have been reported for first-generation Tau PET tracers especially regarding their off-target binding. Here we present the discovery of PI-2620, a next generation PET tracer for the detection of pathological Tau aggregates. PI-2620 displays high affinity to neurofibrillary tangles (NFTs) in AD and non-AD tauopathies. PI-2620 shows excellent selectivity with no off-target binding to amyloid beta or MAO A/B in preclinical models. In vivo biodistribution experiments showed high brain uptake of PI-2620 and rapid washout from the brain in mice and non-human primates with no observed bone uptake. Thus, PI-2620 was selected as lead candidate for clinical studies in Alzheimer's disease patients.

Initial results of the clinical trials in AD subjects showed the expected patterns of tracer uptake in brain regions associated with Tau pathology. Furthermore, no age-related uptake in choroid plexus, striatum, amygdala, or other regions as seen by other tau tracers was observed by PI-2620. Additional clinical tracer validation studies as well as exploration of the use of PI-2620 in therapeutic drug trials are currently ongoing.

O11

To What Extent Can Histology Be Used to Qualify PET Data?

D M Gorman,[1,*] V Tessyman,[2] D M Forster,[1] J P B O'Connor,[3,4] K J Williams[2] and M-C Asselin[1]

[1] Division of Informatics, Imaging and Data Sciences, University of Manchester, UK; [2] Research, Division of Pharmacy and Optometry, University of Manchester, UK; [3] Division of Cancer Sciences, University of Manchester, UK; [4] Department of Radiology, The Christie Hospital NHS Trust, Manchester, UK

* david.gorman@manchester.ac.uk

Hypoxia is a pathological condition commonly occurring within solid tumours when oxygen delivery is insufficient to meet local metabolic demand. Pimonidazole immunohistochemistry (IHC) produces high resolution 2D images of hypoxic cell distributions and is often used to validate non-invasive hypoxia imaging such as [^{18}F]FAZA PET. The hypoxic fraction (HF), the ratio of hypoxic volume over total tumour volume, is a dimensionless metric used to quantify hypoxia that is common to both IHC (area fraction) and PET (volume fraction). In PET, the HF is typically defined by applying a threshold relative to a reference tissue or blood.

Here we used a confidence interval (c.i.)-based threshold derived using pooled muscle data to define the maximum statistically measurable HF from [^{18}F]FAZA PET images of 17 mice with subcutaneous Calu-6 xenografts; this approach has previously been applied in clinical studies [1] and has been adapted by us for preclinical application. Since the initial aim of the preclinical study was to assess the efficacy of the hypoxia targeting drug Atovaquone, the mice were scanned using PET at baseline and 7 days after treatment or vehicle (controls) at the end of which the tumour was excised for IHC analysis. Figure 1a shows that PET derived HFs are 4 times higher than, and uncorrelated with, the IHC derived HFs despite *in vivo* accumulation of pimonidazole and [^{18}F]FAZA occurring via a similar mechanism. Furthermore, other hypoxia related metrics, SUV_{mean} and tumour-to-muscle (T:M) ratio, also do not correlate with IHC derived HF. Busk *et al*. demonstrate that spatial resolution effects in hypoxia imaging confound the interpretation of PET HF [2,3] thus inhibiting cross validation between PET and IHC. Regardless, in this instance, both PET and ICH derived HF independently demonstrate the effect of the drug on hypoxia (Figure 1b).

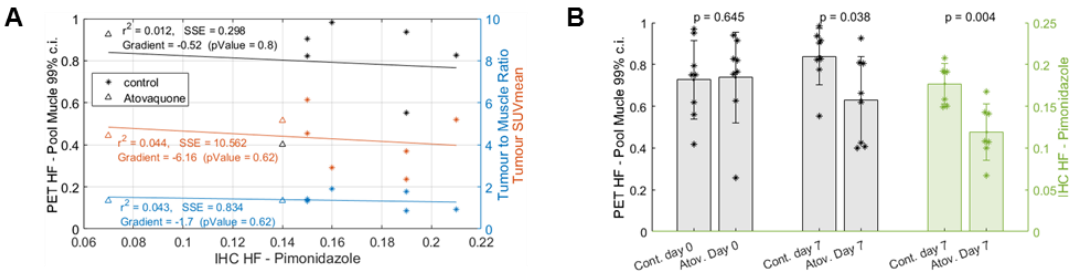

Figure 1. A) Correlation between the HVF, SUVmean, or T:M ratio of subcutaneous Calu-6 xerographs measured using PET and IHC derived HVF. **B)** HVF measured using PET and HIC at baseline and/or after Atovaquone treatment.

We propose that IHC data could potentially be used to estimate the sub-voxel scale hypoxic tissue distribution component of the PET detection limit thus providing insight into tumour type or cell line specific limitations of static PET HF measurements.

[1] Mortensen LS, Johansen J, Kallehauge J *et al*. Radiotherapy and Oncol. **2012**, *105 (1)*, 14–20.
[2] Busk M, Munk OL, Jakobsen SS *et al*. Acta Oncol. **2017**, *56 (11)*, 1583–1590.
[3] Busk M, Munk OL, Jakobsen SS *et al*. Acta Oncol. **2010**, *49 (7)*, 922–933.

Translational In Vivo Tracking of a Cell/Gene Cancer Therapy Using ^{89}Zr-oxine and PET Imaging

P S Patrick,[1] K Kolluri,[2] M Zaw Thin,[1] A Edwards,[2] E K Sage,[2] T Sanderson,[3] J C Dickson,[3] S M Janes,[2] M F Lythgoe[1] and T L Kalber[1,*]

[1] Centre for Advanced Biomedical Imaging, Division of Medicine, UCL; [2] Lungs for Living Research Centre, Division of Medicine, UCL; [3] Institute of Nuclear Medicine, Division of Medicine, UCL

* t.kalber@ucl.ac.uk

The delivery and migration dynamics of cell therapies currently remains unknown in patients, leading to questions of safety and scientific understanding in clinical trials. We are evaluating third-party allogeneic cord-derived MSCs transduced to express the anti-cancer protein TRAIL (TNF-Related Apoptosis Inducing Ligand) as a novel therapy for lung adenocarcinoma in a first-in-man phase I/II clinical trial (TACTICAL; Targeted stem Cells expressing TRAIL as therapy for lung Cancer). To address questions of MSC delivery in patients, we plan to implement a radionuclide-based cell imaging technique in a phase II arm of TACTICAL, using ^{89}Zr-oxine to label MSCs, and positron emission tomography (PET) to monitor whole body distribution. We present here our pre-clinical demonstration of feasibility.

Human TRAIL-expressing cord-derived MSCs were labelled with a range of ^{89}Zr-oxine doses (79 to 332 kBq/10^6 cells) corresponding to a clinical imaging dose of 28 to 116 MBq per 70kg patient receiving 5x10^6 cells/kg. Within this dose range MSCs retained their therapeutic capacity (Figure 1), radio-label, and MSC phenotype (CD73, CD90, CD105 +Ve; HLAII, CD14, CD34, CD45 -Ve) for a month post-labelling. The effects of radiolabelling on metabolism, cell stress, cell cycle, and TRAIL expression were also assessed. In a pre-clinical orthotopic model of lung cancer (CRL2081, human mesothelioma), i.v.-injected ^{89}Zr-oxine labelled TRAIL-MSCs co-localised with lung tumours, as visualised with MRI and PET/CT. MSCs were tracked up to 1 week, revealing their migration dynamics to the lungs, liver, and spleen. Estimates of organ-specific and whole-body effective doses were calculated for patients using OLINDA software and biodistribution data.

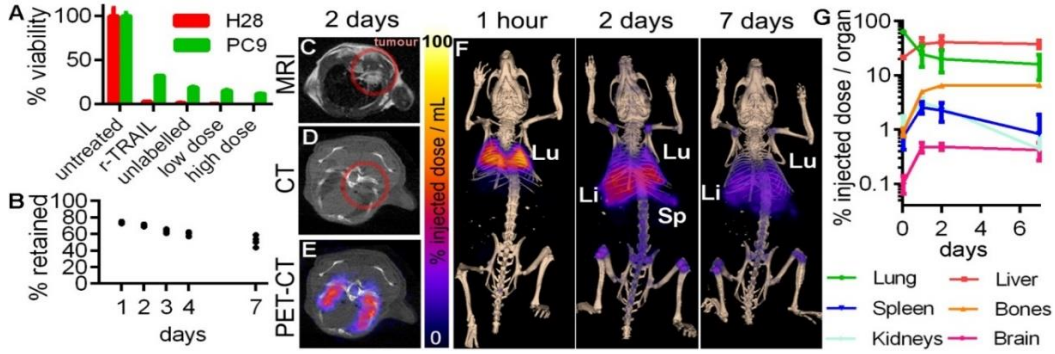

Figure 1. **(A)** TRAIL-MSCs induce apoptosis in TRAIL-sensitive (H28 mesothelioma) and partially resistant (PC9 adenocarcinoma) human lung cancer cells as effectively as recombinant TRAIL (50 ng/μL) and were unaffected by ^{89}Zr-oxine labelling at low (79 kBq/10^6 cells) or high (332 kBq/10^6 cells) ^{89}Zr-oxine doses. **(B)** TRAIL-MSCs retain ^{89}Zr over 1 week. Orthotopic lung xenografts visualised with **(C)** MRI (T_2 RARE, TE = 55 ms), **(D)** X-ray CT, **(E)** CT overlaid with ^{89}Zr PET showing co-localisation of TRAIL-MSCs. **(F)** Full body PET/CT imaging over 7 days, and **(G)** % Injected dose/organ over 7 days shows the distribution dynamics of labelled TRAIL MSCs. Points show means, error bars SD (n=3).

In summary, cord-derived MSCs can be labelled with ^{89}Zr-oxine at a tolerated dose within a clinically relevant time of <40 minutes between thawing and injection. Non-invasive longitudinal imaging of biodistribution can be achieved with PET/CT, showing delivery and retention dynamics across the body. This cell tracking method promises provide valuable feedback on implantation success, migration, and off-target delivery within the TACTICAL trial. This will reveal patient-specific responses and insight on mechanism of action for this and other cell-based therapies.

INVITED LECTURE – O13

Simultaneous Positron Emission Tomography and Ultrafast Ultrasound for Hybrid Molecular, Anatomical and Functional Imaging

A Garofalakis,[1] J Provost,[2] T Viel,[1] J Sourdon,[1] B Berthon,[2] M Perez-Liva,[1] M Pernot,[2] M Tanter[2] and B Tavitian[1,*]

[1] Inserm U970, Paris Cardiovascular Research Center, Paris, France; [2] Inserm U979, Institut Langevin Ondes et Images, Paris, France

* bertrand.tavitian@inserm.fr

Exploring complex diseases such as cancer or ischemic disorders requires a combination of multiple biological parameters, ideally co-registered in space and time. On one hand, high throughput techniques such as GWAS or SIMS extract thousands of bio molecules but are destructive and report the situation in one sample in one (accessible) place and for one timepoint. On the other hand, in vivo imaging techniques depict the full picture of an individual, are non-destructive and can be repeated over time, but report on a limited number of biological parameters. There is a strong trend in modern imaging to try to make the best out of these opposite approaches and to acquire "multiplexed" information. This may be achieved by spectral methods, for instance Multispectral Optoacoustic Tomography, Photoacoustics or MRI Fingerprinting, or by combining different imaging sources from different instruments, the so-called "hybrid imaging" methods. The advantage of the first approach is that it requires only one imaging instrument, the drawback is that it observes the interaction of living matter with a narrow spectrum of energy, often has low penetration power and comes with complex spectral unmixing issues. The advantage of the "hybrid" approach is that it may use widely distinct parts of the electromagnetic spectrum (e.g. PET-MRI), or two forms of energy waves (e.g. mechanical and electromagnetic), with different modes of interactions with tissues likely to provide different information and that can be combined to improve or correct one of the imaging modalities (e.g. attenuation correction of PET by CT); drawback is a significantly increased complexity and cost, and the hybrid combination is summoned to prove useful: as in a good stew, the ingredients must complement each other.

PET and ultrasound are almost ideal as a complementary combination: PET–CT is the most sensitive molecular imaging modality, but it has low spatial and temporal resolution. Ultrasound imaging, especially the recently introduced Ultrafast ultrasound imaging (UUI) technology based on ultrasonic holography, leverages frame rates of up to several thousand images per second to quantitatively map, at high resolution, hemodynamic, biomechanical, electrophysiological and structural parameters. Theoretically, one can expect exquisite sensitivity, quantification, whole body imaging and a relatively large portfolio of molecular imaging targets on one side, together with low cost, simplicity and unmatched resolution on the other side.

We have built PETRUS (PET Registered Ultrasound); a PET–CT–UUI triple-imaging modality that integrates the three imaging modalities in one device for simultaneous, fully co-registered imaging, enabling image fusion independent of motion without increasing acquisition times [1]. PETRUS was assembled from existing, commercially available devices using lightweight and portable UUI instrumentation for which dedicated, customized sequences were developed. We showed that full, markerless, rigid-body three-dimensional registration was accurately achieved by controlling the ultrasound probe with a six-degrees-of-freedom motorized micropositioner and that the presence of the ultrasound

probe had a negligible impact on the quality of the PET volumes [2]. Remarkably, PETRUS provides multi-parametric information currently unobtainable with any other non-invasive imaging method. Here I will present pre-clinical oncology and cardiology applications of fused, simultaneously acquired volumes of PETRUS images that yield unprecedented information.

[1] Provost J, Garofalakis A, Sourdon J *et al*. *Simultaneous Positron Emission Tomography and Ultrafast Ultrasound for Hybrid Molecular, Anatomical, and Functional Imaging*. Nature Biomed. Eng. **2018**, *2 (2)*, 85-94.

[2] Perez-Liva M, Viel T, Yoganathan T *et al*. *Performance evaluation of the PET component of a hybrid PET/CT-ultrafast ultrasound imaging instrument*. Phys. Med. Biol. **2018**, *63 (19)*, 19NT01.

Professor Bertrand Tavitian – Biography

Bertrand Tavitian is Professor in Radiology and Medical Imaging at the Faculty of Medicine of the University Paris Descartes, Director of the Imaging Research Laboratory of the Paris Cardiovascular Research Center (Inserm U970), and Director of the Network for *In Vivo* Imaging at the University Paris Descartes.

His research focuses on translational *in vivo* molecular imaging of gene expression for physiology and pathophysiology, with a particular interest in imaging the relationships between metabolism and vascularization in tumors, heart and brain. Professor Tavitian develops hybrid imaging strategies as well as tools and software for imaging research management and data mining, and he pursues the clinical translation of novel techniques. A personal long-time research interest is in the use of nucleic acids (antisense, aptamers, interfering RNAs, ribozymes etc.) for imaging, both as biotechnological tools for imaging probe development and as pharmacologically active compounds.

Professor Tavitian has a track record of 114 publications in peer-reviewed journals and twelve patent applications. He founded, and was the first president of the European Society for Molecular Imaging (ESMI). His outstanding work has been awarded at multiple occasions. To name a few, he received a Special Award for Nuclear Techniques in Medical Diagnosis and Treatment from the American Nuclear Society (1999), the Eurocancer Great Scientific Prize (2005) and the European Society for Molecular Imaging Award (2007).

[^{18}F]Olaparib: Precision Radiolabelling of PARP Inhibitors for *In Vivo* Imaging

T C Wilson,[1] M-A Xavier,[2] J Knight,[2] S Verhoog,[1] J Baguna-Torres,[2] M Mosley,[2] S Wallington,[2] D Allen,[2] V Kersemans,[2] S Smart,[2] V Gouverneur,[1,*] and B Cornelissen[2,*]

[1] Department of Chemistry, University of Oxford, Oxford, UK; [2] CRUK/MRC Oxford Institute for Radiation Oncology, Department of Oncology, University of Oxford, Oxford, UK

* veronique.gouverneur@chem.ox.ac.uk; bart.cornelissen@oncology.ox.ac.uk

The direct ^{18}F-labeling of Olaparib (Lynparza, Astrazeneca, AZD2281), an FDA approved PARP inhibitor for the treatment of BRCA-mutant ovarian cancer, has proven to be elusive, in part due to the limitations found within the field of radiochemistry [1]. This has led to a compromise either in the radiolabeled structure or the stability of the corresponding precursor, as exemplified by Reiner and Skrydstrup for the labelling of [^{18}F]PARPi and [^{11}C]Olaparib respectively [2,3]. Recently, Gouverneur *et al.* developed a wide range of novel radiofluorination reactions, enabling radiolabelling otherwise challenging motifs [4,5]. Most significantly, the Cu-mediated aromatic nucleophilic ^{18}F-fluorination of aryl pinacol-derived boronic esters [6,7,8]. Here, we demonstrate, for the first time, the successful labelling and isolation of [^{18}F]Olaparib (Figure 1) from the corresponding, bench stable, boronic ester precursor.

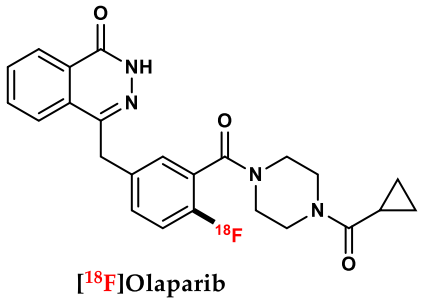

Figure 1. Chemical structure of [^{18}F]Olaparib

This isotopomer of the drug Olaparib, possesses the same PK, lipophilicity, bioavailability and PARP binding spectrum as the cold compound. As such, this has allowed for the direct measurement of biodistribution, uptake, and PARP binding of Olaparib using PET imaging in mouse models of pancreatic ductal adenocarcinoma (PDAC) cell lines.

[1] Campbell MG *et al*. Nat. Chem. **2017**, *9*, 1–3.
[2] Reiner *et al*. Mol. Imaging. Biol. **2016**, *18*, 386–392.
[3] Skrydstrup *et al*. J. Am. Chem. Soc. **2015**, *137*, 1548−1555.
[4] Preshlock S *et al*. Chem. Rev. **2016**, *116*, 719–766.
[5] Wilson T *et al*. Chem. Soc. Rev. **2018**, *47*, 6990–7005.
[6] Gouverneur *et al*. Angew. Chem. Int. Ed. **2014**, *53*, 7751–7755.
[7] Gouverneur *et al*. Chem. Commun. **2016**, *52*, 8361–8364.
[8] Gouverneur *et al*. J. Am. Chem. Soc. **2017**, *139*, 8267−8276.

Optimisation of the [^{18}F]AlF Radiolabelling Method on Trasis AiO Synthesis Platform

C Da Pieve,[1,*] D R Turton,[1] C Vriamont,[2] C Warnier[2] and G Smith[1]

[1] The Institute of Cancer Research, London, UK; [2] Trasis SA, Ans, Belgium

* Chiara.dapieve@icr.ac.uk

The aluminium ^{18}F-fluoride ([^{18}F]AlF) method for radiolabelling of biologically relevant molecules has generated significant interest owing to the capacity to combine the convenient metal-based radiochemistry with the decay characteristics of fluorine-18. Examples of peptides and proteins radiolabelled with [^{18}F]AlF methodology can be found in the literature as well as a general procedure for the automated [^{18}F]AlF-labelling on two synthesis platforms [1,2]. As a safer alternative to manual radiolabelling and with interest in the translation to clinical application, our current study is aimed at developing an optimised automated [^{18}F]AlF radiolabelling process on the Trasis All in One (AiO) platform.

The method was investigated using NOTA-Octreotide as a representative of azamacrocycle-biomolecule conjugates. The focus was placed mainly on the reagent formulation and on the type of buffer. A schematic diagram of the platform is shown in Figure 1. ^{18}F-fluoride (ca. 2 GBq), eluted from the QMA cartridge, was added to a solution of the peptide and $AlCl_3$ in 1 mM ascorbate buffer and ethanol which provided the optimal pH of 4 and peptide radioprotection. After a 15 minutes long incubation at 105 °C, a single purification step using HLB-SPE delivered the final radioconjugate. HPLC analysis of the product showed a high purity (RCP >98%) and high stability. The total production time was 35-40 min.

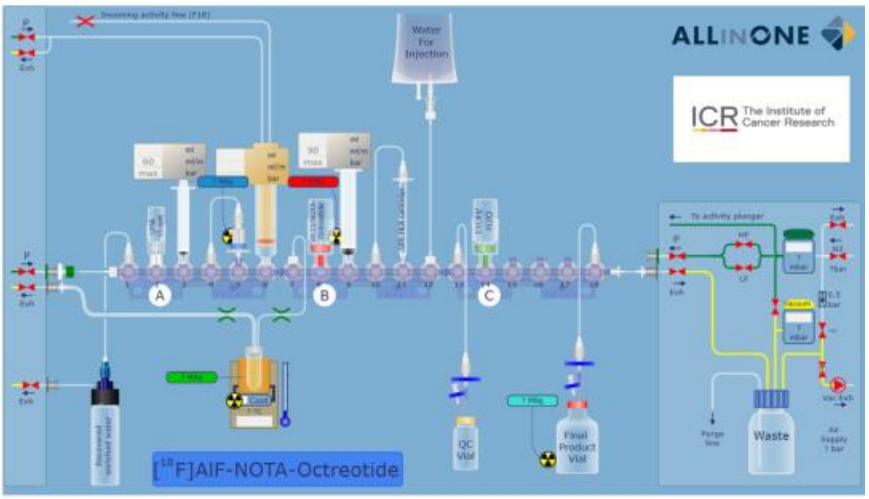

Figure 1. Setup of Trasis AiO platform for the automatic [^{18}F]AlF radiolabelling of NOTA-peptide conjugates

The quick and reproducible method shows great potential for pre-clinical applications and cGMP production of [^{18}F]AlF radiopharmaceuticals for routine clinical use.

[1] McBride W, D'Souza CA, Sharkey RM *et al.* Appl. Radiat. Isot. **2012**, *70*, 200–204.
[2] Allott L, Da Pieve C, Turton DR *et al.* React. Chem. Eng. **2017**, *2*, 68–74.

An Improved Automated Radiosynthesis of [^{18}F]FET-βAG-TOCA

L Allott,[#] C Barnes,[#] D Brickute and E O Aboagye*

Comprehensive Cancer Imaging Centre, Imperial College London, Hammersmith Hospital, Du Cane Road, London, W12 0NN, UK

[#] equal contribution

* e.aboagye@imperial.ac.uk

We previously developed [^{18}F]FET-βAG-TOCA, an octreotide derivative targeting somatostatin receptor type 2 (Figure 1), and reported a successful first-in-human evaluation of distribution, dosimetry and safety in patients bearing neuroendocrine tumours [1]. The peptide was radiolabeled with 2-[^{18}F]fluoroethylazide ([^{18}F]FEA) using copper-catalysed azide-alkyne 1,3-dipolar cycloaddition chemistry (CuAAC "click") in a GMP compliant automated radiosynthesis on the GE FASTlab™. Although validated and sufficient for producing clinical doses, a more reliable automated radiosynthetic method is required to facilitate the national and international dissemination of this radiopharmaceutical into routine clinical practice.

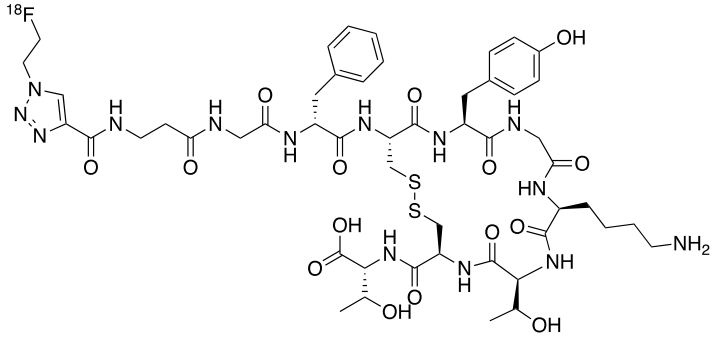

Figure 1. Structure of [^{18}F]FET-βAG-TOCA

We report an improved automated radiosynthesis of [^{18}F]FET-βAG-TOCA with several advantages over the current automated GMP synthesis: 1) SPE cartridge-based purification of [^{18}F]FEA instead of distillation, to avoid the release of radioactive volatiles; 2) simplifying the set-up by removing the off-board reactor, allowing the radiosynthesis to be performed on a single cassette; 3) HPLC purification using a biocompatible mobile phase, to avoid time-consuming C18 SPE reformulation.

The SPE purification of [^{18}F]FEA and an on-cartridge CuAAC "click" reaction improved the isolated radiochemical yield of [^{18}F]FET-βAG-TOCA from 13.3 ± 0.6% to 16.7 ± 0.6% (non-decay corrected); multi-patient doses (ca. 900 MBq) were produced in excellent radiochemical purity ≥ 98% within 75 min. The radioconjugate was radiochemically stable (≥ 98%) over the duration of testing (4 hours). The improved automated radiosynthesis will aid the development of a single, GMP friendly radiosynthesis cassette to reliably produce [^{18}F]FET-βAG-TOCA to satisfy clinical demand. In addition, the automated procedure described can be used, with minimal adaptation, to radiolabel any alkyne-containing peptide with [^{18}F]FEA using the GE FASTlab™ platform.

[1] Dubash SR *et al*. J. Nucl. Med. **2016**, *57*, 1207–1213.

P4

Production of ^{62}Zn-Citrate and ^{62}Cu-Glycine with a Modified ^{62}Zn/^{62}Cu Generator System

Z Yu,[1] D Parker,[2] A D Gee[1] and P J Blower[1,*]

[1] King's College London, School of Biomedical Engineering and Imaging Sciences, St Thomas' Hospital, London SE1 7EH; [2] School of Physics and Astronomy, University of Birmingham, Birmingham B15 2TT

* philip.blower@kcl.ac.uk

Bis(thiosemicarbazonato) complexes of cyclotron generated copper radionuclides such as ^{64}Cu ($t_{1/2}$ = 12.7 h), ^{61}Cu ($t_{1/2}$ = 3.3 h) and ^{60}Cu ($t_{1/2}$ = 23.7 min) are promising agents for non-invasive imaging of hypoxia and myocardial/CNS blood flow with positron emission tomography (PET). The rapid pharmacokinetics of these complexes have potential to allow repeated PET imaging studies in a single session, for example to determine the effect of an intervention such as carbogen breathing on hypoxic tumours. The short half-life generator-produced isotope ^{62}Cu ($t_{1/2}$ = 9 min) would make this possible. Although the 9.3 h half-life of the parent radionuclide ^{62}Zn (not commercially available in EU) limits the shelf life of the generator to one day, it is long enough for delivery to national centres. In this study, we developed an optimised ^{62}Zn/^{62}Cu radionuclide generator system building on Fukumura's method. Both ^{62}Zn-citrate and ^{62}Cu-glycine could be produced with the same generator system.

Production of 1 GBq ^{62}Zn was accomplished by proton irradiation of copper foils with 29 MeV proton particles at a beam current of 30 µA for 1 h at the University of Birmingham (Birmingham MC40 cyclotron). The generator was prepared according to Fukumura's method with modification. In brief, the target was dissolved in a fresh mixture of concentrated H_2O_2 (25 mL) and concentrated HCl (25 mL). To isolate ^{62}Zn, the solution was diluted with water (Cl^- final concentration 3 M) and passed through a Chromabond PS-OH^- cartridge. Excess of HCl solution (2 M) was applied to remove metal contaminants. Parent radionuclide ^{62}Zn was eluted with 20 mL of water and loaded on a Sep-Pak Accell CM plus cartridge. ^{62}Cu was eluted with glycine solution (3 mL, 200 mM). ^{62}Zn-citrate was produced by flush the CM plus cartridge with 2 mL 4% sodium citrate solution. Breakthrough of ^{62}Zn in Cu-glycine solution was evaluated with a HPGe detector. The carrier copper concentration in the final ^{62}Cu elute was measured by ICP-MS.

By replacing the AG1X8 resin columns with Chromabound PS-OH^- anion exchange cartridge, the ^{62}Zn/^{62}Cu generator was ready to elute in 3 hours. The general yield of ^{62}Cu-glycine was 53.93 ± 5.79% (n=4, decay corrected) with very low level of ^{62}Zn breakthrough (<0.2 %) and carrier (< 1ppm).

[1] Fukumura T *et al*. Nucl. Med. Biol. **2006**, *33(6)*, 821–827.
[2] Haynes NG *et al*. J. Nucl. Med. **2000**, *41*, 309–314.

P5

Preliminary Evaluation of Chelating Agents for Biomolecular Labelling with the Long-lived PET Isotope Manganese-52

M Iafrate,[1] W D Shingleton,[2] J Fonslet,[3] G O Fruhwirth[1] and P. J. Blower[1,*]

[1] KCL Imaging Chemistry and Biology, London; [2] GE Healthcare, Amersham; [3] DTU, Denmark

* Philip.blower@kcl.ac.uk

Manganese-52 ($t_{1/2}$ = 5.6 d) has potential application for prolonged longitudinal imaging studies, such as antibody and cell tracking. Since manganese is an essential trace element, it will be important to ensure the imaging signal corresponds to radiomanganese in the administered labelled cell population or antibody rather than leaching into natural biological pathways. Therefore, ^{52}Mn bifunctional conjugates must be highly kinetically stable towards transchelation for *in vivo* use in these contexts. A previous immunoPET imaging study has shown that DOTA was an adequate chelator for ^{52}Mn imaging [1].

In this research, we incubated several Herceptin immunoconjugates (100 μL) of commercially available bifunctional chelators with $^{52}MnCl_2$ at a range of antibody concentrations and mild pH conditions within physiological ranges to identify the lead chelators for future research. Reactions were quenched after 45 minutes with EDTA (50 mM, 2 μL). Labelling efficiencies were analysed by iTLC. There is a clear difference in percent ^{52}Mn bound to chelators at the lowest concentrations tested (Figure 1). Future work will ascertain the number of chelators per immunoconjugate, and the kinetic and *in vivo* stability of lead chelators, which were NOTA, PCTA, and oxo-DOTA.

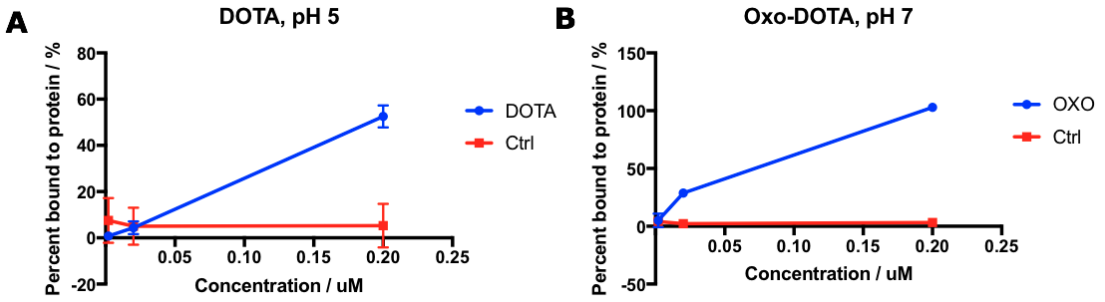

Figure 1. Percent ^{52}Mn bound to selected chelators. Best tested conditions shown in each case: **A**; DOTA pH 5, **B**; Oxo-DOTA, pH 7.

[1] Graves SA, Hernandez R, Fonslet J *et al*. Bioconjugate Chemistry **2015**, *26*, 2118–2124.

^{52}Mn-Sarcophagine: A New Radiometal-Chelator Pair for PET

M S Farleigh,[1,*] N J Long,[2] J Fonslet[3] and M T Ma[1]

[1] School of Biomedical Engineering & Imaging Sciences, King's College London; [2] Chemistry Department, Imperial College London; [3] Technical University of Denmark

* matthew.farleigh@kcl.ac.uk

^{52}Mn (β^+, $t_{1/2}$ 5.6 d) has potential for use in cell tracking, and antibody targeted diagnostic PET imaging by virtue of its relatively long half-life, and favourable imaging properties. To progress ^{52}Mn-based imaging agents, effective chelators that stably retain ^{52}Mn *in vivo* are required. Macrobicyclic sarcophagine ligands are well known for their ability to efficiently and stably chelate a variety of metal ions. In this work, for the first time, a sarcophagine, 1,8-diamino-3,6,10,13,16,19-hexaazabicyclo[6.6.6]icosane, ($(NH_2)_2$sar) was radiolabelled with ^{52}Mn under a variety of conditions. A range of temperatures were investigated (25 – 80 °C) as well as a range of sarcophagine concentrations (1 nm – 1 mM) and reaction times (10 – 120 mins; Figure 1). Our findings suggest that quantitative radiolabeling can be achieved in just 10 minutes at 80 °C with a ligand concentration of 1 mM (Figure 2). This work demonstrates that sarcophagines can be radiolabelled with ^{52}Mn, thus warranting further investigation into this interesting new radiometal-chelator pair whose potential applications to nuclear medicine are numerous.

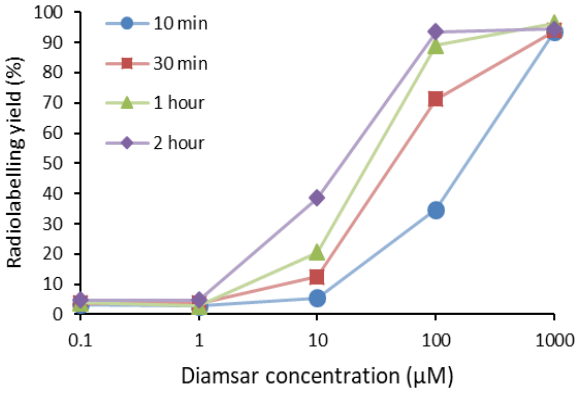

Figure 1. Radiochemical yields for the reaction between $(NH_2)_2$sar and $^{52}Mn^{2+}$ at varying concentrations of $(NH_2)_2$sar with various reaction times. Radiolabelling was conducted at 80 °C.

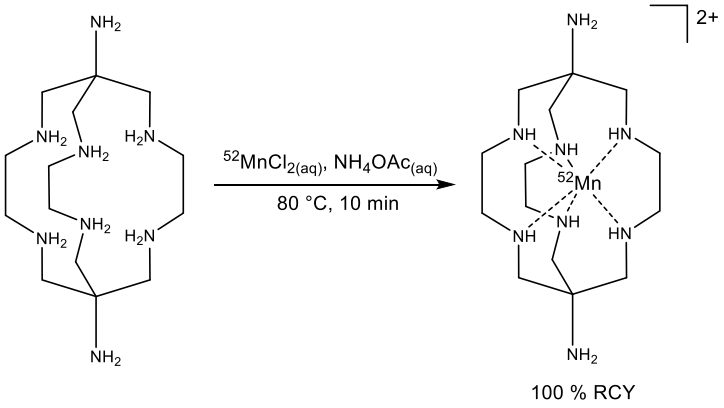

Figure 2. A reaction scheme for the rapid, quantitative radiolabeling of $(NH_2)_2$sar with $^{52}Mn^{2+}$.

Evaluation of DFO-HOPO as an Octadentate Chelator for Zirconium-89

L Allott, C Da Pieve, R Edwards, J Meyers, T Spinks, D M Ciobota, G Kramer-Marek and G Smith*

Division of Radiotherapy and Imaging, The Institute of Cancer Research, Sutton, Surrey

* Graham.Smith@icr.ac.uk

The use of zirconium-89 (^{89}Zr) for preclinical and clinical immuno-positron emission tomography (immuno-PET) is attracting a lot of interest due to its decay characteristics ($t_{1/2}$ = 78.4 h) with the long biological half-life of antibodies. Currently, deferoxamine (DFO, **1**; Figure 1) is the most common chelator used to radiolabel biomolecules with ^{89}Zr. However, the coordination of the radiometal by the hexadentate DFO molecule leads to a certain degree of demetallation of the complex *in vivo* with consequent bone accumulation. Herein, we report the evaluation of an octadentate molecule, DFO-HOPO (**2**), as a suitable chelator for ^{89}Zr and a more stable alternative to DFO [1].

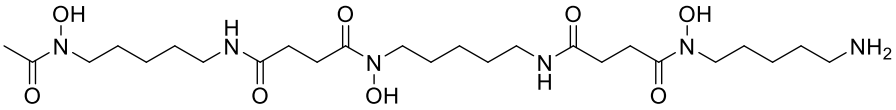

DFO (**1**)

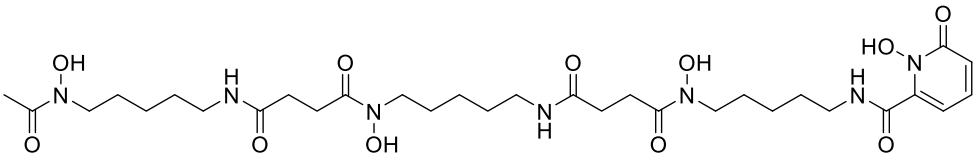

DFO-HOPO (**2**)

Figure 1. Chemical structure of DFO (1) and DFO-HOPO (2)

^{89}Zr–DFO-HOPO complex (^{89}Zr–**2**) stability was assessed by radio-ITLC analysis in a variety of conditions as long as 7 days: in acidic buffer (pH 2), mouse serum and in the presence of an excess of competing chelating agent. Whilst ^{89}Zr–DFO showed various amounts of radioactivity not associated with the chelator, ^{89}Zr-**2** showed no demetallation. Furthermore, *in vivo* studies showed that ^{89}Zr-**2** cleared the body via the renal and hepatobiliary systems comparably to ^{89}Zr–DFO. The molecule shows good potential for the future development of a DFO-HOPO-based bifunctional chelator (BFC) for the radiolabelling of biomolecules with ^{89}Zr.

[1] Allott L, Da Pieve C, Meyers J *et al*. Chem. Commun. **2017**, *53*, 8529−8532.

Surface Mineralisation Mediates Chelate-free Radio-labelling of Iron Oxide Nanoparticles

P S Patrick,[1] L K Bogart,[2] T J Macdonald,[4] P Southern,[2,3] M J Powell,[4] M Zaw-Thin,[1] N H Voelcker,[5] I P Parkin,[4] Q A Pankhurst,[2,3] M F Lythgoe,[1] T L Kalber[1] and J C Bear[4]

[1] Centre for Advanced Biomedical Imaging, University College London; [2] UCL Healthcare Biomagnetics Laboratories; [3] Resonant Circuits Limited, London; [4] UCL Department of Chemistry; [5] Monash Institute of Pharmaceutical Sciences, Monash University, Parkville, Australia

Iron oxide nanoparticles (IONPs) have a wide range of biomedical applications due to their tuneable size, shape, magnetism, and potential for functionalisation. MRI gives sensitive non-invasive detection of IONPs *in vivo*, but in practice this can be ambiguous due to endogenous contrast sources and signal-loss saturation (Figure 1). Radio-labelling circumvents this problem, allowing quantification with nuclear imaging – yet this typically requires further addition of chelators. A recently-reported method achieved labelling without chelators via heating with radiometals [1,2] – thereby simplifying the labelling process. However, the particle-radio-metal interaction was not explained, leaving unanswered questions.

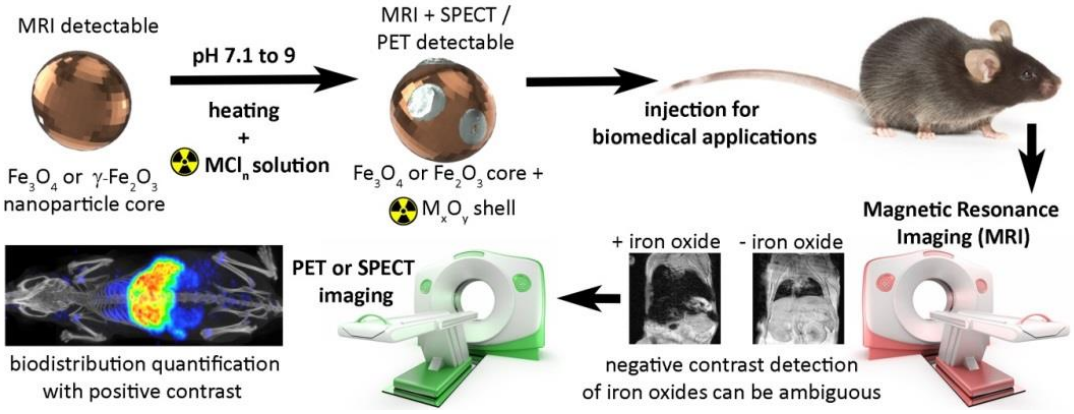

Figure 1. Synthesis of radio-labelled IONPs using radio-metal chloride salts (MCln) to form an oxidised radio-metal coating allows whole-body non-invasive quantitative imaging using PET or SPECT, in addition to high- resolution detection MRI.

Here, we demonstrate that this heat-induced radio-labelling works by mineralization of radio-metals onto the surface of the particle in trace amounts, without changing the original physical size, iron oxide material, magnetic properties, or particle stability in solution. Using both ^{111}In for SPECT, and ^{89}Zr for PET, we show this labelling method is compatible with a panel of magnetite and maghemite-based IONPs having different coatings and sizes, with RCYs of 68 to 95%. For all samples, particles were heated at 90 °C for 90 minutes at pH 8, and labelling efficiency was measured using magnetic separation and thin-layer chromatography. X-ray photo-electron spectroscopy and X-ray diffraction showed that the metal additives form amorphous mineral oxides (In_2O_3 or ZrO_2), and that the starting iron oxides are unaltered. Time-of-flight surface ionisation mass spectroscopy showed that the In and Zr oxides were localized on the particle surface, while Mössbauer spectroscopy, TEM, and SQUID magnetometry showed that the native magnetic and material properties remained unaltered.

To demonstrate this method's utility, we labelled a new, dextran-coated, magnetic hyperthermia iron oxide agent RCL-01 (Resonant Circuits Ltd) [3] using $^{89}ZrCl_4$, giving a 95% RCY. Five mg of ^{89}Zr-RCL-01 was injected subcutaneously in wild-type mice to model the dosing route for melanoma treatment, and PET-CT and MRI were used to track biodistribution for 8 days, showing dispersal from the point of injection across the whole body (Figure 2A). MRI, PET, and CT contrast from the iron oxide showed co-localisation, consistent with retention of the radiolabel on the particle (Figure 2B-E). This method promises rapid radio-labelling and whole-body quantification of IONPs across a range of bio-medical applications.

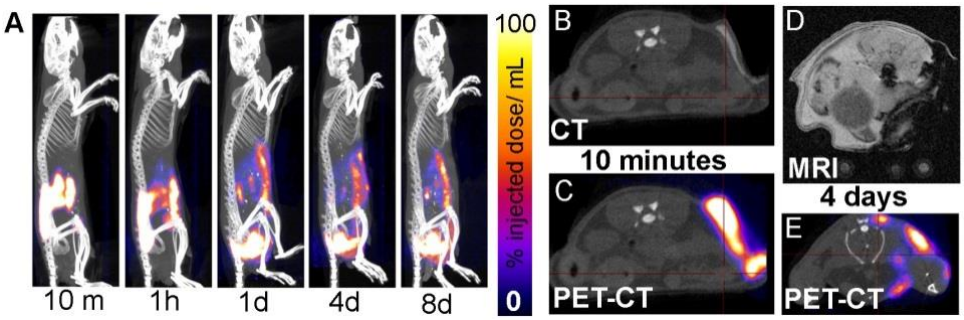

Figure 2. A. PET-CT timecourse of the whole body distribution of subcutaneously injected 89Zr-labelled RCL-01 IONPs. **B.** CT contrast and **C.** PET contrast from iron oxide particles showing subcutaneous location. **D.** MRI and **E.** PET-CT images showing distribution of particles at 4 days post-injection.

[1] Boros *et al*. Chem. Sci. **2015**.
[2] Huan *et al*. Nat. Protocols **2018**.
[3] www.resonantcircuits.com

Visualizing Kinetically Robust $Co^{III}_4L_6$ Assemblies *In Vivo*: SPECT Imaging of the Encapsulated $[^{99m}Tc]TcO_4^-$ Anion

B P Burke,[1] W Grantham,[2] M J Burke,[2] G S Nichol,[2] D Roberts,[1] R Hargreaves,[1] C Cawthorne,[1] P J Lusby[2] and S J Archibald[1,*]

[1] Positron Emission Tomography Research Centre, School of Life Sciences and Department of Chemistry, University of Hull, Cottingham Road, Hull, HU6 7RX, UK; [2] EaStCHEM School of Chemistry, University of Edinburgh, Joseph Black Building, David Brewster Road, Edinburgh, Scotland EH9 3FJ

* S.J.Archibald@Hull.ac.uk

Syntheses of clinical imaging agents for SPECT involve reduction of the $[^{99m}Tc]TcO_4^-$ anion, which can limit applications as it is often incompatible with chelator-biomolecule conjugates. The reliance on a reductive approach to technetium-based imaging agents is a consequence of the assumption that the *"chemical reactivity of the pertechnetate anion is negligible; it does not bind to any ligand*" [1]. Using a kinetically robust $Co^{III}_4L_6$ tetrahedron we now show the feasibility of encapsulating the most widely used precursor in clinical nuclear diagnostic imaging, the gamma emitting $[^{99m}Tc]TcO_4^-$ anion, under conditions compatible with *in vivo* administration (Figure 1). Subsequent SPECT imaging of the caged-anion reveals a marked change in the biodistribution compared to the thyroid-accumulating free oxo-anion, thus moving clinical applications of (metallo)supramolecular species a step closer.

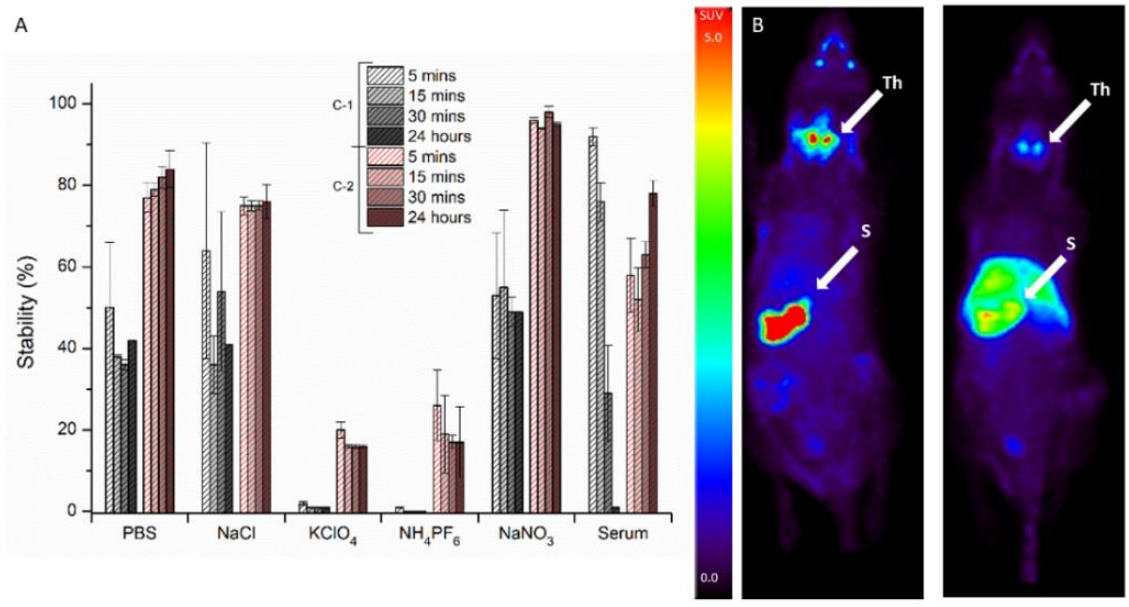

Figure 1. (A) Stability of encapsulated complexes to a range of different anions and conditions. 100 μM solution of salt was added to each cage made at their respective EC_{95} values. **(B)** Comparison of $[^{99m}Tc]TcO_4^-$ uptake in naïve mice (left) vs cage + $[^{99m}Tc]TcO_4^-$ (right).

[1] Zolle I. Technetium-99m Pharmaceuticals: Preparation and Quality Control in Nuclear Medicine; Springer: Berlin, Heidelberg, New York, **2007**.

Biodistribution of Manganese in Healthy Mice Using ^{52}Mn

G Firth,[1] J Blower,[1] J Bordoloi,[1] J Fonslet[2] and P J Blower[1,*]

[1] School of Biomedical Engineering & Imaging Sciences, King's College London, St Thomas' Hospital, London, SE1 7EH, UK; [2] The Hevesy Lab, Technical University of Denmark, 4000 Roskilde, Denmark

* philip.blower@kcl.ac.uk

^{52}Mn ($t_{1/2}$ = 5.6 days) is a positron emitting radionuclide that has the potential to non-invasively study manganese trafficking on a whole body scale to better understand the role of manganese in biological processes and health *in vivo*. This could help elucidate potential changes to the transport of manganese in a range of pathological diseases. In this project we address the whole body distribution of ^{52}Mn, administered intravenously as $MnCl_2$ in healthy BALB/c mice. The data will be used in later studies as a healthy control. [^{52}Mn]$MnCl_2$ was administered i.v. at time 0 h, a dynamic PET scan followed from 0-1 h and PET/CT scans were then performed at 4, 24, 48 and 72 h. The mice (n = 3) were then euthanised at 96 h to provide *ex* vivo biodistribution data. Fast blood clearance was observed initially with an estimated biological half-life of 1.35 min. Activity at 1 h was localised primarily to the abdominal organs with small amounts of radioactivity observed in the heart and joints. Retention of ^{52}Mn varied over time for each organ, with activity associated with the salivary glands increasing over time. Prominent uptake at 96 h was seen in the liver (8.21 ± 0.62 %ID/g), pancreas (22.99 ± 3.44% ID/g), salivary glands (9.25 ± 0.18% ID/g) and kidneys (20.87 ± 3.11% ID/g). Maximum intensity projection (MIP) PET images at 1 and 4h also demonstrated heart and intestine uptake which decreased over time as ^{52}Mn was excreted *via* the faeces. Modest brain uptake (2.30 ± 0.24% ID/g) was observed at 96 h. The research described sets the foundation for the study of ^{52}Mn trafficking using PET, and will be developed further to investigate the importance of manganese in a range of diseases.

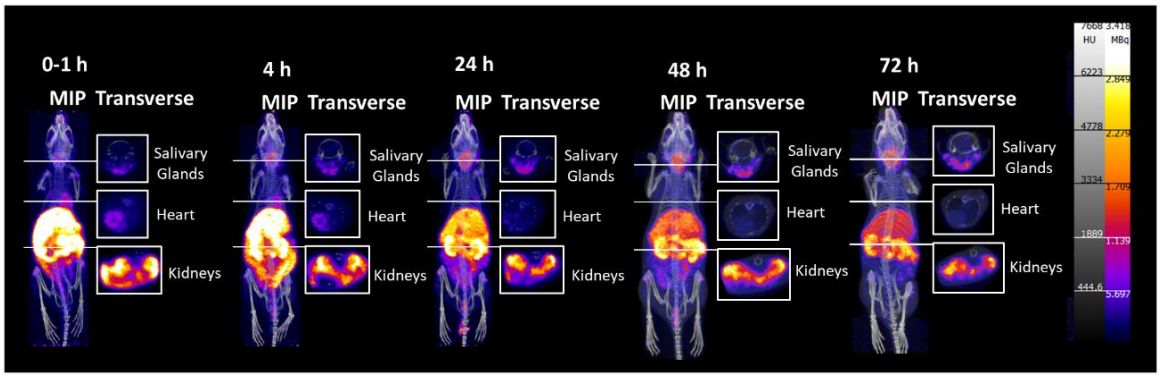

Figure 1. PET/CT images of ^{52}Mn biodistribution at various time points: representative maximum intensity projection (MIP) and transverse slices of PET-CT images of a healthy BALB/c mouse injected with [^{52}Mn]$MnCl_2$ (1.5MBq, 100 µL) at 1 h, 4 h, 24 h, 48 h and 72 h post injection.

Towards Dual Isotope In Vivo PET/SPECT Imaging – A Pilot Study

J E Blower, J K Bordoloi, K Sunassee, L Livieratos, M Farleigh, A Rigby, C Poyiatzis, H O'Brien, J Jackson, J Bezer, P J Blower*

School of Biomedical Engineering and Imaging Sciences, King's College London, 4th Floor Lambeth Wing, St Thomas' Hospital, London SE1 7EH, UK

* philip.blower@kcl.ac.uk

Two ^{18}F-labelled tracers for hNIS, [^{18}F]BF_4^- and [^{18}F]SO_3F^-, have been developed as potential PET analogues of [^{99m}Tc]pertechnetate [1]. [^{18}F]BF_4^- has recently undergone a Phase 1 clinical trial in patients with thyroid cancer and a study in healthy volunteers [2]. This work aims to compare the *in vivo* properties of [^{18}F]BF_4^- and [^{18}F]SO_3F^- in mice bearing hNIS-expressing tumours.

Since these tracers possess identical physical emission profiles, they cannot be compared simultaneously in the same animal. To overcome this, each was compared by pairing with SPECT tracer $^{99m}TcO_4^-$ as a same-animal control (that is, each animal was imaged with [^{99m}Tc]pertechnetate and either [^{18}F]BF_4^- OR [^{18}F]SO_3F^- to allow controlled comparison of the two PET tracers. Although ^{18}F and ^{99m}Tc possess different emission profiles, their impact on the SPECT and PET scans respectively, could be significant and lead to confounding results. Mixed-isotope ^{18}F/^{99m}Tc phantom experiments were carried out to determine the crossover effects of each isotope on the scans, and ultimately, to help design the optimal protocol for *in vivo* dual isotope imaging using ^{18}F and ^{99m}Tc.

The impact of ^{18}F on the SPECT detectors was particularly significant: 511 keV photons from ^{18}F undergo Compton scattering and enter the ^{99m}Tc energy window leading to an over-estimation of ^{99m}Tc activity, and an increase in noise. However, it was found that the more ^{99m}Tc present in relation to ^{18}F, the less impact the ^{18}F had on the SPECT quantification: > 1:70 ratio of ^{18}F:^{99m}Tc was found to mitigate this effect completely.

Based on the phantom study findings, a final dual-isotope *in vivo* protocol was proposed and tested in a pilot study to compare the behaviour of [^{18}F]BF_4^- and [^{18}F]SO_3F^-, using [^{99m}Tc]TcO_4^- as a control, in mice bearing hNIS-expressing tumours, with interesting results: differences in uptake between [^{18}F]BF_4^- and [^{18}F]SO_3F^- were observed. Various methods to remove the contribution of the ^{18}F emissions from the final SPECT image are being investigated.

[1] Khoshnevisan A, Chuamsaamarkkee K, Boudiemeline M *et al.* ^{18}F-Fluorosulfate for PET Imaging of the Sodium-Iodide Symporter: Synthesis and Biologic Evaluation In Vitro and In Vivo. *J. Nucl. Med.* **2017**, *58*, 156–161.

[2] O'Doherty J, Jauregui-Osoro M, Brothwood T *et al.* ^{18}F-Tetrafluorborate, a PET Probe for Imaging Sodium/Iodide Symporter Expression: Whole-Body Biodistribution, Safety, and Radiation Dosimetry in Thyroid Cancer Patients. *J. Nucl. Med*. **2017**, *58*, 1666–1671.

Insights into Trace Metal Metabolism in Health and Disease from PET: ‘‘PET Metallomics’’

J J Bartnicka and P J Blower*

King’s College London, School of Biomedical Engineering and Imaging Sciences, St. Thomas’ Hospital, London, United Kingdom

* philip.blower@kcl.ac.uk

Essential trace metals such as copper, zinc, iron, and manganese perform critical functions in cellular and physiologic processes including catalytic, regulatory, and signaling roles. Disturbed metal homeostasis is associated with the pathogenesis of diseases such as dementia, cancer, and inherited metabolic abnormalities. Intracellular pathways involving essential metals have been extensively studied but whole-body fluxes and transport between different compartments remain poorly understood. The growing availability of PET scanners and positron-emitting isotopes of key essential metals, particularly ^{64}Cu, ^{63}Zn, and ^{52}Mn, provide new tools with which to study these processes *in vivo* [1].

This project aims to use this methodology to understand the trafficking of copper, zinc and manganese in normal physiology, as well as in disease states. Radiometals are often used for imaging in non-physiological ionic formulations (such as chloride salts) but the plasma equilibria resulting from their intravenous injection are not well characterized. It is important to study the speciation of radiometals (for example, their complexation by plasma proteins and low-molecular weight components), as well as the role of those different species for the delivery of metals to target tissues. This will allow us to devise the more physiologically relevant methods of radiometal delivery to study its trafficking *in vivo*.

In the context of a specific translational application, feasibility of PET imaging with ^{64}Cu and ^{62}Cu to image copper homeostasis in tumours *in vivo* will be evaluated as a prognostic tool for their response to cisplatin therapy - due to the emerging role of copper transporters in cisplatin trafficking in tumours. Other future studies will involve studying trace metal trafficking in cancer, dementia and diabetes models and patients using ^{63}Zn, ^{51}Mn and ^{52}Mn.

[1] Bartnicka JJ, Blower PJ. *Insights into Trace Metal Metabolism in Health and Disease from PET: “PET Metallomics”.* J. Nucl. Med. **2018**, *59*, 1355–1359.

P13

^{68}Ga Biodistribution and Binding to Transferrin: Effects of Bicarbonate and Anaesthesia

F Al-salemee,* J E Blower and P J Blower

School of Biomedical Engineering and Imaging Sciences, King's College London, London, UK

* fahad.al-salemee@kcl.ac.uk

Background: When administered unchelated, $^{68/67}Ga^{3+}$ has a variable and unpredictable biodistribution. Transferrin is the major Ga transporter in blood and Ga-transferrin binding requires bicarbonate. Anaesthesia depresses respiration, potentially affecting blood [HCO_3^-]. We examined the effect of bicarbonate on ^{68}Ga-transferrin binding and cell uptake, and the effect of anaesthesia on ^{68}Ga biodistribution.

Methods: ^{68}Ga-apotransferrin binding was assessed at varying [HCO_3^-] using PD10 size-exclusion chromatography. A375 melanoma cells were incubated with ^{68}Ga and human apotransferrin at different bicarbonate levels. Ten BALB/c mice (5 isoflurane-anaesthetised, 5 not) were intravenously injected with ammonium-acetate-buffered ^{68}Ga eluted on three different occasions from an Eckert & Ziegler generator, and *ex vivo* biodistribution was determined 2 hours later.

Results: *In vitro*, without bicarbonate, 11.5±0.7% radioactivity was transferrin-associated, compared to 38.9±2.37, 34.0±1.6 and 34.1±0.1% with 5, 10 and 20 mM HCO_3^-, respectively (n=3). 1.7±0.1% activity was cell-associated at 0 mM bicarbonate, compared with 3.4±0.3, 3.3±0.1 and 3.2±0.02 at 5, 10 and 20 mM, respectively (n=4). *In vivo*, tissue biodistribution did not differ significantly between anaesthetised and non-anaesthetised mice (n=5). However, liver and spleen uptake (%ID/g) was significantly higher for mice injected with the first (vs. second) generator elution (liver: 15.4±1.0% vs. 6.2±0.2%, spleen: 11.2±2.5% vs. 3.6±0.2%) (n=4).

Conclusions: The presence of bicarbonate significantly improves ^{68}Ga-transferrin binding and cellular uptake. Anaesthesia has no effect on the biodistribution of weakly-chelated ^{68}Ga. ^{68}Ga partitioning between liver/spleen and bones varies significantly between, but not within, generator elutions, suggesting that variable chemical composition of ^{68}Ga, rather than variable physiology of the subject, is responsible for variable biodistribution.

In Vivo Development and Validation of Dual Isotope SPECT/CT for the Assessment of Gastrointestinal Transit

T Alahmad,[1] C Finucane,[2] H Fitzke,[1] S Macholl,[2] R Kashani[2] and J Sosabowski[2,*]

[1] UCL Centre for Advanced Biomedical Imaging, London, UK; [2] Centre for Molecular Oncology and Imaging, Barts Cancer Institute, Queen Mary University of London, London EC1M 6BQ, UK

* alahmadta@gmail.com

Purpose: To evaluate a non-invasive imaging technique using translational dual-isotope SPECT/CT [1] to quantitatively analyze upper gastrointestinal (GI) motility.

Methods: Stomach volumes were measured after intravenous injection of 30 MBq of ^{99m}Tc-pertechnetate and GI transit assessed following oral gavage of 20 MBq (300 µL) ^{111}In-DTPA radiolabeled liquid meal of either a non-nutrient meal of PBS (G1); nutrient meal of Ensure PLUS 1.5 kCal/mL (G2); or a nutrient meal with prior dose of a prokinetic - neostigmine bromide (1 µg/kg) (G3). SPECT imaging was performed at 0, 30, 45, 60, 75, and 90 minutes post-dosing to measure gastric volumes and transit of the labelled meal and compared with *ex vivo* biodistribution 2 hours post-gavage.

Results: Following a non-nutrient meal (G1), stomach volumes had decreased at 30 mins post-gavage compared to baseline. Following a nutrient meal (G2 & G3) they did not decrease until 45 mins. A significant difference was observed between the non-nutrient and nutrient groups at 30 min post-gavage (p = 0.005) and volumes decreased more rapidly following administration of neostigmine bromide (G3). This corresponded with *ex vivo* biodistribution of ^{111}In, which found that 10.37 ± 0.27% of the meal remained in the stomach at 2 h post-gavage in G1, compared to 29.73 ±7.33% in G2 and 22.39 ±9.41% in G3.

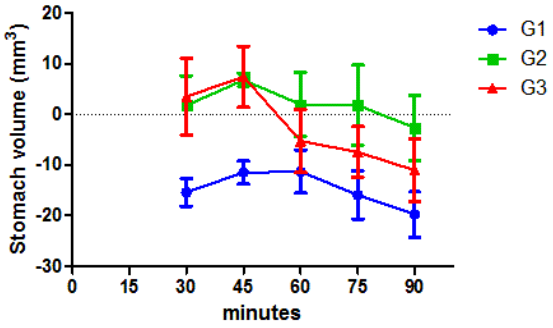

Figure 1. Mean change (± standard deviation) in stomach volume compared to baseline volume assessed with ^{99m}Tc-pertechnetate.

Conclusion: As expected, transit of the non-nutrient meal (G1) was more rapid than the nutrient meal (G2) and mice treated with the prokinetic (G3) prior to oral gavage exhibited faster gastric emptying compared to the untreated mice.

Discussion: This study has demonstrated the validation of non-invasive dual isotope SPECT imaging technique with quantification accuracy of the upper GI motility. This non-invasive method would enable dramatic reductions in the number of animals used in experiments and in future could be applied to different models including pain, stress and

neurodegeneration to characterize the effect of different pathologies on gastrointestinal function [2].

[1] Simonian H *et al*. *Simultaneous assessment of gastric accommodation and emptying of solid and liquid meals*. Gastroenterology **2003**, *124(4)*, A53.
[2] Camilleri M and D Linden. *Measurement of Gastrointestinal and Colonic Motor Functions in Humans and Animals.* Cellular and Molecular Gastroenterology and Hepatology **2016**, *2(4)*, 412–428.

Acknowledgments: I would like to thank J Foster for her help with HO license protocol, S Martin for her help with PO dosing, and J Brook for helping with VivoQuant.

Structural Features of Graphene Nanomaterials Alter Their Biodistribution in Mice

D A Jasim,[1,*] C Ménard-Moyon,[2] H Boutin,[3] M Fairclough,[3] A Bianco,[2] C Prenant,[3] K Kostarelos[1,*]

[1] Nanomedicine Lab, National Graphene Institute & Faculty of Biology, Medicine and Health, University of Manchester, Manchester, UK; [2] CNRS, Institut de Biologie Moléculaire et Cellulaire, Laboratoire d'Immunopathologie et Chimie Thérapeutique, 67000 Strasbourg, France; [3] Wolfson Molecular Imaging Centre, University of Manchester, Manchester, UK

* dhifaf.jasim@manchester.ac.uk; kostas.kostarelos@manchester.ac.uk

Graphene-based nanomaterials have attracted a great deal of interest recently due to their unique properties for use in many fields including biomedicine [1]. The biodistribution of graphene oxide (GO) materials after intravenous (i.v.) administration in mice has shown major accumulation in spleen, liver and lungs. Extensive urinary excretion has also been reported [2]. In this study, the biodistribution of GO materials with differing structural properties was studied. The GO materials were functionalized with a chelating moiety and labelled with radioisotopes for positron emission tomography (PET) and single photon emission computed tomography (SPECT) whole body dynamic imaging. The effect of GO sheet thickness and lateral size were studied.

The results revealed that 24 h following i.v. administration in mice, the thicker GO sheets accumulated to a greater extent in the liver and spleen compared to the thinner ones. The latter were excreted in urine to a greater extent. GO materials of three distinct lateral size distributions demonstrated uptake in liver and spleen, while more of the largest (>1 μm) sheets accumulated in the lungs. Interestingly, there was extensive urinary excretion of all three materials that seemed to be dependent much less by lateral dimensions, indicating that sheet thickness is a more critical design parameter that can determine the kinetics and excretion of 2D materials. This study provides a systematic understanding of how 2D materials with different structural features can behave *in vivo* and can be valuable in the development of their possible pharmacological applications.

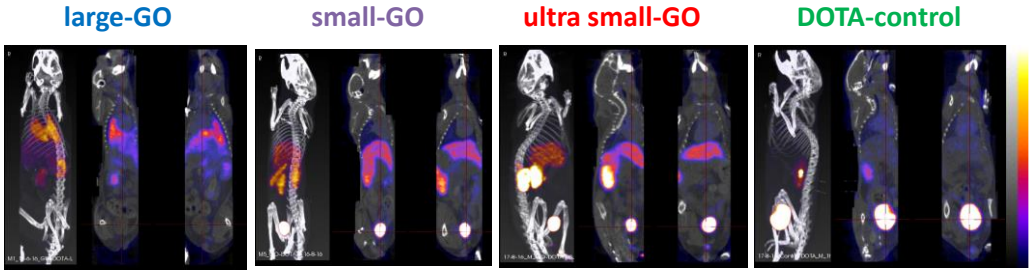

Figure 1. Biodistribution of graphene materials with differing lateral dimensions.

[1] Kostarelos K, Novoselov K. Nature Nanotechnology **2014**, *9*, 744–745.
[2] Jasim DA, Ménard-Moyon C, Begin D, Bianco A, Kostarelos, K. Chemical Science **2015**, *6*, 3952–3964.

Laponite Nanocrystal Radiolabelling: Characterisation of Pptential in Drug Delivery Application Using PET and SPECT Imaging Probe

G Clemente,[1] B Burke,[1] D Roberts,[1] J Domarkas,[1] C Cawthorne,[1,3] C Wilson[2] and S J Archibald[1,*]

[1] PET Research Centre, University of Hull, Hull, United Kingdom; [2] Listerdale Life Sciences, BV Nijmegen, Netherlands; [3] Current: Nuclear Medicine and Molecular Imaging, Department of Imaging and Pathology, and MoSAIC- Molecular Small Animal Imaging Centre, KU Leuven, Leuven, Belgium

* s.j.archibald@hull.ac.uk

Laponite nanocrystals can be used as a drug delivery system offering high loading capacity, selective release, low toxicity and swelling characteristics which can be modified by formulation [1]. In this work we aim demonstrate the use of short-lived radioisotopes to characterise Laponite nanosystems in a robust and sensitive manner. Laponite can be radiolabelled directly using gallium-68 which can then be used to a) understand how formulation and modification affects biodistribution and to b) mimic *in vivo* conditions to model aggregate disruption and subsequent therapeutic release in drug delivery applications, see Figure 1. In addition, encapsulation and release of example cationic bioactive species [^{68}Ga]Ga-transferrin and [^{99m}Tc]Tc-sestamibi is studied to show the potential to use radiolabelled species to understand uptake and release behaviour in drug delivery applications.

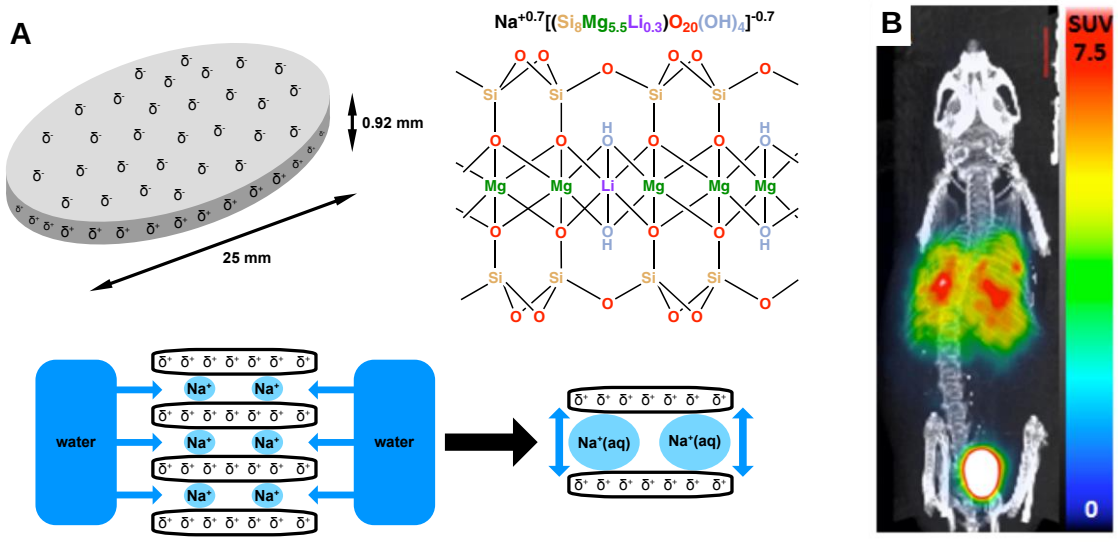

Figure 1. (A) Structure of Laponite nanocrystals, **(B)** *In vivo* mouse image of [^{68}Ga]Ga-laponite fused PET-CT coronal slice image at 80-90 minutes post-injection.

Gallium-68 ions strongly interact with the laponite surface for chelator- free labelling. Radiolabelled proteins and clinical imaging agents can be adsorbed and selectively released. This allows iterative optimisation of drug delivery systems with the nanocrystals.

[1] Li K, Wang S, Wen S, Tang Y, Li J, Shi X, Zhao Q. ACS Appl. Mat. Interf. **2014**, *6 (15)*, 12328–12334.

Non-invasive Whole-body *In Vivo* Imaging of Reporter Gene Engineered Human iPSC-derived Hepatocytes

C Ashmore-Harris,[1,2] S J I Blackford,[2] E Kurtys,[1] G O Fruhwirth,[1,*] and T S Rashid[2,3*]

[1] Department of Imaging Chemistry & Biology, School of Biomedical Engineering & Imaging Sciences, St Thomas' Hospital, King's College London, London, SE1 7EH, UK; [2] Centre for Stem Cells & Regenerative Medicine, School of Basic and Medical Biosciences, Guy's Hospital, King's College London, London, SE1 9RT, UK; [3] Institute of Liver Studies, King's College Hospital NHS Foundation Trust, London, SE5 9RS, UKWolfson Molecular Imaging Centre, University of Manchester, Manchester, UK

* Gilbert.Fruhwirth@kcl.ac.uk; Tamir.rashid@kcl.ac.uk

Primary hepatocyte transplantation (HTx) is well established as a safe cell therapy for patients with liver disease, but wider application is circumvented by poor cell engraftment due to limitations in hepatocyte quality and transplantation strategies. Hepatocyte-like cells (HLCs) derived from human induced pluripotent stem cells (hiPSC) are considered a promising alternative but also require optimisation of transplantation for which whole-body *in vivo* imaging would be highly advantageous to assess engraftment non-invasively and monitor the transplanted cells in the short- and long-term.

Here, we report a lentiviral transduction approach designed to engineer hiPSC-derived HLCs during differentiation. This strategy resulted in the successful production of sodium iodide symporter (NIS)-expressing HLCs that were functionally characterised, injected intraperitoneally into mice, and subsequently imaged using radionuclide tomography.

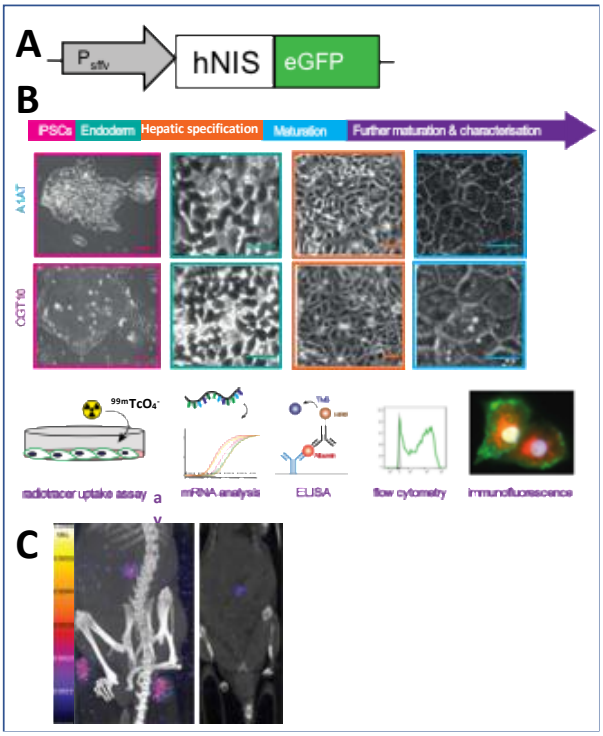

Figure 1. Generation of *in vivo* trackable hNIS-mGFP expressing HLCs. **A)** Reporter gene cassette, hNIS is fused to monomeric GFP under the spleen focus forming virus promoter. **B)** Differentiation pathway of human induced pluripotent stem cells to HLCs, immature HLCs with the expected cuboidal morphology are transduced and subject to further maturation and characterisation relative to untransduced HLCs *in vitro*. **C)** hNIS-mGFP expressing HLCs are pre-labelled with $^{99m}TcO_4^-$, injected intraperitoneally and imaged by SPECT/CT.

Exploring Manganese-52 Porphyrin and Ionophore Complexes as Cell and Liposome Labelling Agents

P J Gawne,[1,*] F Man,[1] J Fonslet,[2] J Bordoloi,[1] P Jimenez-Royo,[3] M Cleveland,[3] M Pereira,[4] P J Blower,[1] N J Long[5] and R T M de Rosales[1]

[1] School of Imaging Sciences & Biomedical Engineering, King's College London, St. Thomas' Hospital, London, SE1 7EH, UK; [2] The Hevesy Lab, Technical University of Denmark, Roskilde, Denmark; [3] GSK Medicines Research Centre, Stevenage, UK; [4] Department of Chemistry, University of Coimbra, Portugal; [5] Department of Chemistry, Imperial College London, London, UK

* peter.gawne@kcl.ac.uk

We recently reported [^{52}Mn]Mn(oxinate)$_2$ ($t_{1/2}$ = 5.6 d) as a cell/liposome labelling agent. The neutral, lipophilic metal complex can passively cross lipid bilayers and release the radionuclide which is trapped by binding to intracellular macromolecules, or intraliposomal drugs. Due to its promising liposome labelling properties [1], we explored the cell-labelling ability of [^{52}Mn]Mn(oxinate)$_2$ in comparison with a stable lipophilic ^{52}Mn porphyrin complex, [^{52}Mn]Mn-PPh1.

[^{52}Mn]Mn(oxinate)$_2$ was used to radiolabel various cell lines, and the cell viability and cellular retention of the radiometal tested, followed by a preliminary comparison with [^{52}Mn]Mn-PPh1. Additionally, the clinically-available nanomedicine DOXIL® was radiolabelled using [^{52}Mn]Mn(oxinate)$_2$ and tracked *in vivo*. B6CBAF1 mice were injected with [^{52}Mn]Mn-DOXIL and imaged over 3 days, with *ex vivo* biodistribution performed 3 d post-injection. [^{52}Mn]Mn(oxinate)$_2$ uptake in MDA-MB 231 cells was higher than with [^{52}Mn]Mn-PPh1 (42% and 12%, respectively). However, cellular retention of ^{52}Mn using oxine was three-fold lower than with the stable ^{52}Mn porphyrin complex (14% and 45%, respectively). PET images of [^{52}Mn]Mn-DOXIL at 1 h and 24 h post-injection showed a distribution consistent with previously imaged liposomal nanomedicines. PET imaging and *ex vivo* biodistribution at 3 d post-injection showed a profile consistent with release of free manganese-52, which may be indicative of drug release (Figure 1).

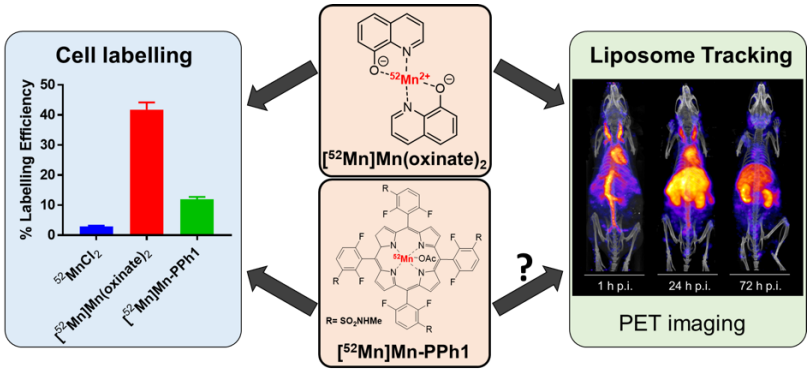

Figure 1. Structure and applications of [^{52}Mn]Mn(oxinate)$_2$ and [^{52}Mn]Mn-PPh1.

Whilst the cell tracking ability of [^{52}Mn]Mn(oxinate)$_2$ is limited by its cellular retention, [^{52}Mn]Mn-PPh1 shows promise as cell labelling agent. We also propose that [^{52}Mn]Mn(oxinate)$_2$ is an effective means to image liposomal drug delivery and release [2].

[1] Edmonds S *et al*. *ACS Nano* **2016**, *10*, 10294−10307.
[2] Gawne P *et al*. *Dalton Trans*. **2018**, *47*, 9283−9293.

P19

The Development of a Bifunctional Contrast Agent for Investigating the Behaviour of Administered Cells

N McCallum,[1,2,*] P Murray,[1] M J Rosseinsky,[2] H Poptani[1]

[1] Department of Cellular and Molecular Physiology, Institute of Translational Medicine, University of Liverpool, Liverpool, UK; [2] Materials Innovation Factory, Department of Chemistry, School of Physical Sciences, University of Liverpool, Liverpool, UK

* N.Mccallum@liverpool.ac.uk

Following systemic administration, most cell therapies die within 24 hours. However, there is evidence to suggest that these cells can still have long-lasting therapeutic effects on the body. It is thought that administered cells act through interactions with the innate immune system. Pre-clinical imaging is necessary for greater understanding of these interactions, as well as for tracking the fate and biodistribution of cells.

MRI and PET-CT are widely used diagnostic tools for clinical and pre-clinical imaging applications. PET-CT is famed for its high sensitivity and its ability to produce a full body image but is limited by its poor spatial resolution. On the other hand, MRI offers fantastic spatial resolution (40-100 μm) but lacks in sensitivity and has poor temporal resolution [1].

We aim to design a bifunctional nanoparticle for cell labelling which can be applied in both MR and PET imaging; combining the advantages that both techniques provide to improve diagnostic performance. Overall, we would achieve high spatial resolution, high sensitivity and morphological and functional analysis in one single agent. This would allow for monitoring whole-body distribution of administered cells with PET and intra-organ distribution of cells with MR. With aid of the positron emitter, cells could be tracked for up to 3 weeks, helping the development of safe and efficacious cell therapies (Figure 1).

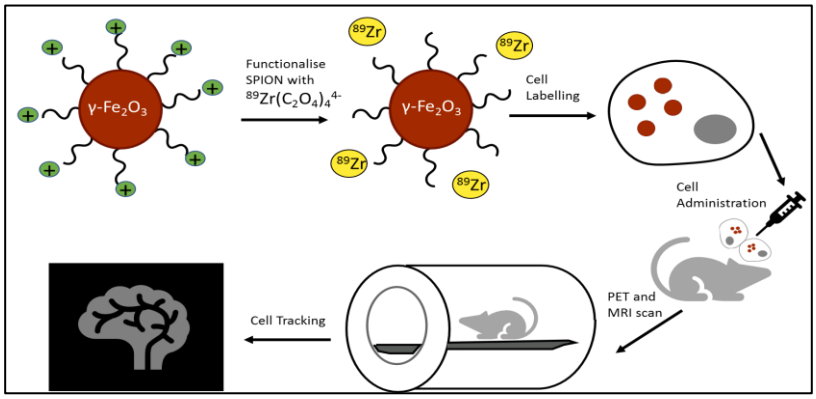

Figure 1. Macrophage tracking using a hybrid PET/MRI nanoparticle. Polycationic SPIONs are first functionalised with an anionic ^{89}Zr complex via electrostatics. Cells are then labelled with the hybrid particle and then administered into the host for non-invasive imaging. A PET scan is performed first due to the decaying isotope followed by an MRI scan.

The hybrid particle will be created through chelate-free, electrostatic coordination of a polycationic SPION (Superparamagnetic Iron Oxide Nanoparticle) and an anionic zirconium complex, $^{89}Zr(C_2O_4)^{4-}$. Initial work in this study will involve the use of cold, non-radioactive zirconium to show that electrostatic coordination is a viable process.

[1] Scarfe L *et al*. NPJ Regenerative Medicine **2017**, *2*, 28.

P20

PET Tracking of ^{89}Zr-labeled Gamma-delta T-cells in a Xenograft Model of Breast Cancer: Liposomal Alendronate Increases Tumour Accumulation

F Man,[1,*] L Lim,[1] A Volpe,[1] A Gabizon,[2] H Shmeeda,[2] B Draper,[3] A C Parente-Pereira,[3] J Maher,[3] P J Blower,[1] G O Fruhwirth[1] and R T M de Rosales[1]

[1] School of Biomedical Engineering and Imaging Sciences, King's College London, St Thomas' Hospital, London, UK; [2] Oncology Institute, Shaare Zedek Medical Center and Hebrew University−School of Medicine, Jerusalem 9103102, Israel; [3] Division of Cancer Studies, King's College London, Guy's Hospital, London, UK

* francis.man@kcl.ac.uk

Introduction: The development of cellular immunotherapies against cancer would greatly benefit from *in vivo* cell tracking solutions. Vγ9Vδ2-T cells are a highly cytotoxic subset of T cells, used successfully in several clinical trials in cancer immunotherapy. Using the recently developed PET tracer [^{89}Zr]Zr(oxinate)$_4$ ($t_{1/2}$ = 78.4 h), human Vγ9Vδ2-T cells were tracked in a xenograft breast cancer model, using PEGylated liposomal alendronate (PLA) to attract Vγ9Vδ2-T cells towards tumour tissue.

Methods: MBA-MB-231.hNIS-GFP breast cancer cells were injected s.c. in female SCID/beige mice. In one group (*n*=9), tumours were sensitised by i.v. administration of PLA (5 mg/kg alendronate) 4 days prior to Vγ9Vδ2-T cell injection. Control groups received placebo liposomes (*n*=4), non-liposomal alendronate (*n*=3) or Vγ9Vδ2-T cells alone (*n*=5). γδ-T cells isolated from peripheral blood were radiolabelled with [^{89}Zr]Zr(oxinate)$_4$ and injected in the tail vein. Animals were imaged by PET/CT and by SPECT/CT (^{99m}Tc). The cancer-cell-killing ability of radiolabelled γδ-T cells was evaluated *in vitro*.

Results: Vγ9Vδ2-T cells radiolabelled with ^{89}Zr showed the expected biodistribution/pharmacokinetics. Radiolabelling did not affect their ability to kill tumour cells *in vitro*. Vγ9Vδ2-T *in vitro* proliferation was only affected by amounts of ^{89}Zr ≥50 mBq/cell. Accumulation of Vγ9Vδ2-T cells in tumours was demonstrated by PET/CT and confirmed by histology. Tumour uptake was higher in the PLA-treated group than in control groups (Vγ9Vδ2-T +PLA: 2.1 ± 0.8 %ID/g versus Vγ9Vδ2-T without PLA: 1.2 ± 0.3 %ID/g, *n*=9-12, p=0.0018) (Figure 1). Radiolabelling of liposomes with ^{111}In demonstrated accumulation of PLA in the tumour.

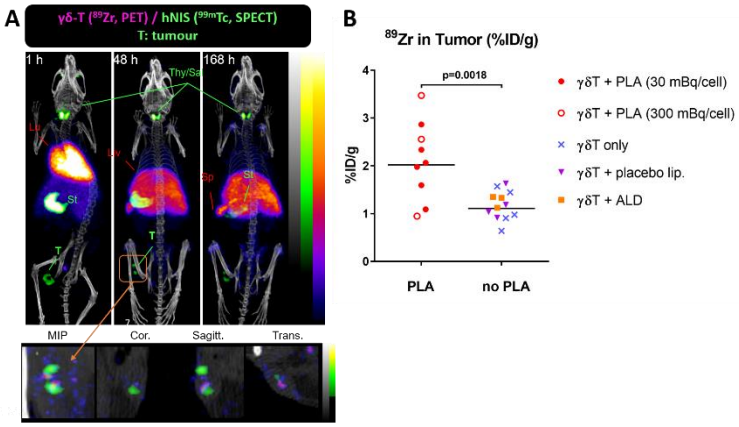

Figure 1. A) PET/SPECT/CT imaging of γδ-T cells (^{89}Zr, red) and tumours (^{99m}Tc, green) on days 0, 2 and 7. **B)** Effect of PLA on the tumour uptake of ^{89}Zr-labelled γδ-T cells, 7 days after injection.

Conclusion: We demonstrated that [^{89}Zr]Zr(oxinate)$_4$ allows efficient delivery of ^{89}Zr to γδ-T cells and sufficient retention for *in vivo* tracking by PET over 7 days. *In vitro* studies showed no adverse effect of radiolabelling on γδ-T cell functionality. Accumulation of γδ-T cells in tumour tissue was enhanced by pretreatment with aminobisphosphonate-loaded liposomes.

Multi-modal Imaging of Stem Cell Delivery to Breast Tumour

M Zaw Thin,[1] R Bofinger,[2] J Connell,[1] S Patrick,[1] H Hailes,[2] A Tabor,[2] M Lythgoe,[1] D Stuckey[1] and T L Kalber[1,*]

[1] University College London, Centre for Advanced Biomedical Imaging, London, UK; [2] University College London, Department of Chemistry, London, UK

* t.kalber@ucl.ac.uk

Stem cells have been used as selective anticancer agents[1]. *In vivo* imaging of stem cells homing to tumours could provide a tool to inform on and improve cell delivery. The main aim of this study was to compare the efficiency of intravenous (IV) and intracardiac (IC) injection routes in delivering stem cells to distal tumours using multi-modal imaging.

Luciferase expressing human adipose-derived stem cells (ADSC) were labelled with iron oxide nanoparticles conjugated to Indium-111, thereby producing cells with tri-modal imaging capabilities (MRI, SPECT and BLI). 150,000 labelled cells were injected either IV or IC into mice bearing 4T1 orthotopic breast tumours and imaged with BLI, SPECT/CT and MRI serially over 3 days. At 1 hour after IC injection, BLI showed the presence of ADSCs in tumours while BLI signals were only detected in tumours at day 3 after IV injection. SPECT data at day 0 after IC injection showed the percentage of ADSCs in tumours was 2-fold higher than IV injection. MRI also showed the presence of SPION labelled cells in tumours after IC injection. The imaging data were further confirmed by histological analysis which showed the engrafted ADSCs in the tumour at day 3 after IC injection (Figure 1).

In summary, these results demonstrate that IC injection is more efficient than IV in delivering cells to tumour tissue. The results from this study also highlight the advantages of combining a genetic BLI reporter with a novel SPECT/MRI nanoparticle to quantitatively assess stem cell delivery to tumours.

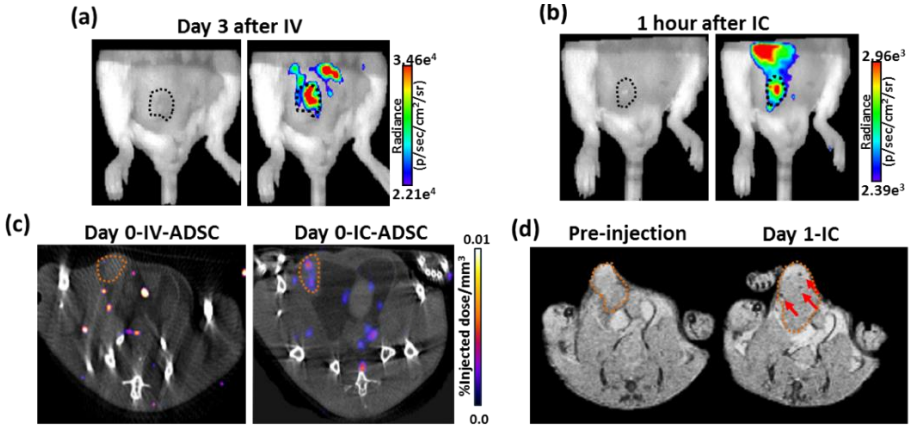

Figure 1. Multi-modal imaging of ^{111}In-DOTA-SPION labelled ADSCs engraftment in tumour following IV or IC injection (a & b) BLI signal in tumour at day 3 after IV injection and 1 hour after IC injection. (c) SPECT/CT images of dual labelled ADSCs at day 0 after IV and IC injection showing the tumour uptake in a mouse with IC injection. (d) T_2^*-weighted MR images of tumour before injection and day 1 after IC injection of dual labelled ADSCs showing the presence of focal hypointensitiy within the tumour.

[1] Sage EK, Kolluri KK, McNulty K, Lourenco Sda S *et al*. Thorax **2014**, *69(7)*, 638–647.

Synthesis and Evaluation of ^{18}F-radiolabeled Anticancer Agents as Tracers of Nucleic Acid Metabolism

A King, A Doepner, D Turton, D Ciobota, G Kramer-Marek, Y-L Cheung and G Smith*

Division of Radiotherapy & Imaging, The Institute of Cancer Research, 123 Old Brompton Road, London, SW7 3RP

* graham.smith@icr.ac.uk

Trifluridine (TFT), floxuridine (FUDR) and 5-fluorouracil (5-FU) are nucleic acid-derived anticancer agents that disrupt DNA synthesis pathways. However, their effectiveness is difficult to predict, due to inter-individual differences in nucleic acid metabolism. The intrinsic presence of fluorine in these compounds creates an opportunity to probe their pharmacokinetic properties using positron emission tomography (PET).

Using an automated ^{18}F-trifluoromethylation procedure, we have developed the first radiosynthesis of [^{18}F]TFT. Furthermore, we present a novel route to non-radioactive TFT from an iodinated nucleoside precursor. Biodistribution and PET-imaging data were obtained using a HCT116 xenograft model in mice, and the tumors were clearly identifiable 60 minutes post-injection. *In vivo* metabolite analysis of selected tissues revealed the presence of parent [^{18}F]TFT, together with known [^{18}F]TFT metabolites.

Our preliminary data also suggest that uracil and uridine precursors that are iodinated at the 5-position can be ^{18}F-fluorinated using [^{18}F]fluoride; subsequently we have used this method to radiolabel [^{18}F]FUDR and 5-[^{18}F]FU analogues. An investigation is underway to elucidate the reaction mechanism.

In a clinical setting, [^{18}F]TFT, [^{18}F]FUDR and 5-[^{18}F]FU may provide useful predictions of treatment response, for the development of personalized treatment plans. We present improved methods to access these radiotracers, enabling more thorough research into their role as PET probes.

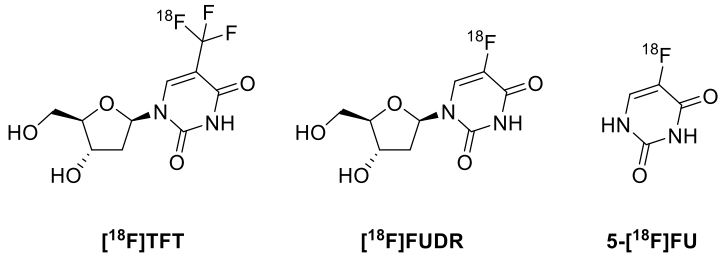

Figure 1. Radiolabelled derivatives of TFT, FUDR and 5-FU.

Synthesis and Evaluation of [^{68}Ga]Ga-THP-Pam: A Hydroxyapatite-targeting PET Agent with Rapid, Facile Radiolabelling

G P Keeling,[1] P J Blower,[1] G Smith,[2] S Y A Terry[1] and R T M de Rosales[1]

[1] Department of Imaging Chemistry and Biology, School of Biomedical Engineering and Imaging Sciences, King's College London, London, UK; [2] Theragnostics Ltd.

* george.keeling@kcl.ac.uk

Bone metastases are found in up to 85% of terminal lung, prostate and breast cancer patients and commonly exhibit high mineral turnover. Calcium minerals can also be present in arterial calcification and due to the lack of these minerals in soft tissues, may be detected with bone-seeking imaging agents. Bisphosphonates (BP) have high affinity for hydroxyapatite and other calcium minerals, particularly in regions of high mineral turnover, such as those found in bone metastases [1]. While several BP tracers exist, there are no PET BP-tracers in clinical use, with [^{18}F]NaF being the current standard for clinical imaging of bone metastases. Here, we report the synthesis, ^{68}Ga radiolabelling and *in vitro* evaluation of a pamidronate conjugate of the gallium chelator (*tris*)hydroxypyridinone (THP) with rapid radiochemistry and high affinity for bone mineral. The conjugate (THP-pamidronate or THP-Pam) can be efficiently radiolabelled with generator-produced gallium-68. [^{68}Ga]Ga-THP-Pam shows efficient binding to hydroxyapatite *in vitro* supporting its future evaluation *in vivo* (Figure 1). Given the excellent kit-based radiolabelling properties of THP, we propose [^{68}Ga]Ga-THP-Pam has a high potential as a bone imaging tool, in particular for facilities and regions lacking access to cyclotron produced [^{18}F]NaF.

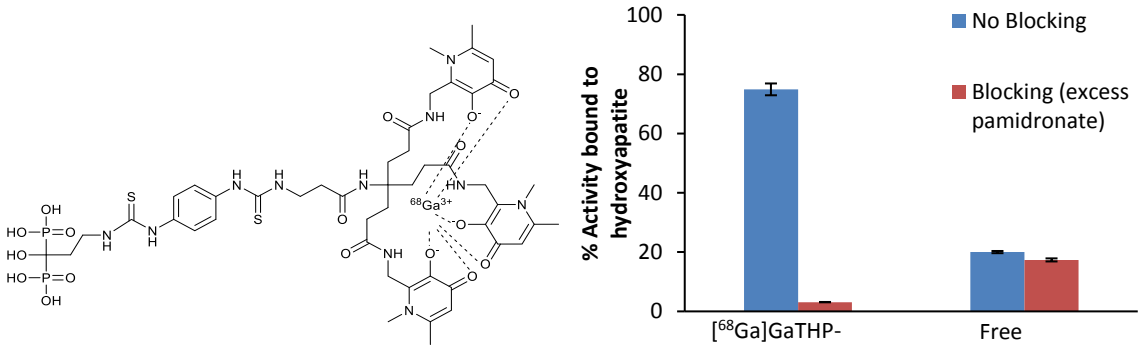

Figure 1. [^{68}Ga]GaTHP-Pam. Left: Structure of [^{68}Ga]GaTHP-pamidronate. Right: Binding of [^{68}Ga]GaTHP-Pam to hydroxyapatite with a neutralised [^{68}Ga]$GaCl_3$ control for comparison.

[1] Cole LE, Vargo-Gogola T, Roeder RK. *Targeted delivery to bone and mineral deposits using bisphosphonate ligands*. Adv. Drug Delivery Rev. **2016**, *99*, 12–27.

^{44}Sc-AAZTA-PSMA: Synthesis, Characterisation and Preclinical Evaluation of PET Tracer

I Hawala,[1] S Ghiani,[2] R Stefania,[1] D Szikra,[3] G Trencsényi,[3] G Nagy,[3] A Maiocchi[2] and S Aime[1]

[1] Dipartimento di Biotecnologie Molecolari e Scienze per la salute, Centro di Imaging Molecolare, Università degli Studi di Torino, Via Nizza 52, 10126, Torino (TO), Italy; [2] Bracco Imaging Spa, Bracco Research Centre, Via Ribes 5,10010, Colleretto Giacosa (TO), Italy; [3] Scanomed Ltd. Nagyerdei krt. 98, 4032 Debrecen, Hungary

* silvio.aime@unito.it

The standard diagnostic strategy of prostate cancer relies on the determination of the Prostate-Specific Antigen (PSA) in the blood, rectal exploration screening and biopsies. Recently, scandium 44 has received much attention as a potential radionuclide with favourable characteristics for PET imaging applications.

A polyaminopolycarboxylate heptadentate ligand based on a 1,4-diazepine scaffold (AAZTA) has been thoroughly studied as chelator for Gd^{3+} ions for MRI applications [1]. The excellent results of the equilibrium, kinetic, and labelling studies led to a preliminary assessment of the *in vitro* and *in vivo* behaviour of ^{44}Sc(AAZTA)$^{-}$ and two derivatives (^{44}Sc(CNAAZTA-BSA) and ^{44}Sc(CNAAZTA-c(RGDfK) by assuming that the physicochemical properties of Sc(AAZTA) are maintained in his bioconjugates [2]. Herein we report our preclinical results of a ^{44}Sc-labeled PSMA binding motif, based peptide for *in vivo* PET imaging of PSMA expression in a preclinical cancer model. The bioconjugate has been synthesized combining solid phase peptide synthesis (SPPS) and solution chemistry and the desired product has been obtained with good chemical yield and high purity. Subsequently, the radiolabelling with ^{44}Sc has been performed producing the radionuclide from natural calcium target in cyclotron and good radiochemical yields under mild condition (pH 3.8, 298 K) has been achieved.

In conclusion, this work has demonstrated the suitability of AAZTA PSMA 617 conjugate for the complexation with ^{44}Sc and PET image acquisition for PCa diagnosis.

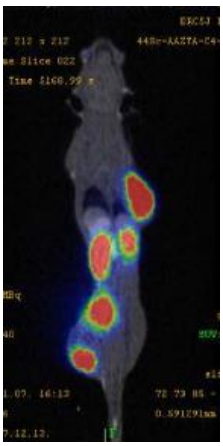

Figure 1. Example of *in vivo* uptake of ^{44}Sc-AAZTA-PSMA on LNCaP tumour-bearing mice (PET-MRI image; 0-90 min dynamic scan).

[1] Manzoni *et al.* ChemMedChem **2012**, *7*, 1084–1093.
[2] Nagy *et al.* Angew. Chem. Int. Ed. **2017**, *56*, 1–6.

Development and Evaluation of a ^{18}F-Radiolabeled Monocyclam Derivative for Imaging CXCR4 Expression

M Braga, D Brickute, E Stevens, S Trousil and Eric O Aboagye*

Cancer Imaging Centre, Department of Surgery and Cancer, Imperial College London

* eric.aboagye@imperial.ac.uk

C-X-C chemokine receptor type 4 (CXCR4) is a G-protein coupled receptor that upon binding to its ligand, CXCL12, elicits biological activities that result in tumor progression; thus, it has been the subject of significant investigation for detection and treatment of disease. Previous methodology for detection of CXCR4 utilized predominantly peptidic radioprobes or small molecules labeled with long-lived radiometals. We report here the development of a ^{18}F-radiolabeled cyclam-based small molecule radioprobe, [^{18}F]MCFB, for imaging CXCR4 expression.

The affinity of [^{18}F]MCFB for CXCR4 was similar to that of AMD3465 (89.8 and 111.0 nM, respectively). *In vitro* binding assays show that the tracer depicted differential CXCR4 expression, which was blocked in the presence of AMD3465, demonstrating specificity of [^{18}F]MCFB. PET imaging studies showed distinct uptake of radioprobe in lymphoma and breast cancer xenografts (Figure 1). High liver and kidney uptake were seen with [^{18}F]MCFB leading us to further examine the basis of its pharmacokinetics. Substrate competition following the intravenous injection of metformin led to a marked decrease in urinary excretion of [^{18}F]MCFB, with moderate changes observed in other organs, including the liver. Our results suggest involvement of organic cation transporters (OCTs) in renal elimination of the tracer but not liver uptake. In aggregate, the ^{18}F radiolabeled monocyclam, [^{18}F]MCFB, has potential to detect tumor CXCR4 in non-hepatic tissue.

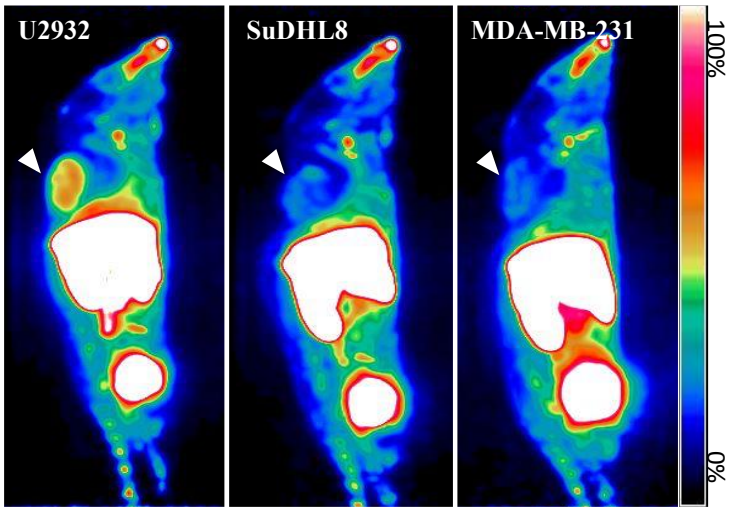

Figure 1. Representative orthogonal [^{18}F]MCFB-PET images derived from summed 60 min dynamic scans in U2932, SuDHL8 and MDA-MB-231 xenograft-bearing mice.

Positron Emission Tomography Imaging of CXCR4 Using ^{18}F AND ^{68}Ga Radiolabelled Configurationally Restricted Tetraazamacrocyclic Antagonists

N Perujo Holland,[1] B P Burke,[1] I Renard,[1] R E Lee,[1] C S Miranda,[1] J Domarkas,[1] T D'Huys,[2] D Schols,[2] C Cawthorne[1,3] and S J Archibald[1,*]

[1] School of Life Sciences, Chemistry Department and Positron Emission Tomography Research Centre, University of Hull, Cottingham Road, Hull HU6 7RX, UK; [2] Rega Institute for Medical Research, KU, Leuven, Belgium; [3] Current: Nuclear Medicine and Molecular Imaging, Department of Imaging and Pathology, and MoSAIC- Molecular Small Animal Imaging Centre, KU Leuven, Leuven, Belgium

* s.j.archibald@hull.ac.uk

CXCR4 and its ligand CXCL12 have a crucial role in tumour growth, metastasis, angiogenesis and the cancer cell-microenvironment interaction. The non-invasive imaging of CXCR4 would enable the identification of potential candidates for CXCR4 targeting therapies and drugs, along with improved disease staging and treatment planning.[1] Based on the structure of the clinically approved CXCR4 antagonist, AMD3100, configurationally restricted tetraazamacrocyclic metal complexed analogues have been synthesised in our group. Metal complex formation and configurational restriction using an ethylene bridge optimises binding to receptor aspartate residues and results in an increase in affinity and receptor residence time compared to AMD3100.[2] Positron emission tomography (PET) radiopharmaceuticals can be formed by modifying macrocyclic derivatives to incorporate ^{18}F and ^{68}Ga radionuclides, which are more routinely available clinically. The uptake of such tracers can be blocked by another CXCR4 antagonist showing that binding of the tracer is specific and that the complex is stable *in vivo* (Figure 1).

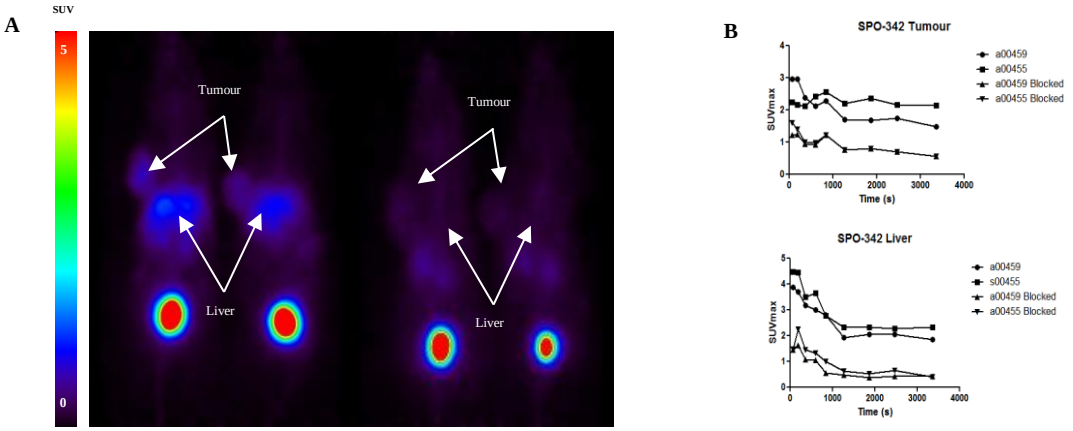

Figure 1. A) PET imaging of CXCR4 over-expressing tumour bearing animals injected with 1.6 MBq of tracer (left) and 2.2 MBq of tracer following injection of a blocking agent (right). **B)** SUV_{max} data of unblocked and blocked liver and tumour signals.

[1] Amor-Coarasa A, Kelly J, Ponnala S *et al*. Nucl. Med. Biol. **2018**, *60*, 37–44.
[2] Maples RD, Cain AN, Burke BP *et al*. Chem. Eur. J. **2016**, *22*, 12916–12930.

P27

Synthesis, *In Vitro* and *In Vivo* Validation of Configurationally Restricted Azamacrocyclic CXCR4- and ACKR3-specific Binding Agents for PET Imaging and Therapeutic Applications in Cancer

I Renard,[1] K L Nicholson,[1] T D'Huys,[2] B P Burke,[1] J Domarkas,[1] T J Hubin,[3] D Schols,[2] C Cawthorne[1,4] and S J Archibald[1,*]

[1] Department of Chemistry and Positron Emission Tomography Research Centre, University of Hull, UK; [2] Rega Institute for Medical Research, KU, Leuven, Belgium; [3] Department of Chemistry and Physics, Southwestern Oklahoma State University, USA; [4] Nuclear Medicine and Molecular Imaging, Department of Imaging and Pathology, and MoSAIC- Molecular Small Animal Imaging Centre, KU Leuven, Leuven, Belgium

* s.j.archibald@hull.ac.uk

Chemokine receptors are implicated in various diseases, such as asthma, rheumatoid arthritis, AIDS and cancer, hence they represent interesting targets for the development of antagonists and imaging agents. Among these receptors, CXCR4 and ACKR3 (CXCR7) have been shown to be over-expressed in different types of cancers [1] and have been the focus of extensive research. Successfully targeting and imaging these receptors could allow earlier diagnosis of some cancers, inform treatment selection and lead to better outcome for the patient.

Our group has previously synthesized and characterised configurationally restricted azamacrocyclic metal complexes that bind to CXCR4 and demonstrated their antagonistic properties *in vitro* [2]. We have produced a library of these macrocyclic compounds (and their copper(II), zinc(II) and nickel(II) complexes) specific to CXCR4 with affinities up to 4 nM. We then extended our work to the *in vitro* validation of a related set of novel compounds that bind to ACKR3, as well as CXCR4. The SAR are currently under investigation with preliminary results showing affinity for ACKR3 below 100 nM. Some of these derivatives were also successfully radiolabelled with ^{64}Cu and showed high tumour accumulation in animals implanted with CXCR4-overexpressing xenografts. A wider range of compounds have been characterised through *in vivo* blocking studies of the CXCR4-specific PET tracer [^{68}Ga]Pentixafor with doses as low as 4 mg/kg.

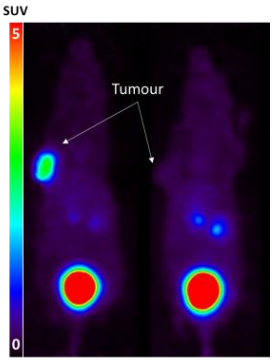

Figure 1. Blocking by SJA372, a novel high affinity CXCR4 antagonist. Coronal maximum intensity projections (46-66 min) of tumour-bearing animals injected with [^{68}Ga]Pentixafor (left) and injection of the tracer following injection of a blocking dose of SJA372 (right).

[1] Wani NA *et al*. Breast Cancer Research **2014**, *16*, R54.
[2] Kahn A *et al*. J. Am. Chem. Soc. **2009**, *131*, 3416.

cCPE Peptides for SPECT Imaging of Claudin-4 Overexpression in Pancreatic Cancer

J Baguña Torres,[1] M Mosley,[1] S Koustoulidou,[1] S Hopkins,[1] S Knapp,[2] A Chaikuad,[2] V Kersemans[1] and B Cornelissen[1]

[1] Cancer Research UK and Medical Research Council Oxford Institute for Radiation Oncology, University of Oxford, UK; [2] Structural Genomics, University of Oxford, ORCRB, Old Road Campus, Oxford, UK

Background: Overexpression of tight junction protein claudin-4 has been detected in primary and metastatic pancreatic cancer tissue and is associated with better prognosis in patients [1,2]. Non-invasive measurement of claudin-4 expression by imaging methods could provide a means for accelerating disease detection and stratifying patients into risk groups. A GST-tagged version of the C-terminus of *Clostridium perfringens* enterotoxin (cCPE), a natural ligand for claudin-4, was previously used to delineate claudin-4 overexpression by SPECT but showed modest binding affinity and slow blood clearance *in vivo* [3].

Methods: Based on the crystal structure of cCPE, a series of smaller-sized $cCPE_{194-319}$ mutants (S313A, H194, S307A+N309A+S313A, D284A and L254F+K257D) with putatively improved binding affinity and specificity for claudin-4 were generated by site-directed mutagenesis[4]. All peptides were conjugated site-specifically on a C-terminal cysteine using maleimide-DTPA to allow radiolabelling with ^{111}In. The binding affinity of all radioconjugates was evaluated in claudin-4-overexpressing Panc-1 cells and HT1080 negative controls. *In vivo* SPECT imaging was performed using BALB/c nude mice bearing Panc-1 or HT1080 tumour xenografts.

Results: Uptake of all cCPE-based radioconjugates was significantly higher in Panc-1 cells compared to HT1080 negative controls (Figure 1).

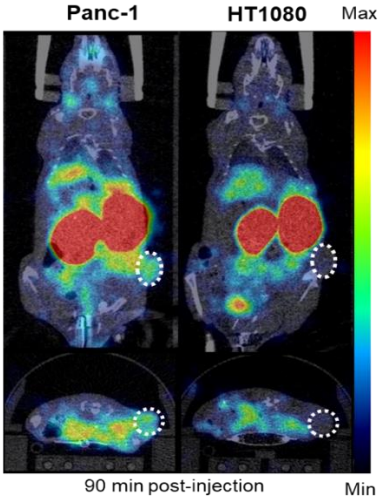

Figure 1. Representative SPECT/CT images of mice carrying Panc-1 (claudin-4-positive) and HT1080 (claudin-4-negative) xenografts (white circles) 90 min after intravenous administration of ^{111}In-radiolabelled cCPE mutant (L254F+K257D).

All peptides showed a marked improvement in affinity for claudin-4 *in vitro* when compared to wildtype ^{111}In-cCPE.GST (K_d values of 2.2±0.8, 3±0.1, 5.5±1.1, 8.3±2.8 and 9.4±0.5 vs. 14.8±1.3 nM). Blood clearance of all cCPE probes, as measured by SPECT,

was considerably faster when compared to that of ^{111}In-cCPE.GST ($t_{1/2}$<2 min). All radiopeptides showed significantly higher accumulation in Panc-1 xenografts than HT1080 tumours at 90 min post-injection (2.7±0.7, 2.3±0.9, 2±0.4, 2±0.2 and 6.3±0.6 vs. 0.4±0.1, 0.5±0.1, 0.3±0.1, 0.7±0.1 and 0.7±0.1 %ID/g; P<0.01, P<0.01, P<0.05, P<0.05 and P<0.001 respectively).

Conclusion: These optimised cCPE-based SPECT imaging agents show great promise as claudin-4-targeting vectors for *in vivo* imaging of claudin-4 overexpression in pancreatic cancer.

[1] Nichols *et al*. Am. J. Clin. Pathol. **2004**, *121*, 226–230.
[2] Tsutsumi *et al*. Ann. Surg. Oncol. **2012**, *19*, 491–499.
[3] Mosley *et al*. J. Nucl. Med. **2015**, *56*, 745–751.
[4] Van Itallie *et al*. J. Biol. Chem. **2008**, *283(1)*, 268–274.

Prediction of Chemotherapy Resistance in Ovarian Cancer with [^{18}F]FSPG PET

H Greenwood,[1] P McCormick,[1] M Glaser,[2] T Gendron,[2] R Pereira,[1] K Sander,[2] N Koglin,[3] M F Lythgoe,[1] E Årstad[2] and T H Witney[1,*]

[1] Centre for Advanced Biomedical Imaging, University College London, London, UK; [2] Institute of Nuclear Medicine and Department of Chemistry, University College London, London, UK; [3] Piramal Imaging GmbH, Berlin, Germany

* t.witney@ucl.ac.uk

Drug-resistance is a major obstacle preventing effective treatment in high grade serous ovarian cancer (HGSOC). Currently, there is no satisfactory way to identify patients that are refractive to the standard of care [1,2]. The positron emission tomography (PET) radiotracer (4*S*)-4-(3-[^{18}F]fluoropropyl)-L-glutamate ([^{18}F]FSPG) is a substrate for the glutamate/cystine antiporter system xc-, which plays a central role in maintaining antioxidant homeostasis. We propose [^{18}F]FSPG PET imaging as a non-invasive method to measure upregulated antioxidant pathways present in drug-resistant tumours, allowing the prediction of drug resistance in HGSOC. Using matched drug-sensitive and drug-resistant human ovarian cancer cell lines (Figure 1A), a significant decrease in intracellular reactive oxygen species (ROS; Figure 1B) and increase in intracellular glutathione (GSH; Figure 1C) corresponded to a reduction in [^{18}F]FSPG cell retention in drug-resistant *vs* drug-sensitive cell lines (Figure 1D). The potential mechanism driving changes in [^{18}F]FSPG retention was investigated, with a dramatic 94% decrease in the intracellular concentration of cystine measured in the chemotherapy resistant cell lines *vs* sensitive. We reasoned this was the result of an increased flux of cystine into de novo GSH biosynthesis.

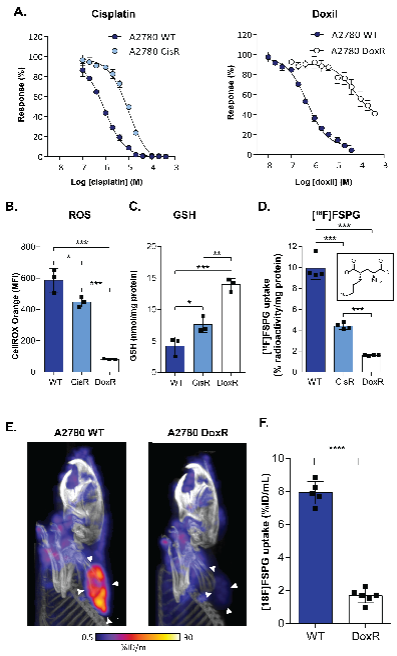

Figure 1. [^{18}F]FSPG uptake is reduced in drug-resistant ovarian cancer. **A)** Cell viability in A2780 cells after cisplatin or doxil treatment. **B)** Intracellular ROS and **C)** GSH in A2780 cells. **D)** The effect of drug sensitivity on [^{18}F]FSPG uptake (insert: [^{18}F]FSPG chemical structure). **E)** PET/CT maximum intensity projection images of WT and DoxR tumour-bearing mice 40-60 min p.i. White arrows indicates the tumour. **F)** Quantification of [^{18}F]FSPG tumour uptake (n = 5, WT; n = 6, DoxR).

Using static PET imaging (Figure 1E), [^{18}F]FSPG tumour uptake was reduced 80% in chemotherapy resistant tumour-bearing mice compared to chemotherapy-sensitive (Figure 1F), corresponding to a 21-fold increase in oxidised to reduced GSH. These results confirm the sensitivity of [^{18}F]FSPG to upregulated antioxidant pathways in drug-resistant A2780 tumours. [^{18}F]FSPG may therefore enable the identification of HGSOC patients that are refractory to standard-of-care, allowing the transferal of drug-resistant patients to alternative therapies, thereby improving the outcome of this disease.

[1] Ovarian cancer statistics. Cancer Research UK **2012**.
[2] Bowtell *et al*. Nat. Rev. Cancer **2015**, *15*, 668–679.

Synthesis and Biological Evaluation of 4-((Diethylamino)methyl) benzaldehyde-based Substrates for the Detection of Aldehyde Dehydrogenase 1A1 Activity

R Pereira,[1,3] T Genderon,[2,3] C Sanghera,[1] H E Greenwood,[1] J Newcombe,[3,4] P N McCormick,[1] K Sander,[2,3] M Topf,[4] E Årstad,[2,3] and T H Witney[1,*]

[1] Centre for Advanced Biomedical Imaging, University College London, 72 Huntley Street, London WC1E 6DD, UK; [2] Institute of Nuclear Medicine, University College London, 235 Euston Road, London NW1 2BU, UK; [3] Department of Chemistry, University College London, 20 Gordon Street, London WC1H 0AJ, UK; [4] Department of Biological Sciences, Birkbeck, University of London, Malet Street, London, WC1E 7HX, UK

* t.witney@ucl.ac.uk

Aldehyde dehydrogenases (ALDHs) catalyse the oxidation of aldehydes to carboxylic acids [1], with elevated ALDH1A1 expression in human cancers linked to metastases and poor overall survival [2]. Despite ALDH1A1 being a poor prognostic factor, the non-invasive assessment of ALDH activity is challenging. Previous attempts to develop ALDH1A1-specific radiotracers have so far failed due to poor cellular retention of the tracer [3]. Here, we report the synthesis and biological evaluation of an ^{18}F-fluorinated aldehyde-based probe for the detection of ALDH1A1 activity in tumour cells.

Stemming from a focused medicinal chemistry approach *N*-ethyl-6-(fluoro)-*N*-(4-formyl benzyl) nicotinamide, **4b** (Figure 1A), was shown to have good ALDH1A1 selectivity and enzyme affinity, and consequently was taken forward for radiolabelling and evaluation in tumour cells. [^{18}F]**4b** was synthesised from **7** in 39 ± 5% radiochemical yield (Figure 1B).

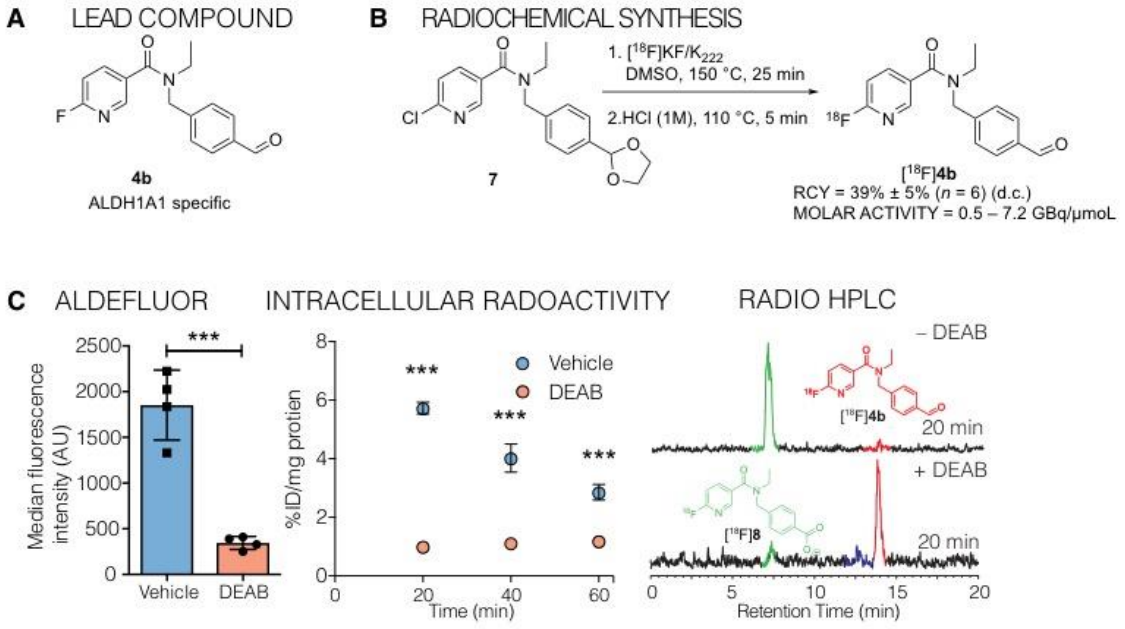

Figure 1. Evaluation of a novel ALDH1A1-specific radiotracer. **A)** Lead compound from structure optimization studies. **B)** Radiochemical synthesis of [^{18}F]**4b**. **C)** ALDH activity in HCT116 mut cells, as measured by ALDH-mediated trapping of Aldefluor and detection by flow cytometry (left). ALDH activity determined by [^{18}F]**4b** trapping via oxidation to the carboxylate [^{18}F]**8** (centre). Radio-HPLC suggests the uptake is specific as there is no oxidation in the presence of the ALDH1A1 inhibitor, DEAB (right).

In ALDH1A1-expressing HCT116 Kras$^{G13D/-}$ mutant human colorectal cancer cells, incubation of [^{18}F]**4b** showed rapid cell uptake and retention, reaching 5.7 ± 0.2% radioactivity/mg protein at 20 min (n = 3). Treatment of cells with DEAB – an ALDH1A1 inhibitor – resulted in an 83% reduction in cell-radioactivity to 1.0 ± 0.1% radioactivity/mg protein (P = 0.0005; n = 3), indicating ALDH-specific intracellular trapping of [^{18}F]**4b** as its carboxylate [^{18}F]**8** which was confirmed *via* Radio-HPLC (Figure 1C). DEAB treatment of the cells reduced the production of [^{18}F]**8** to 10% of control lysates (Figure 1C).

Together, this data shows [^{18}F]**4b** to be a specific and sensitive marker of ALDH activity in HCT116 Kras$^{G13D/-}$ tumour cells. *In vivo* positron emission tomography imaging in balb/c mice revealed high uptake of [^{18}F]**4b** in the lungs and liver, with radioactivity cleared through the urinary tract; however, rapid oxidation limited tissue uptake. Future strategies will focus on the development of ALDH1A1 radiotracers with improved *in vivo* stability.

[1] Singh S *et al*. Free Radic. Biol. Med. **2013**, *56*, 89–101.
[2] Raha D *et al*. Cancer Res. **2014**, *74*, 3579–3590.
[3] Vaidyanathan G *et al*. Nucl. Med. Biol. **2009**, *36 (8)*, 919–929.

PET Imaging of PARP Expression Using [^{18}F]Olaparib

T C Wilson,[1,#] M-A Xavier,[2,#] J Knight,[2] S Verhoog,[1] J Baguna-Torres,[2] M Mosley,[2] S L Hopkins,[2] S Wallington,[2] D Allen,[2] V Kersemans,[2] R Hueting,[2] S Smart,[2] V Gouverneur[1,*] and Bart Cornelissen[2,*]

[1] Department of Chemistry, University of Oxford, Oxford, UK; [2] CRUK/MRC Oxford Institute for Radiation Oncology, Department of Oncology, University of Oxford, Oxford, UK

* veronique.gouverneur@chem.ox.ac.uk; bart.cornelissen@oncology.ox.ac.uk

We developed a radiolabelled structural equivalent of the FDA-approved PARP inhibitor olaparib, substituting fluoride for ^{18}F to allow PET imaging (Figure 1).

In vitro, [^{18}F]olaparib was taken up differently among PDAC cell lines: PSN1 > MiaPaCa-2 > Capan-1. PARP1 expression levels determined by Western blot analysis were in line with cell uptake of [^{18}F]olaparib. Cell-associated uptake of [^{18}F]olaparib in all three cell lines could be blocked by more than 99% with addition of an excess of cold, unlabelled PARP inhibitor. [^{18}F]olaparib uptake in all cells was increased 48h after receiving gamma-irradiation (10 Gy).

In vivo, dynamic PET imaging of wild type naïve mice injected with 3 MBq of [^{18}F]olaparib revealed a weighted blood half-life of 19.3 min. Tumour uptake of [^{18}F]olaparib in PSN1 mouse xenografts were consistent with expression of PARP1 determined by immunohistochemistry, in vitro uptake and immunoblotting analysis. *Ex-vivo* biodistribution analysis showed uptake of 3.16 ± 0.36%ID/g of [^{18}F]olaparib in PSN1 tumours. Two hours after irradiation of PSN1 tumour (10 Gy), uptake of [18F]olaparib increased by 70% (P=0.025). Western blot analysis demonstrated that PARP1 expression in PSN1 tumour increased in the irradiated group. Tumour uptake was significantly decreased after co-administration of an excess of cold, unlabelled olaparib (1.20 ± 0.17%ID/g; P = 0.0016). Taken together, we demonstrated that [^{18}F]olaparib can be used for quantifying olaparib tumour accumulation, *in vitro* and *in vivo*.

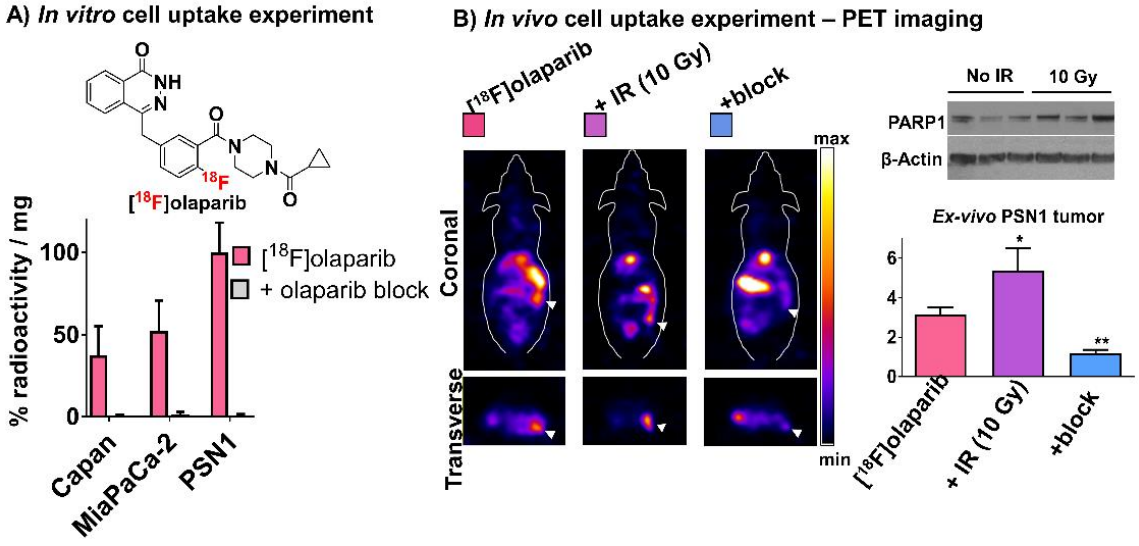

Figure 1. [^{18}F]Olaparib uptake in a pancreatic ductal adenocarcinoma cell lines.

Radiolabelled Bacillus Anthracis Toxin-based Probes for Molecular Imaging of MMP Activity in Tumour Models

M-A Xavier,[1] J Baguna-Torres,[1] S Hopkins,[1] S Liu,[2] T Bugge,[2] S Leppla,[2] and B Cornelissen[1,*]

[1] CRUK and MRC - Oxford Institute for Radiation Oncology, University of Oxford, UK; [2] National Institutes of Health, Bethesda, Maryland, USA

* bart.cornelissen@oncology.ox.ac.uk

Increased activity of matrix metalloproteinases (MMP) types 2, 9 and 14 is associated with poor prognosis and metastasis in different solid tumour types. The protective antigen-binding domain (PAWT) of the binary anthrax lethal toxin (LT) was reengineered [1] to enable pore formation in cell membranes only when cleaved by MMPs (PAL1), instead of the furin enzyme (PAWT). The anthrax lethal factor (LF) is then able to translocate through these pores into the cytosol of tumour cells. The current work describes the use of radiolabelled LF^{E687A} (LF with a defective catalytic domain) associated with PAL1 to image MMP activity non-invasively in preclinical tumour models by SPECT.

After radiolabelling LF^{E687A} with [^{111}In], the ability of PAL1 to deliver [^{111}In]LF^{E687A} into MDA-MB-231 cells was demonstrated by uptake assays which correlated with protein expression levels of MMP14 and LT native receptor CMG2. Activation of PAL1 was effectively blocked by GM6001 (a broad spectrum MMP inhibitor) in MDA-MB-231 cells, further suggesting MMP selectivity. Evaluation of the *in vivo* biodistribution of [^{111}In]LF^{E687A} in the presence of PAL1 was performed by SPECT/CT in naive mice and MMP14-expressing MDA-MB-231 tumour-bearing mice. MDA-MB-231 tumour bearing xenografts demonstrated that co-administration of PAL1/[^{111}In]LF^{E687A} leads to tumour uptake of 7.19±0.43 % ID/g, significantly higher than control groups (P=0.0013) which consisted of [^{111}In]LF^{E687A} alone or an excess of unlabelled [^{111}In]LF^{E687A} prior to PAL1/[^{111}In]LF^{E687A} injections (Figure 1).

Taken together, our results indicate that radiolabelled forms of mutated anthrax lethal toxin hold promise for non-invasive imaging of MMP activity in cancer patients.

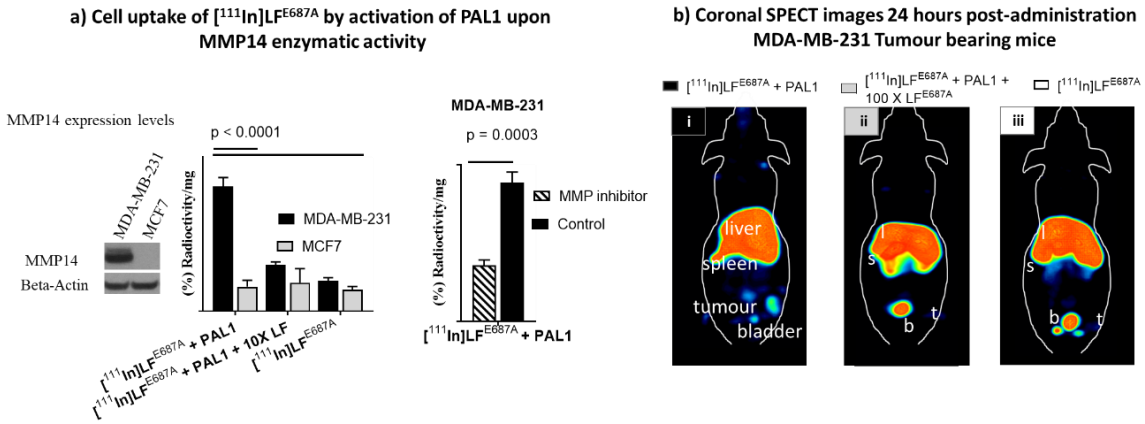

Figure 1. Tumour delivery of [^{111}In]LFE687A by PAL1 pores upon MMP activation. **A)** *in vitro* and **b)** *in vivo*.

[1] Liu S *et al*. *Tumor Cell-selective Cytotoxicity of Matrix Metalloproteinase-activated Anthrax Toxin*. Cancer Research **2000**, *60 (21)*, 6061–6067.

^{18}F-mFBG Monitors Changes in NET-1 Expression with AZD2014 Treatment

S Turnock,[1] D R Turton,[1] D M Ciobota,[1] O Yogev,[1] L Chesler,[1] T Wilson,[2] G Smith,[1] V Gouverneur[2] and G Kramer-Marek[1]

[1] The Institute of Cancer Research, London, 123 Old Brompton Road, London, SW7 3RP, UK; [2] University of Oxford, Mansfield Road, Oxford, OX1 3TA, UK

The radio-labelled norepinephrine analogue ^{18}F-mFBG (*meta*-fluorobenzylguanidine) has been recently developed as an alternative to the mainstay imaging tracer ^{123}I-mIBG (*meta*-iodobenzylguanadine) in order to improve diagnostic imaging of norepinephrine transporter 1 (NET-1) expressing tumours, such as neuroblastoma (NB), using Positron Emission Tomography (PET) [1]. We hypothesise that imaging the dynamics of NET-1 expression with PET will guide novel combinatorial approaches that will improve outcomes of ^{131}I-mIBG radiotherapy for high-risk NB patients.

The specificity of ^{18}F-mFBG tracer uptake in NB cells lines with different NET-1 protein expression was evaluated *in vitro;* and tracer pharmacokinetics studied *in vivo* using Kelly and SK-N-BE(2)C xenografts followed by *ex vivo* tumour investigation. Changes in NET-1 expression level and mTOR function post-treatment with dual mTORC1/2 inhibitor AZD2014 were evaluated by Western blot (WB) and the radiotracer uptake assay *in vitro.*

In vivo, mice were randomised between vehicle and AZD2014 (20 or 25 mg/kg/day), and imaged with ^{18}F-mFBG (1-4 hr post injection (p.i.)). *Ex vivo* biodistribution of major organs, WB analysis of tumour lysates, autoradiography and IHC of tumour sections were correlated with PET data.

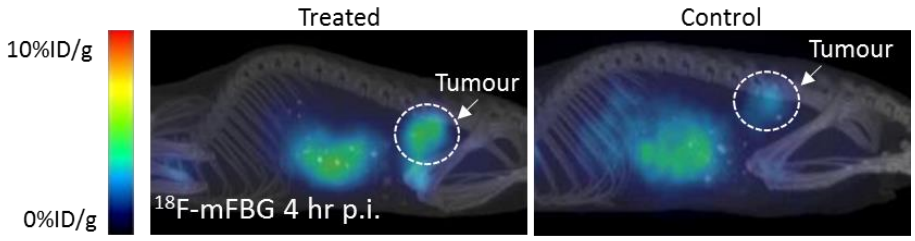

Figure 1. PET/CT images of SK-N-BE(2)C xenografts (4 hr p.i.) treated for 3 days with 20 mg/kg/day AZD2014 (Left), compared to vehicle alone (Right).

^{18}F-mFBG uptake correlated with NET-1 protein expression in NB cell lines. PET imaging allowed for accurate delineation of NET-1 positive SK-N-BE(2)C xenografts. Following AZD2014 treatment, there was a concentration-dependent increase in NET-1 protein expression, and subsequent radiotracer uptake, in both Kelly and SK-N-BE(2)C cells *in vitro*. PET quantification analysis of SK-N-BE(2)C xenografts showed an increase in ^{18}F-mFBG tracer uptake following 3 days treatment with AZD2014, paralleled by biodistribution and an increase in tumour NET-1 protein expression confirmed by WB.

^{18}F-mFBG can quantitatively assess different levels of NET-1 *in vitro* and *in vivo*, and therefore could provide guidance for ^{131}I-mIBG dose optimisation and monitoring drug responses that improve NET-1-mediated uptake of ^{131}I-mIBG.

[1] Pandit-Taskar N *et al*. *Biodistribution and dosimetry of ^{18}F-Meta Fluorobenzylguanadine (mFBG)*. J. Nucl. Med. **2018**, *59*, 147–153.

Biodistribution of the Gallium Anti-cancer Drug KP46 in a Mouse Melanoma Model Using ^{68}Ga

J E Blower, J J Bartnicka, C Imberti and P J Blower*

School of Biomedical Engineering and Imaging Sciences, King's College London, London, UK

* philip.blower@kcl.ac.uk

Gallium compounds, such as gallium nitrate, have been investigated as anti-cancer drugs but their mechanism and trafficking are obscure. Gallium tris(oxinate) (known as KP46) is cytotoxic against several human cancer cell lines [1], and has been assessed in Phase 1 trials for treating renal carcinoma [2]. Here, we performed the first PET imaging with ^{68}Ga-tris(oxinate) to determine its fate *in vivo*. Uptake of ^{68}Ga-tris(oxinate) and ^{68}Ga-acetate was assessed in A375 melanoma cells. Serum speciation was investigated by incubating ^{68}Ga-tris(oxinate) or ^{68}Ga-acetate with human serum and fractionating using PD10 size-exclusion chromatography. Dynamic PET-imaging and *ex vivo* biodistribution (4 h p.i.) of the tracers was performed on A375 xenografted mice.

Intracellular/extracellular radioactivity concentration ratios in cells incubated with ^{68}Ga-tris(oxinate) reached twice (101.8 ± 31.7) those in cells incubated with ^{68}Ga-acetate (43.1 ± 18.7). In serum speciation, ~70% of the eluted ^{68}Ga-acetate activity eluted in early fractions corresponding to apo-transferrin, in a bicarbonate-dependent manner, whereas 100% of the eluted ^{68}Ga-tris(oxinate) activity was bound to protein, independent of bicarbonate, probably via hydrophobic interaction. *In vivo*, ^{68}Ga-tris(oxinate) exhibited lower accumulation in tumours (2.5 ± 0.9 %ID/g, tumour:blood ratio 0.47) than ^{68}Ga-acetate (5.8 ± 2.4 %ID/g). Notably, higher myocardial uptake of ^{68}Ga-tris(oxinate) (16.9 ± 2.1 %ID/g) compared to ^{68}Ga-acetate (2.0 ± 0.8 %ID/g) was observed. We conclude that when administered intravenously, ^{68}Ga-tris(oxinate) shows no specific tumour targeting and is a poor vehicle for delivery of ^{68}Ga to this tumour, suggesting that gallium delivery is not its main mechanism of action. ^{68}Ga-acetate delivers more gallium to tumour than ^{68}Ga-tris(oxinate).

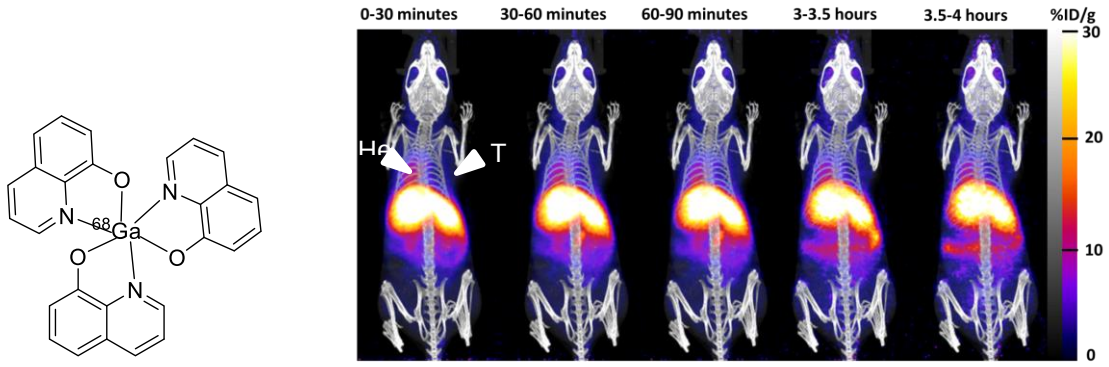

Figure 1. Structure of ^{68}Ga-tris(oxinate) (left); representative PET/CT MIPs of ^{68}Ga-tris(oxinate) over 4 h in female NSG mice inoculated with A375 melanoma cells (n=5). Heart (He) and tumour (Tu) indicated with white arrow (right).

[1] Jungwirth U, Gojo J, Tuder T *et al*. Molecular Cancer Therapeutics **2014**, *13*, 2436.
[2] Hofheinz RD, Dittrich C, Jakupec MA *et al*. International Journal of Clinical Pharmacology and Therapeutics **2005**, *43*, 590.

First Steps Towards Monitoring Immune Checkpoint Expression Levels after Reovirus Treatment *In Vivo* Using ^{89}Zr-based ImmunoPET

J Hoebart,[1] S Turnock,[1] I Titley,[2] C Da Pieve,[1] F Raes,[1] P Lawrence,[2] A Sadanandam,[2] G Smith,[1] A Melcher,[1] K Harrington[1] and Gabriela Kramer-Marek[1,*]

[1] The Institute of Cancer Research, Division of Radiotherapy and Imaging, London, UK; [2] The Institute of Cancer Research, Division of Molecular Pathology, London, UK

* Gabriela.Kramer-Marek@icr.ac.uk

Immune checkpoint inhibitor therapy (ICPI) has shown promising effects in patients with head and neck squamous cell carcinoma (HNSCC), including increased survival and reduced toxicities when compared to standard of care alternatives [1]. Inhibiting immune checkpoint receptors, present on cancer cells, e.g. PD-L1, and immune cells, e.g. PD-1, enables partial restoration of the immune response against cancer. This effect can be enhanced when ICPI is combined with oncolytic virus treatment (e.g. Reovirus), which has been shown to increase intratumoural PD-L1 levels. However, little is still known about the dynamics of immune checkpoint receptors and their relevance in the interplay of virotherapy and ICPI in the whole-body context.

Therefore, Positron Emission Tomography (PET) was chosen as a non-invasive tool to study immune checkpoint expression levels *in vivo*.

The murine HNSCC cell lines MOC1 and MOC2 were characterised via flow cytometry *in vitro*. Further, both cell lines were established as mouse models *in vivo*. Cells isolated from mouse tumours were investigated using flow cytometry and tumour sections were stained via immunohistochemistry. A ^{89}Zr-based PD-L1 tracer was prepared and its target specificity was assessed *in vitro* (cell binding assay) and *in vivo* (PET imaging).

PD-L1 expression was highly upregulated post-IFNγ but not Reovirus treatment in MOC1 and MOC2 cells *in vitro*. Flow cytometry analysis of tumour samples revealed higher levels of PD-1 and PD-L1 on the CD45^{+} cell population derived from MOC1 tumours. The ^{89}Zr-DFO-PD-L1 tracer showed promising target specificity *in vitro* and *in vivo*. Notably, tracer accumulation was increased in tumours which have been treated via intratumoural Reovirus injections when compared to the control group.

The first study to validate the ^{89}Zr-DFO-PD-L1 probe showed promising target specificity which encourages its potential as a non-invasive tool to study changes in immune checkpoint levels, e.g. PD-L1, after Reovirus treatment in mouse models of HNSCC.

[1] Ferris R L *et al*. *Nivolumab for recurrent squamous-cell carcinoma of the head and neck*. N. Engl. J. Med. **2016**, *375*, 1856–1867.

Role of ^{18}F-FACBC PET in Monitoring Tumour Response to ADT Therapy in Prostate Cancer

G Malviya,[1,*] R Patel,[1] E Johnson,[1] A Mrowinska,[1] E Mui,[1] S Champion,[2] S Pimlott,[2] D Lewis[1,3] and H Leung[1,3,4]

[1] Cancer Research UK Beatson Institute, Garscube Estate, Switchback Road, Glasgow, UK; [2] West of Scotland PET Centre, Greater Glasgow and Clyde NHS Trust, Glasgow, UK; [3] Institute of Cancer Sciences, University of Glasgow, Glasgow, UK; [4] Department of Urology, Greater Glasgow and Clyde NHS Trust, Glasgow, UK

* g.malviya@beatson.gla.ac.uk

In prostate cancer treatment, tumour heterogeneity and treatment resistance are major challenges. Metastatic castration-resistant prostate cancer (mCRPC) is the most lethal form of treatment-resistant prostate cancer. Despite initial favourable responses to androgen deprivation therapy (ADT), the majority of prostate cancer patients progress to mCRPC which remains incurable. Monitoring treatment response during the response phase in a temporal manner may help in the early identification of patients at risk of early treatment resistance, providing the basis for patient selection to receive combination therapy and/or early second line intervention aimed at improving patient outcome. We used functional metabolic imaging using an FDA approved radiotracer, FACBC (anti-1-amino-3-^{18}F-fluorocyclobutane-1-carboxylic acid), to monitor tumour response to ADT in murine orthograft models of CRPC [1]. FACBC is a synthetic L-leucine analogue that is taken up into cells via the LAT1 and ASCT2 transporters. Due to tumour heterogeneity especially under therapeutic stress, evolving CRPC may arise from a combination of androgen receptor (AR) dependent and independent mechanisms. Typically, AR-dependent CRPC arises from enhanced intra-tumoural *de novo* androgen biosynthesis to drive AR function, and may therefore exhibit increased vulnerability to sterol metabolising enzyme inhibitors such as abiraterone. We synthesised ^{18}F-FACBC on a GE Fastlab Synthesiser using cassettes provided by Blue Earth Diagnostics (BED, Oxford, UK) with ≥99% radiochemical purity. Isogenic androgen responsive and castrate resistant human prostate cancer cells (CWR22 and 22Rv, respectively) were implanted into the anterior lobes of the prostate in CD-1 Nu mice to generate orthografts tumour model (n=3 per group). Mice were anesthetised using isoflurane during imaging procedures. Ultrasound was performed to evaluate size of the tumours before PET/MR imaging. T1 GRE 3D Coronal/Sagittal MR scans were performed to obtain anatomical references. For PET imaging, both mice groups received ~14MBq ^{18}F-FACBC intravenously and 15 min static PET scans were performed. Standard uptake values (SUV) were calculated in the prostate tumours volumes defined on the MR images. Using ADT sensitive and CRPC pre-clinical prostate orthograft models [2], we show sustained ^{18}F-FACBC uptake in residual proliferating tumours. Overall, in addition to its diagnostic potential, ^{18}F-FACBC based imaging may be useful in monitoring treatment response and detection of treatment-resistant residual prostate cancer.

[1] Cunningham D and Z You. *In vitro and in vivo model systems used in prostate cancer research*. J. Biol Methods. **2015**, *2 (1)*, e17.

[2] Patel R, Fleming J, Mui E *et al. Sprouty2 loss-induced IL6 drives castration-resistant prostate cancer through scavenger receptor B1*. EMBO Mol. Med. **2018**, *10 (4)*.

Acknowledgments: Authors want to thank Blue Earth Diagnostics for providing Fastlab cassettes for ^{18}F-FACBC synthesis.

The Synthesis and Validation of Multimodal PET/Fluorescence Zinc Sensing Probes as Potential Imaging Agents for Prostate Cancer

G Firth,[1] T W Price,[1,2] M Kinnon,[1] C Eling,[3] N Long,[4] J Sturge[1] and G J Stasiuk[1,2,*]

[1] School of Life Sciences; [2] Positron Emission Tomography Research Centre, [3] Department of Chemistry, University of Hull, HU6 7RX, UK; [4] Department of Chemistry, Imperial College London, SW7 2AZ, UK

* G.stasiuk@hull.ac.uk

Prostate cancer (PCa) is the 2nd most common cancer worldwide for males, and the 4th most common cancer overall, accounting for 15% of all male cancers in 2012 [1]. PCa is asymptomatic in its early stages and advances in medical imaging are improving diagnosis, however novel simple non-invasive diagnostic tests are needed to catch the disease early. Zinc has emerged as a promising diagnostic target in PCa progression as it's accumulation in PCa cells is significantly lower compared to normal prostate [2]. We herein propose a fluorescent imaging probe, 2-((2-(2-fluoroethoxy)ethyl)amino)-*N*-(quinolin-8-yl)acetamide (AQA-F) shown in Figure 1, that changes emission profile when binding the metal zinc. A stokes shift of 90 nm can be observed upon zinc binding, enhancing the emission wavelength from 410 to 500 nm, with a K_d of 13.5×10^{-6} M. A 6-fold increase in fluorescence intensity is observed upon the addition of one equivalent of zinc. This significant increase in fluorescence intensity is specific to zinc and is not observed with the other transition metals that were tested. AQA-F can therefore be translated into *in vitro* studies where the endogenous localisation and uptake of the probe can be assessed. This research sets the foundation for a zinc sensing probe that has the ability to be radiolabelled with ^{18}F in 8.6% radiochemical yield with a 97% radiochemical purity and can be utilised for the diagnosis of prostate cancer.

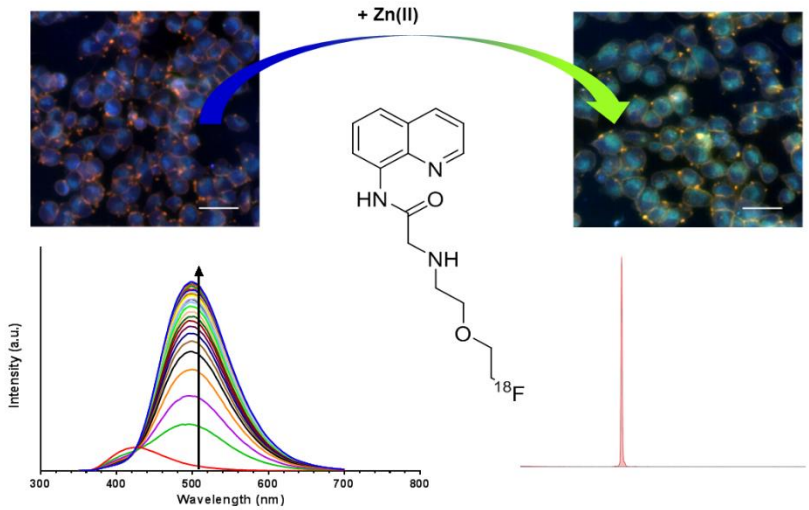

Figure 1. Cellular studies in prostate cells. Fluorescence spectra for AQA-F (0.1 mM) in HEPES buffer (10 mM, pH = 7.68) with increasing concentrations of zinc (0-3 equivalents) and radiotrace of [^{18}F]AQA-F.

[1] Hassanipour-Azgomi S *et al*. *Incidence and mortality of prostate cancer and their relationship with the Human Development Index worldwide*. Prostate International **2016**, *4 (3)*, 118–124.

[2] Franklin RB *et al*. hZIP1 zinc uptake transporter down regulation and zinc depletion in prostate cancer. Molecular Cancer **2015**, *4 (32)*, 1–13.

A Dual Reporter Iodinated Labelling Reagent for Cancer PET Imaging and Fluorescence-Guided Surgery

Z Lu,[1,2] T T Pham,[2] V Rajkumar,[3] Z Yu,[2] R B Pedley,[3] E Årstad[4] and R Yan[2,*]

[1] Department of Nuclear Medicine, the First Affiliated Hospital of Dalian Medical University, People's Republic of China; [2] School of Imaging Sciences and Biomedical Engineering, St. Thomas' Hospital, King's College London, SE1 7EH, London, UK; [3] UCL Cancer Institute, University College London, 72 Huntley Street, London, WC1E 6BT, UK; [4] Institute of Nuclear Medicine and Department of Chemistry, University College London, 235 Euston Road (T-5), London, NW1 2BU, UK

* ran.yan@kcl.ac.uk

The combination of early diagnosis and complete surgical resection of malignant tumor is the best modality to treat cancer. We have developed a dual modality labelling reagent, ^{124}I-Green, that has the potential to unite cancer diagnosis with positron emission tomography (PET) and surgery guided by its excellent target-to-background fluorescence.

^{124}I-Green was synthesised with excellent radiochemical yields of 92±5 % (n = 4) using an improved one-pot three-component radioiodination reaction. The carcinoembryonic antigen (CEA) specific antibody A5B7 was conjugated with ^{124}I-Green. The EC_{50} of the ^{124}I-Green A5B7 conjugate towards CEA was 22 nM similar to that of the native A5B7 (26 nM). The CEA-expressing human colorectal carcinoma SW1222 cells were stained with the ^{124}I-Green A5B7 conjugate emitted bright green fluorescence that was largely blocked by the native A5B7. The biodistribution, PET/CT and *ex vivo* fluorescence imaging of the ^{124}I-Green A5B7 conjugate was performed in the SW1222 xenograft bearing mice (n=3) at 24, 48, and 72 h post intravenous injection. Tumor uptakes of the ^{124}I-Green A5B7 conjugate around 20.21±2.70, 13.31±0.73, and 10.64±1.86 %ID/g (n = 3) was observed at 24, 48, and 72 h, respectively. The SW1222 xenografts were clearly visualized by both PET/CT and *ex vivo* fluorescence imaging with excellent target to background contrast (Figure 1). The encouraging results warrant further studies towards translation of the ^{124}I-Green to the PET cancer imaging and fluorescence-guided surgery.

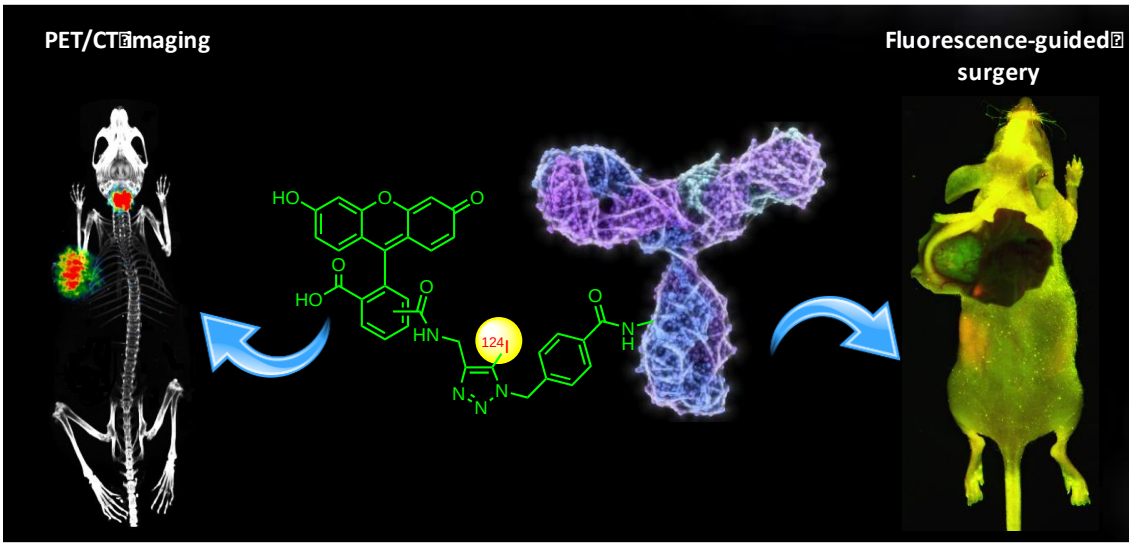

Figure 1. Structural illustration of the ^{124}I-Green anti-CEA monoclonal antibody A5B7 conjugate for the sequential PET/CT and ex vivo fluorescence imaging of SW1222 human colorectal xenograft.

Deuterium Isotopic Substitution in ^{64}CuATSM: Effects on Redox Potential and Hypoxic Trapping

J E Blower,[1] F Baark,[1] T Eykyn,[1] V Pell,[1] R A Atkinson,[2] K B Holt,[3] S Teague,[4] R Southworth[1] and P J Blower[1,*]

[1] School of Biomedical Engineering and Imaging Sciences, King's College London, London, UK; [2] Centre for Biomolecular Spectroscopy and Randall Division of Cell and Molecular Biophysics, King's College London, UK; [3] Department of Chemistry, University College London, London, UK; [4] Department of Chemistry, King's College London, London, UK

* philip.blower@kcl.ac.uk

Hypoxia selectivity of copper bisthiosemicarbazone PET tracers such as ^{64}CuATSM is achieved by subtle manipulation of the ligand, controlling redox potential and lipophilicity by alkylation of the ligand diamine backbone. This is believed to involve pi-electron donation by the methyl C-H bonds (hyperconjugation; Figure 1). Substitution of hydrogen for heavier deuterium in the ligand backbone could therefore perturb the frontier orbitals affecting the redox potential and the rate of dissociation of copper in hypoxic environments. This work aimed to evaluate this effect.

Deuterated 2,3-butanedione was synthesised via hydrogen-deuterium exchange of 2,3-butanedione in acidified D_2O, and used for synthesis of CuATSM-d_6. Reduction and oxidation potential of CuATSM and CuATSM-d_6 were measured using cyclic voltammetry. Differences in electron distribution were analysed using ^{15}N NMR. The biological behaviour of radiolabelled ^{64}CuATSM-d_6 was assessed using the Langendorff isolated perfused normoxic and hypoxic rat heart model.

First synthesis of CuATSM-d_6 was achieved. Cyclic voltammetry showed minimal electrochemical differences between CuATSM and CuATSM-d_6. In ATSM-d_6, ^{15}N NMR showed a chemical shift on the coordinating nitrogen atoms of +0.239 ppm (downfield) compared to ATSM. In heart perfusion experiments, both complexes showed hypoxic-selective trapping but without significant differences in retention between ^{64}CuATSM and ^{64}CuATSM-d_6 under normoxic and hypoxic conditions.

While the substitution of hydrogen for deuterium atoms on the ligand backbone altered electronic distribution across the ligand, this effect was not enough to significantly affect redox potentials or the hypoxia selectivity of the parent ligand.

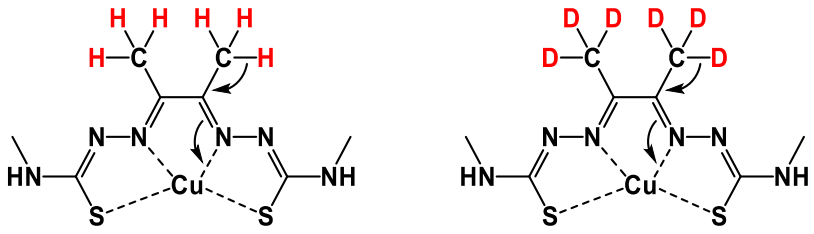

Figure 1. Structure of CuATSM *vs* the proposed CuATSM-d_6 and the hyperconjugation effect.

A Novel ^{18}F-labelled Molecular Probe for *In Vivo* Detection of Oxidative Stress using Positron Emission Tomography

F Mota*, V Pell, N Singh, F Baark, E Waters, R Southworth and Ran Yan

School of Biomedical Engineering and Imaging Sciences, Department of Imaging Chemistry and Biology, St Thomas' Hospital, 4th floor Lambeth Wing, King's College London

* filipa.da.mota.quinteiro@kcl.ac.uk

Background: Reactive oxygen species (ROS) are endogenously generated by the mitochondrial electron transport chain, and play important roles in the regulation of cell growth, neurotransmission, and the immune system. In elevated level, however, ROS ultimately lead to oxidation of DNA, proteins, and cell membranes. The resulting oxidative stress underlies the pathogenesis of numerous disease states including neurodegenerative disease, cardiovascular disease, and chemotherapy-induced cardiotoxicity.

Methods and results: We are exploring new chemical entities as potential radiotracers for the direct detection of ROS *in vivo* using positron emission tomography (PET). Our radiotracer candidates are cell membrane permeable and susceptible to ROS oxidation, leading to changes in physicochemical properties that favour prolonged intracellular retention. Lead compound [^{18}F]FM074 was tested in a rat model of Doxorubicin-induced cardiotoxicity using osmotic mini-pumps to deliver a cumulative dose of 30 mg/kg Doxorubicin (pilot study at n = 4) or vehicle control (n = 3) at a constant rate for six days. Quantitative PET data analysis showed that [^{18}F]FM074 had two-fold increased retention and a significantly higher ($p<0.05$) left ventricle to myocardial blood pool uptake ratio in the hearts of Doxorubicin-treated animals *vs* control (Figure 1).

Conclusions: We have designed and validated a novel radiotracer candidate, [^{18}F]FM074, for the direct detection of ROS *in vivo* by PET. It has favourable pharmacokinetics and low baseline retention in healthy subjects, and shows significantly higher uptake in the hearts of Doxorubicin-treated rats *vs* vehicle controls in a pilot study.

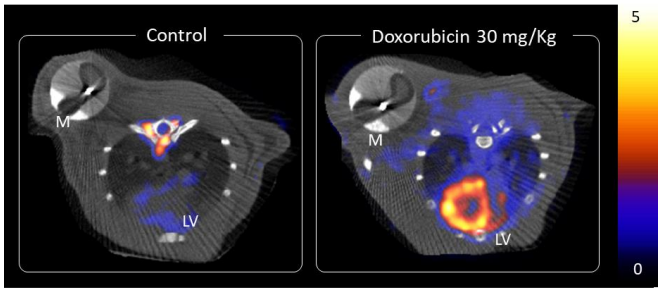

Figure 1. Axial PET/CT images of [^{18}F]FM074 in a rat model of Doxorubicin-induced cardiotoxicity. Wistar rats received 30 mg/kg of Doxorubicin (right) or saline (left) via osmotic mini-pump for 6 days.

Validation of ROS Sensitive PET Tracers: Towards In Vivo Imaging of Oxidative Stress

E C T Waters,* F Baark, V R Pell, F Mota, T Eykyn, R Yan and R Southworth

School of Biomedical Engineering and Imaging Sciences, King's College London

* edward.waters@kcl.ac.uk

Reactive oxygen species (ROS) are a common mediator in the pathogenicity of numerous human diseases, the toxicity of many drugs and the mode of action of several cancer therapy regimens. Detecting changes in tissue redox status by PET imaging of ROS could be used to gain invaluable information in these pathologies, with the potential to enable earlier diagnosis of disease, drug toxicity or response to therapy. While several new ROS-sensing PET tracers have recently been postulated, none have yet been fully validated in terms of parallel independent biomarkers of oxidative stress or exclusion of the confounding effects of alterations in tissue perfusion. We have therefore developed a model of ROS generation in the isolated perfused rat heart, which allows such validation and characterisation work to be performed and demonstrate here its utility in evaluating our pilot ROS sensing tracer; an analogue of dihydroethidine labelled with ^{18}F.

The pilot tracer candidate [^{18}F]dihydroethidine was synthesised in a non-decay corrected radiochemical yield of 12 ± 3% (n=10) with a molar activity of > 74 GBq·µmol^{-1}. The logD7.4 was 1.58 ± 0.11 (n=6) for the neutral tracer and -0.22 ± 0.04 (n=6) for its oxidised form., which would allow tissue penetration and ROS-dependent trapping respectively. Chemoselectivity of the tracer candidate to a range of proximal ROS was assessed *in vitro* and oxidation was assessed by HPLC. The tracer showed selectivity for both superoxide (25% oxidation after 5 minutes and 50% oxidation after 1 hour; n=3) and hydroxyl radicals (20% oxidation after 5 minutes and 1 hour; n=3).

The capacity of [^{18}F]dihydroethidine to measure ROS generation in an isolated perfused heart was measured with a custom triple γ-detector array. We developed a titratable pharmacological method of ROS formation using menadione, which redox-cycles at the active site of flavoenzymes catalysing the generation of superoxide. ROS generation was validated using relevant biomarkers. Total glutathione concentration (GSH) in treated hearts was 67.1 ± 1.5% (n=3) of control, PKG1α showed an increase in oxidation from 11.0 ± 0.1% in controls to 68.1 ± 0.2% in menadione treated hearts. Under these conditions of ROS generation, [^{18}F]dihydroethidine was administered to the heart by constant infusion, the rate of uptake of the tracer increased 61.7 ± 6.3% (n=2) when compared to control.

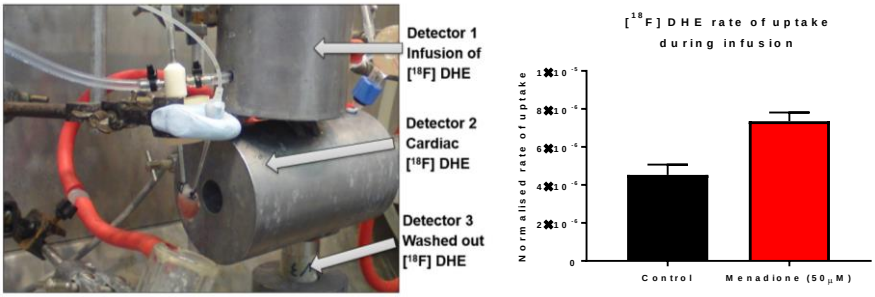

Figure 1. Left) Custom triple γ-detector array measuring radioactivity in an isolated perfused rat heart. **Right)** Rate of uptake of [^{18}F]dihydroethidine in control and menadione perfused heart measured by detector 2.

Imaging Chronic Cardiac Disease Using Hypoxia Targeting PET Agents

V Pell,[1,*] F Baark,[1] F Mota,[1] K Sander,[2] E Årstad,[2] J Clark[3] and R Southworth[1]

[1] School of Biomedical Engineering & Imaging Sciences, King's College London, London, UK; [2] Radiochemistry, Division of Medicine and Department of Chemistry, University College London, London, UK; [3] School of Cardiovascular Medicine & Sciences, King's College London, London, UK

* victoria.pell@kcl.ac.uk

Hypoxia plays a key role in the pathology of chronic cardiovascular diseases such as cardiac hypertrophy and heart failure. The imaging modalities used in cardiac imaging, however, largely report on changes in cardiac structure or function which provide a limited window for intervention. Currently available hypoxic PET tracers are however suited to detecting extreme hypoxia, such as that which occurs in tumours or severe ischemia. Consequently, there remains a need for an imaging method that will aid in the identification of cardiac diseases in which milder hypoxia is implicated. We have demonstrated that the PET tracer ^{64}Cu-CTS out-performs the more established ^{64}Cu-ATSM in identifying hypoxic myocardium *ex vivo*. The *ex vivo* model is however limited in replicating cardiovascular disease and provides little insight into pharmacokinetic properties *in vivo*.

Using a mouse model of pressure-overload induced heart failure we aimed to characterise the hypoxia selectivity and pharmacokinetics of novel PET tracers. Mice (n=6) were subjected to abdominal aortic constriction (AAC) or a sham operation. AAC mice exhibited extensive cardiac hypertrophy and reduced cardiac function as determined by serial cardiac echocardiography. 10 weeks post-surgery mice were culled for histological analysis and a subset of mice were imaged via PET/CT with the novel hypoxic tracer ^{18}F-KS-178. Preliminary analysis showed an increase in LV/blood SUV ratio in an AAC mouse compared to control suggesting ^{18}F-KS-178 could be a promising tool for the detection of hypoxia in chronic cardiovascular disease.

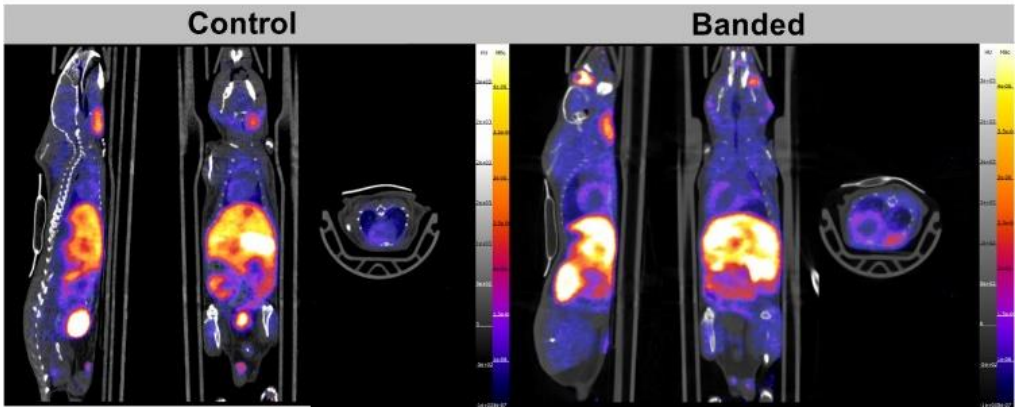

Figure 1. PET/CT imaging of a control and AAC mouse with hypoxic PET tracer ^{18}F-KS-178. Mice subjected to either abdominal aortic banding or a sham procedure were injected (i.v) with 3-5 MBq of ^{18}F-KS-178 and subjected to PET/CT imaging. LV:Blood ratio was higher in the banded mouse compared to control.

Understanding the Cardiac Metabolic Phenotype of a Mouse Model of Barth's Syndrome Using PET/MR Imaging

E Johnson, E Anderson, A Mrowinska, G Malviya, D Soloviev, D Strathdee and D Lewis*

Beatson Institute for Cancer Research, Garscube Estate, Switchback Road, Bearsden, Glasgow G61 1BD, Scotland, UK

* d.lewis@beatson.gla.ac.uk

Background: Barth syndrome is a serious X-linked inherited genetic disease estimated to affect about 1 in 300,000 individuals worldwide resulting in a broad range of clinical features. It is characterised by dilated cardiomyopathy, lipid abnormalities and growth delay caused by mutations in Taz, a mitochondrial transacylase required for the production of the phospholipid, cardiolipin. The molecular mechanisms underlying the development and progression of Barth syndrome are still poorly understood. To study this further we generated a whole body germline knockout of the Taz gene and characterised resulting the phenotype using molecular imaging.

Key Results: Mutation in the Taz gene resulted in a pronounced reduction in cardiolipin levels and development of severely compromised cardiac function with the failure of proper mitochondrial maturation. This is accompanied by an alteration in metabolism, mitochondrial morphology and the induction of the mitochondrial unfolded protein stress response. Using whole-body [11C]acetate PET imaging we observed a halving of the myocardial oxygen consumption rate in the Taz knockout compared to wild-type mice (Kmono 0.007± 0.0004 v 0.014 ± 0.002 sec-1; p=0.03). This was accompanied by an increase in myocardial glucose utilisation measured by [18F]FDG imaging (SUVmean 8.57 ± 0.03 v 17.26 ± 5.8) suggesting a marked metabolic shift from oxidative to glycolytic metabolism as part of a cardiac stress response in Barth syndrome.

Conclusion: Reversing the induction of this stress response may represent an effective therapy and metabolic PET imaging can provide a method to non-invasively identify cardiac metabolic stress and monitor the effectiveness of novel therapies.

P44

Non-invasive Imaging of Mitochondrial Dysfunction and Anthracycline Cardiotoxicity by Repurposing ^{99m}Tc Sestamibi SPECT Imaging

F Baark, Z Md Saffee, E Waters, V R Pell, F Mota, M Veronese, J E Clark, T R Eykyn, L Livieratos, P J Blower and R Southworth

School of Biomedical Engineering & Imaging Sciences, King's College London, UK

Anthracyclines are a first in line therapy used to treat numerous malignancies including leukemia, lymphoma, myeloma, lung, ovarian, gastric, thyroid and breast carcinoma. However, they are highly toxic to the heart, inducing coronary heart disease, valvular heart disease, cardiomyopathy, and heart failure. Cardiotoxicity critically limits chemotherapeutic dose, and can develop years or decades after therapy. During this latency period, cardiotoxicity is only monitored clinically by evaluating changes in cardiac structure and contractility, typically using echocardiography or MUGA scanning. However, anthracycline cardiotoxicity is initiated at the subcellular level, commonly associated with mitochondrial dysfunction and elevated oxidative stress, meaning these techniques are not sensitive enough and diagnose too late in the pathology to allow meaningful intervention or personalised dosage regimes.

Mitochondrial dysfunction is fundamental to anthracycline cardiotoxicity, mediated in part by severe iron overload and oxidative stress. We are developing nuclear imaging approaches to probe mitochondrial function and oxidative stress as predictors of evolving cardiotoxicity. Fluorescent lipophilic cations like TMRE are used experimentally to report on mitochondrial membrane potential ($\Delta\Psi_m$), but are of limited utility clinically. The SPECT tracer ^{99m}Tc sestamibi (MIBI) is used clinically to visualize cardiac perfusion, but being a lipophilic cation, its cardiac retention is more accurately a function of both perfusion and $\Delta\Psi_m$. Correcting scans for variations in perfusion would allow ^{99m}Tc-sestamibi to be repurposed to specifically report on $\Delta\Psi$m.

In the Langendorff heart we have demonstrated a dose-dependent MIBI washout proportional with mitochondrial uncouplers or doxorubicin. In an *in vivo* rat model of chronic cardiotoxicity (using osmotic minipumps loaded with doxorubicin over 4 weeks, and 4 weeks to allow injury to develop), we demonstrate dose-dependent loss of cardiac MIBI retention before any detectable changes in cardiac function, as measured by echocardiography. Cardiac MIBI retention decreased from 1.4% ± 0.1 (injected dose per gram) in control animals to 0.79% ± 0.08 with our top dose of doxorubicin. We have also go on to show that a co-infusion of doxorubicin with the iron chelator deferiprone limits anthracycline cardiotoxicity and mitochondrial iron overload, and restores cardiac MIBI retention (increasing from 0.79% ± 0.08 with doxorubicin alone to 1.2% ± 0.2 in the Deferiprone group). We believe this demonstrates the potential of MIBI imaging as an early readout of evolving cardiotoxicity and as a means of evaluating novel cardioprotectant strategies.

Can ^{68}Ga(HP3-RGD3) Image Early Onset of Rheumatoid Arthritis Preclinically?

F Clarke,[1] M T Ma,[2] T J Peel,[1] N K Ramakrishnan,[2] K Sunassee,[2] J K Bordoloi,[2] G H Cornish,[1] A P Cope[1] and S Y A Terry[2,*]

[1] King's College London, Centre for Inflammation Biology and Cancer Immunology, School of Immunology and Microbial Sciences, London, SE1 1UL, United Kingdom; [2] King's College London, Department of Imaging Chemistry and Biology, London, United Kingdom

* samantha.terry@kcl.ac.uk

Purpose: Rheumatoid arthritis is an autoimmune disease characterized by systemic inflammation. If identified early, it can be treated successfully with disease-modifying anti-rheumatic drugs. Here, we investigated ^{68}Ga(HP$_3$-RGD$_3$) as a PET imaging tool to detect arthritis early-on by targeting integrin a_vb_3, found on osteoclasts, macrophages and new blood vessels.

Methods: C57Bl/6 mice were injected with arthritogenic serum (n=10-20/group) and mice presenting mild or severe arthritis were imaged by PET/CT with ^{68}Ga(HP$_3$-RGD$_3$) at 1h p.i. on day 6 and 8 (9-16 MBq/4 μg) or used for biodistribution only (1.5-6MBq/4 μg). In a final study, ankle joints were removed from healthy and arthritic mice on day 10 for staining with H+E and flow cytometry was used to identify immune cell populations in the joints and joint-draining lymph nodes at the peak of disease (Day 5).

Results: Mice imaged at day 6 did not have external signs of arthritis nor could PET/CT visualise early signs of arthritis (Figure 1). In biodistribution studies, a difference in joint uptake of ^{68}Ga(HP$_3$-RGD$_3$) was seen between mice receiving arthritogenic serum and PBS. For example, tracer uptake in the feet and ankles was 0.84±0.16 %ID and 0.67±0.22 %ID (p=0.007), respectively. At day 8, imaging could differentiate between severely arthritic joints (increased diameter >0.5mm) and joints with little inflammation, even within the same mouse. In biodistribution data, tracer uptake in severely arthritic joints was 0.26±0.02 %ID in wrists and 0.68±0.18 %ID in ankles, whereas wrists measured 0.14±0.02 %ID and ankles 0.29±0.03 %ID in non-arthritic mice. In blockade studies, radiotracer uptake in severely arthritic joints measured 0.08±0.01 %ID in wrists and 0.24±0.02 %ID in ankles (p = 0.0005). Joints and joint-draining lymph nodes from arthritic mice showed enhanced cell infiltration and erosion as well as a greater number of T cells, monocytes, dendritic cells and neutrophils, respectively, compared to healthy mice.

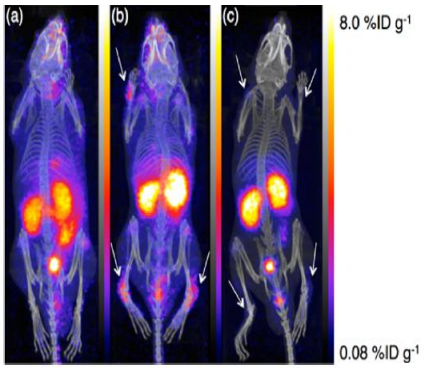

Figure 1. PET/CT maximum intensity projections of mice administered [^{68}Ga(HP3-RGD$_3$)] (8−13 MBq, 4 mg) 1 h post injection. **a)** healthy C57Bl/6 mouse; **b)** severely arthritic mouse at Day 8; **c)** severely arthritic mouse co-administered with c(RGDfK) at Day 8. Arrows indicate arthritic joints.

Conclusion: In mice, ^{68}Ga(HP$_3$-RGD$_3$, is an excellent and specific tracer to image arthritis but only where disease is established.The combination of early diagnosis and complete surgical resection of malignant tumor is the best modality to treat cancer. We have developed a dual modality labelling reagent, ^{124}I-Green, that has the potential to unite cancer diagnosis with positron emission tomography (PET) and surgery guided by its excellent target-to-background fluorescence.

Acknowledgements: Funding for the project was in part provided by the Rosetrees Trust.

Evaluation of TSPO PET In Vivo Imaging in a Rat Model of Neuroinflammation

M Vicente-Rodríguez,[1,4] N Singh,[1] D Cash,[1,4] M Veronese,[1] C Simmons,[1,4] A K Haji-Dheere,[3] J Bordoloi,[3] R O Awais,[5] K Sander,[5] E Årstad,[5] F Turkheimer[1,4] and C Parker[2,4]

[1] Department of Neuroimaging, Institute of Psychiatry, Psychology & Neuroscience, King's College London, London, United Kingdom; [2] GlaxoSmithKline, Stevenage, London, United Kingdom; [3] PET Centre, St Thomas' Hospital, London, United Kingdom; [4] The Wellcome Trust Consortium for the Neuroimmunology of Mood Disorders and Alzheimer's Disease (NIMA); [5] Radiochemistry, Institute of Nuclear Medicine and Department of Chemistry, University College London, United Kingdom

The aim of the study was to evaluate the utility of *in vivo* TSPO PET imaging in a rat model of low level neuroinflammation induced by a systemic injection of LPS. To assess neuroinflammation we characterized two different TSPO PET tracers, [^{11}C]PK11195 and [^{18}F]DPA714 in a rat model of intracranial LPS, which is known to induce a robust focal neuroinflammatory reaction. For the intracranial LPS model, the rats were treated with unilateral stereotaxic injection of LPS (1ug) into the right striatum (n=3) and for the systemic LPS model, the rats were injected with either LPS (0.5mg/kg, i.p. n=4) or Veh (PBS, n=4). Animals were imaged in a microPET/CT scanner for 40 minutes after intravenous administration of ~ 10-15 MBq [^{11}C]PK11195 or 60 minutes of [^{18}F]DPA714 and SUV values for various brain regions determined. Blood and plasma samples were collected from the systemic LPS rat model to study peripheral tracer distribution. All experiments were ethically reviewed and performed in accordance with the UK Animals (Scientific Procedures) Act 1986 and the GSK Policy on the Care, Welfare and Treatment of Animals. In intracranial model, 4 days after lesioning, *in vivo* microPET data demonstrated a significantly higher uptake of both [^{11}C]PK11195 and [^{18}F]DPA714 in the LPS-injected side vs the non-injected side (Figure 1). AUC was significantly higher for [^{18}F]DPA714 compared to [^{11}C]PK11195, in the intracranial model.

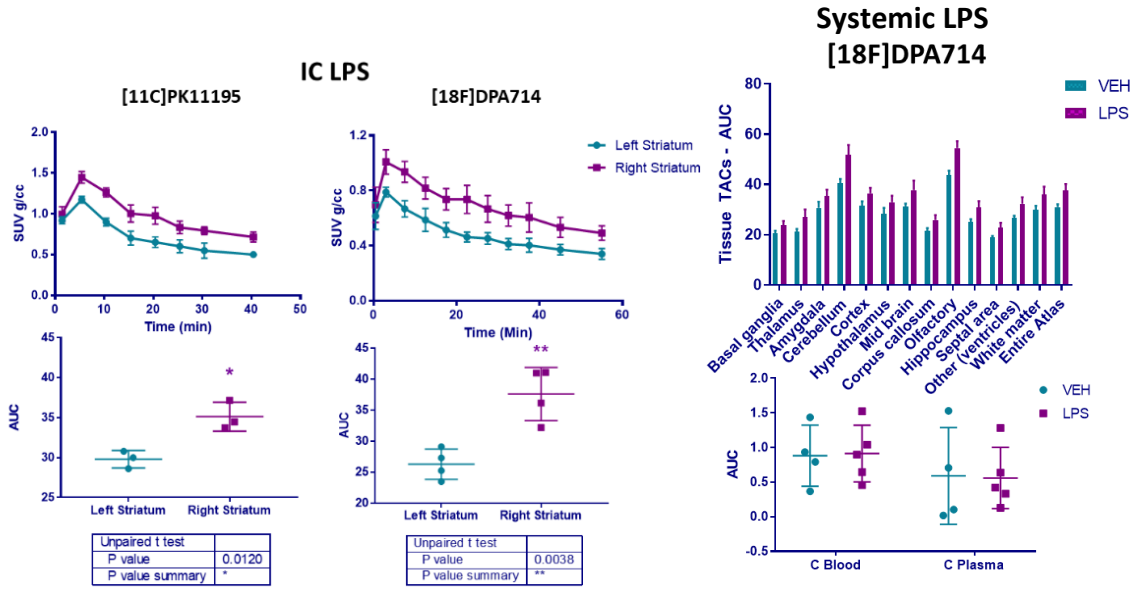

Figure 1. Time activity curves (TACs) and Area Under Curve (AUC) of TACs for different brain regions.

Therefore, [^{18}F]DPA714 tracer was used to asses neuroinflammation in the systemic LPS rat model. An increased uptake in LPS group was found across all regions. Cerebellum,

thalamus and olfactory bulb had higher activity in LPS compared to vehicle (>20%), while the lowest difference was in amygdala (11%). No difference in peripheral distribution of the tracer was found. [^{18}F]DPA714 PET imaging may be useful in monitoring subtle, low level inflammation in the brain.

Acknowledgements: This study was part funded by GSK and a grant from the Wellcome Trust (Grant number: 104025/Z/14/Z).

Imaging of the Dementias – What Do Tau PET Tracers Really Show?

M C Wren,[1,2] T Lashley,[2] E Årstad[1] and K Sander[1,*]

[1] University College London, Radiochemistry, Institute of Nuclear Medicine and Department of Chemistry, 5 Gower Place, London WC1E 6BS; [2] University College London, Queen Square Brain Bank for Neurological Disorders, Institute of Neurology, 1 Wakefield Street, London WC1N 1PJ

* k.sander@ucl.ac.uk

Imaging of pathological tau with positron emission tomography (PET) has the potential to allow early diagnosis of the dementias and monitoring of disease progression, including assessment of therapeutic interventions, *in vivo*. The first generation of tau PET tracers, including the carbazole flortaucipir and the 2-arylquinolines of the THK series, are now used in clinical research; however, concerns have been raised about off-target binding and low sensitivity.

With the aim to determine the nature of tau pathology depicted by structurally distinct tau ligands we carried out a microscopic neuropathological evaluation in human *post-mortem* brain tissue of cases with primary and secondary tauopathies. In end stage Alzheimer's disease cases, fluorescent imaging with the carbazole T726 and the 2-arylquinoline THK-5117 revealed high inter- and intra-case variability of tracer binding, and this was corroborated by quantitative phosphorimaging with the PET tracer [^{18}F]THK-5117. Microscopic analysis of the pathological inclusions revealed that the fluorescent tracers preferentially bind to premature tau aggregates. Whilst T726 binding was limited to neuronal tau, THK-5117 additionally depicted neuritic tau. Neither tracer depicted tau in pre-symptomatic disease (Figure 1).

Our results highlight limitations of the first generation of tau PET tracers, in particular lack of correlation between pathological tau load and tracer binding, limited sensitivity to tau in early disease, and high variability in tracer binding between and within cases. Concerns remain that these limitations may also affect the next generation tracers as they target the same high affinity binding site. Therefore, it is crucial to assess novel tau PET tracers before translation into clinical studies [1].

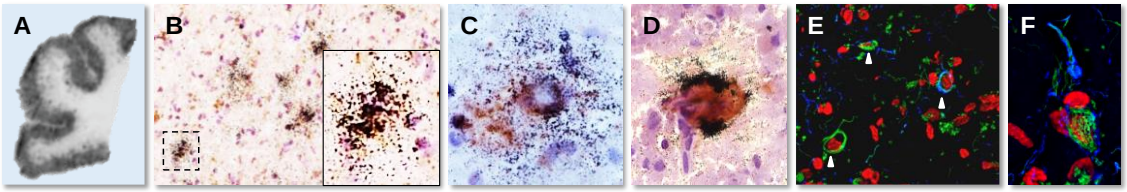

Figure 1. Neuropathological assessment of THK-5117 in a case with Alzheimer's disease. **A)** Distribution of [^{18}F]THK-5117 binding in the frontal cortex. **B–D)** [^{18}F]THK-5117 binding to tau neurofibrillary tangles (B; co-staining with tau antibody AT8) and neuritic plaques (C/D; co-staining with AT8 and the amyloid-beta antibody Aβ-XP). **E/F)** Binding of THK-5117 to a subset of AT8 immunodecorated neurofibrillary tangles (THK-5117 in green, AT8 in blue, nuclear marker Nissl Neurotrace 640 in red).

[1] Wren MC, Lashley T, Årstad E, Sander K. *Large inter- and intra-case variability of first generation tau PET ligand binding in neurodegenerative dementias*. Acta Neuropath. Comm. **2018**, *6*, 34.

Acknowledgements: We acknowledge funding by the Leonard Wolfson Experimental Neurology Centre, Alzheimer's Research UK and the NIHR Queen Square Dementia Biomedical Research Unit. This work was undertaken at UCLH/UCL, which is funded in part by the Department of Health's NIHR Biomedical Research Centres funding scheme.

Development of [^{11}C]Leucine PET as a Tool to Measure Brain Protein Synthesis in Rats

D Bochicchio,[1] M Vandesquille,[1] K Herholz,[1] C Parker,[2] R Hinz[1] and H Boutin[1]

[1] University of Manchester, Manchester, UK; [2] GlaxoSmithKline, Stevenage, UK

* daniela.bochicchio@postgrad.manchester.ac.uk

Alzheimer's disease (AD) is characterised by severe alterations of cognitive function and memory. Memory consolidation depends on protein synthesis which promotes neuronal plasticity and new connections, and all are altered in AD [1]. In the CNS, appropriate protein synthesis is essential to stabilize the formation of long-term memory [2]. Different studies have shown alterations in these pathways by AD in animal models and patients [3]. [^{11}C]leucine is a good tracer to measure protein synthesis rate (PSR) by PET because leucine has a good uptake at the blood brain barrier, a limited amount of metabolites being produced during its catabolism and in brain leucine is used only in proteins incorporation [4].

The aim of this study is to model PSR in rats and validate an image-derived input function (IDIF), based on the time-activity curve of the heart left ventricle validated against an arterial input function obtained with the Twilite® sampler and discrete arterial blood and plasma samples. The IDIF should be enabling the future evaluation of PSR in the TgF344-AD rat model of AD. All experiments were ethically reviewed and performed in accordance with the UK Animals (Scientific Procedures) Act 1986 and the GSK Policy on the Care, Welfare and Treatment of Animals. Male Wistar rats (n=6) were scanned using PET-CT for 60min following [^{11}C]leucine administration (tail vein i.v, 30-60MBq). Brain and heart-ventricular time-activity curves were extracted from the PET images. Online measurement of blood radioactivity was performed using a Twilite™ detector; blood samples were also taken at 2, 5 10, 20, 30 40 and 60min for γ-counting. Brain activity was also evaluated by γ-counting at the end of the scan.

γ-counting and PET measures over the left ventricle are in good agreement both in term of absolute activity and pharmacokinetics. Following the injection peak, the activity rapidly decreases due to distribution of [^{11}C]leucine into the body up to 20min post-injection. The blood activity then increases slowly due to an increase in radiolabelled proteins in plasma in agreement with previous studies in human and in rat [5]. All the brain TACs show a similar trend characterised by a peak during the first 5 minutes, followed by a modest washout and then a plateau from 20 minutes onward. These data are in agreement with previous results [6]. PET measurements and γ-counting of brain regions are in good agreement, highlighting that PET measurements are accurate.

[1] Ma T *et al*. Nat. Neurosci. **2013**, *16*, 1299–1305; Garcia-Esparcia P *et al*. Am. J. Neurodegener. Dis. **2017**, *6*, 15–25.
[2] Bishu S *et al*. J. Cereb. Blood Flow Metab. **2008**, *28*, 1502–1513.
[3] Pasini S *et al*. Cell Rep. **2015**, *11*, 183–191; Hoozemans JJ *et al*. Acta Neuropathol. **2015**, *110*, 165–172.
[4] Oldendorf WH. Am. J. Physiol. **1971**, *221*, 1629–1639; Keen RE *et al*. J. Cereb. Blood Flow Metab. **1989**, *9*, 429–445; Hellyer PJ *et al*. Neuroimage **2017**, *155*, 209–216.
[5] Sundaram SK *et al*. J. Nucl. Med. **2006**, *47*, 1787–1795; Lauenstein L *et al*. Neurosurg. Rev. **1987**, *10*, 147–150.
[6] Smith CB *et al*. J. Cereb. Blood Flow Metab. **2005**, *25*, 629–640; Veronese M *et al*. J. Cereb. Blood Flow Metab. **2012**, *32*, 1073–1085; Hawkins RA *et al*. J. Cereb. Blood Flow Metab. **1989**, *9*, 446–460.

Assessment of Multiple Animal Scanning on NEMA-NU4 Image Quality for the Sedecal SuperArgus2R Preclinical PET Scanner

N Efthimiou,[1,*] I Renald,[1] S Archibald[1,2] and C Cawthorne[1,3,4]

[1] PET Research Centre, Faculty of Health Sciences, University of Hull, UK; [2] Faculty of Science and Engineering, School of Mathematics and Physical Sciences, University of Hull, UK; [3] Nuclear Medicine and Molecular Imaging, Department of Imaging and Pathology, KU Leuven, Leuven, Belgium; [4] MoSAIC-Molecular Small Animal Imaging Centre, KU Leuven, Leuven, Belgium

* n.efthymiou@hull.ac.uk

Introduction: A common practice to increase the throughput in preclinical PET imaging is to concurrently scan multiple animals. However increased activity and attenuation in the FOV leads to more random events and an increased likelihood for scatter, which can impact image quality (IQ) of the resulting scans. Here we assessed the impact of an additional mouse-sized body on IQ using the NEMA-NU4 phantom, when located at side of the FOV.

Methods: Image quality was assessed using a NEMA NU4 phantom, solo and in combination with a 20ml syringe, using a Sedecal preclinical PET/CT scanner. Due to the limited axial FOV, two bed positions (10 min each), were used. Data were reconstructed using 3DOSEM with 16 subsets and 2 iterations, with randoms, scatter and PSF correction as used for routine scans.

Results: The uniformity analysis showed an increase in the $\%STD_{unif}$ from 7% to 8.05%, attributed to the presence of an extra body in the FOV which increases the total attenuation and a reduction in the number of detected events along some LORs that increased noise. The addition of the syringe also reduced the spatial resolution of the scanner, especially for the smallest rods, and increased the %STD of the axial profiles, with a visible impact on the 2mm rod. The spill over ratio (SOR) in air is significantly increased in the case of the two phantoms.

Future Work: A validated GATE simulation model will be used to further assess the nature of the resulted image quality degradations.

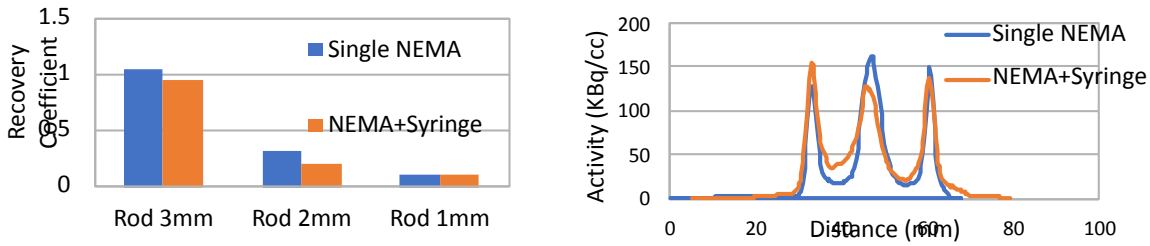

Figure 1. A) Recovery coefficients for the three thinner rods and **B)** line profile through the cold regions of the phantom (air and water) for both the single NEMA and NEMA + syringe acquisitions.

[1] Siepel FJ *et al*. *Scanning multiple mice in a small-animal PET scanner: Influence on image quality*. Nucl. Inst. Meth. Phys. A, 621, 6075–6610.

[2] Herranz E *et al*. Non-inVaSiVe eSTiMaTe of inPuT funCTion froM PeT iMageS of SMall MiCe, European Society for Molecular Imaging 2009.

INTERNET ACCESS DURING THE MEETING

There are two wireless networks at The Crick Institute. ‘Eduroam’ is a common guest wireless network available at academic institutions. ‘WiFi Guest’ can be accessed by Crick guests, who are not affiliated with academia.

HOW TO USE ‘EDUROAM’

‘Eduroam’ is an international service that allows users to connect to a wireless network at participating institutions using the same ‘eduroam’ network. Visitors from a participating institution can connect to ‘eduroam’ at The Crick Insitute. Your device may request that you trust a certificate called ‘Crick Self Signed’, please do this.

HOW TO USE ‘WIFI GUEST’

The Crick’s guest wireless network is ‘WiFi Guest’ and it is powered by ‘The Cloud’, which is used in over 20,000 Wi-Fi spots in the UK. There is a simple login process, similar to that used with Wi-Fi on trains and in other public spaces.

Connect to ‘WiFi Guest’, open your browser, visit any website and click ‘Get online at The Francis Crick Institute’.

If you have not used a Wi-Fi network powered by ‘The Cloud’ before, click ‘Create Account’ and enter your details.

If you have previously used ‘The Cloud’ — for example, at a railway station, restaurant, pub etc. – you can enter your existing credentials and click ‘Continue’.

SPEAKERS AND JUDGES

SPEAKERS

Christopher J Cawthorne

Peter J Gawne

Thibault Gendron

David M Gorman

Gabriela Kramer-Marek

David Y Lewis

André Müller

Edward S O'Neill

Wim J G Oyen

Stephen J Paisey

P Stephen Patrick

Richard Southworth

Bertrand Tavitian

POSTER PITCH AND POSTER JUDGES

Marie-Claude Asselin

Bart Cornelissen

Philip J Blower

Gilbert Fruhwirt

Mark F Lythgoe

Graham Smith

COMMITTEES

PNI ORGANISING COMMITTEE

Thibault Gendron

S Peter Johnson

Tammy L Kalber

Kerstin Sander

Bernard Siow

Thomas Snoeks

Timothy H Witney

PNI SCIENTIFIC COMMITTEE

Christopher J Cawthorne

Gabriela Kramer-Marek

David Y Lewis

James O'Connor

Kerstin Sander

Bernard Siow

Rafael Torres Martin de Rosales

Vessela Vassileva

LIST OF EXHIBITORS

EXHIBITORS AT THE PNI

Aspect Imaging

Bartec / Mediso

Bruker

Elysia Raytest

Imaging Equipment

Invicro

MILabs

Southern Scientific / LabLogic

Trasis

LIST OF ATTENDEES

Mrs Sarah **Able**
University of Oxford
sarah.able@oncology.ox.ac.uk

Ms Taibah **Alahmad**
University College London
alahmadta@gmail.com

Miss Aishah **Alenezi**
Cardiff University
alenezia2@cardiff.ac.uk

Dr Louis **Allott**
Imperial College London
l.allott@imperial.ac.uk

Ms Hanan **Almutairi**
Cardiff University
almutairih@cardiff.ac.uk

Dr Fahad **Al-salemee**
King's College London
fahad.al-salemee@kcl.ac.uk

Dr Kurt **Anderson**
The Francis Crick Institute
kurt.anderson@crick.ac.uk

Prof Steve **Archibald**
University of Hull
s.j.archibald@hull.ac.uk

Prof Erik **Arstad**
University College London
e.arstad@ucl.ac.uk

Ms Candice **Ashmore-Harris**
King's College London
candice.ashmore-harris@kcl.ac.uk

Dr Marie-Claude **Asselin**
University of Manchester
marie-claude.asselin@manchester.ac.uk

Dr Robert **Atkinson**
Reckitt Benckiser
robert.atkinson@rb.com

Dr Bala **Attili**
University of Cambridge
ba396@cam.ac.uk

Dr Ramla **Awais**
University College London
r.awais@ucl.ac.uk

Mr Friedrich **Baark**
King's College London
friedrich.baark@kcl.ac.uk

Dr Adam **Badar**
MILabs
a.badar@milabs.com

Dr Julia **Baguna Torres**
University of Oxford
julia.bagunatorres@oncology.ox.ac.uk

Mr Scott **Baker**
LabLogic Systems Limited
sbaker@lablogic.com

Mr Chris **Barnes**
Imperial College London
chris.barnes@imperial.ac.uk

Miss Joanna **Bartnicka**
King's College London
joanna.bartnicka@kcl.ac.uk

Miss Alice **Beckley**
Imperial College London
aa.beckley15@imperial.ac.uk

Dr Romain **Bejot**
Ipsen
romain.bejot@ipsen.com

Dr Donald **Bell**
The Francis Crick Institute
donald.bell@crick.ac.uk

Dr Helen **Betts**
Nottingham University Hospitals
helen.betts2@nuh.nhs.uk

Dr Julia **Blower**
King's College London
julia.blower@kcl.ac.uk

Prof Phil **Blower**
King's College London
philip.blower@kcl.ac.uk

Dr Diana **Brickute**
Imperial College London
d.brickute@imperial.ac.uk

Prof Kevin **Brindle**
Cancer Research UK - Cambridge Institute
kmb1001@cam.ac.uk

Mr Andy **Brown**
Aspect Imaging
abrown@aspectimaging.com

Dr David **Brown**
RenaSci Ltd.
david.brown@renasci.co.uk

Miss Lucy **Buckwell**
lucybuckwell1@gmail.com

Dr Benjamin **Burke**
University of Hull
b.burke@hull.ac.uk

Dr Christopher **Cawthorne**
KU leuven
christopher.cawthorne@kuleuven.be

Miss Cen **Chen**
Imperial College London
c.chen@imperial.ac.uk

Dr Juliette **Chupin**
Invicro
j.t.m.chupin@qmul.ac.uk

Miss Maria **Clara Liuzzi**
University of Glasgow
m.liuzzi.1@research.gla.ac.uk

Mr Simon **Corbett**
University College London
simon.corbett.15@ucl.ac.uk

Miss Ines **Costa**
King's College London
ines.meloo.costa@gmail.com

Dr Marta **Costa-Braga**
Imperial College London
m.braga13@imperial.ac.uk

Dr Chiara **Da Pieve**
The Institute of Cancer Research
chiara.dapieve@icr.ac.uk

Mr Christopher **Davis**
King's College London
christopher.davis@kcl.ac.uk

Mr Vittorio **De Santis**
King's College London
vittorio.de_santis@kcl.ac.uk

Dr Katie **Dexter**
Barts Cancer Institute
k.dexter@qmul.ac.uk

Dr Gemma **Dias**
University of Oxford
gemma.dias@oncology.ox.ac.uk

Ms Juozas **Domarkas**
University of Hull
j.domarkas@hull.ac.uk

Miss Georgina **Dowsett**
RenaSci Ltd.
georgina.dowsett@renasci.co.uk

Dr Richard **Edwards**
The Institute of Cancer research
redwards@icr.ac.uk

Dr Sebastian **Eigner**
Bruker
sebastian.eigner@bruker.com

Dr Nadia **Falzone**
Cancer Research UK - University of Oxford
nadia.falzone@oncology.ox.ac.uk

Mr Matt **Farleigh**
King's College London
matthew.farleigh@kcl.ac.uk

Mr George **Firth**
King's College London
george.firth@kcl.ac.uk

Ms Heather **Fitzke**
University College London
h.fitzke@ucl.ac.uk

Dr Julie **Foster**
Barts Cancer Institute
j.m.foster@qmul.ac.uk

Mr Peter **Gawne**
King's College London
peter.gawne@kcl.ac.uk

Dr Thibault **Gendron**
University College London
t.gendron@ucl.ac.uk

Dr Matthias **Glaser**
University College London
matthias.glaser@ucl.ac.uk

Dr David **Gorman**
University of Manchester
david.gorman@manchester.ac.uk

Miss Hannah **Greenwood**
University College London
hannah.greenwood.16@ucl.ac.uk

Miss Caroline **Haegeman**
Imperial College London
caroline.haegeman13@imperial.ac.uk

Mr Ivan **Hawala**
University of Turin
ihawala@unito.it

Mr George **Herbert**
University of Hull
g.herbert@2014.hull.ac.uk

Miss Julia **Hoebart**
The Institute of Cancer Research
julia.hoebart@icr.ac.uk

Dr Samantha **Hopkins**
University of Oxford
samantha.higgins@oncology.ox.ac.uk

Miss Ai **Hui Doreen Lau**
University of Cambridge
la399@cam.ac.uk

Miss Madeleine **Iafrate**
King's College London
madeleine.iafrate@kcl.ac.uk

Miss Jessica **Jackson**
King's College London
jessica.1.jackson@kcl.ac.uk

Mr Kurt **Jacobson**
Bruker
kurt.jacobson@bruker.com

Dr Dhifaf **Jasim**
University of Manchester
dhifaf.jasim@manchester.ac.uk

Dr Peter **Johnson**
The Francis Crick Institute
peter.johnson@crick.ac.uk

Prof Terry **Jones**
University of California
terry.jones40@googlemail.com

Ms Holly **Joyce**
The Francis Crick Institute / UCL
holly.joyce@crick.ac.uk

Dr Tammy **Kalber**
University College London
t.kalber@ucl.ac.uk

Mr George **Keeling**
King's College London
george.keeling@kcl.ac.uk

Miss Azalea **Khan**
King's College London
azalea.khan@kcl.ac.uk

Dr James **Knight**
Newcastle University
james.knight2@newcastle.ac.uk

Mr Hiroshi **Kondo**
The Francis Crick Institute
hiroshi.kondo@crick.ac.uk

Miss Sofia **Koustoulidou**
MILabs
s.koustoulidou@milabs.com

Ms Doris **Kracht**
European Society for Molecular Imaging
office@e-smi.eu

Dr Gabriela **Kramer-Marek**
The Institute of Cancer Research
gkramermarek@icr.ac.uk

Miss Alix **Le Marois**
The Francis Crick Institute
alix.lemarois@crick.ac.uk

Miss Laura **Lechermann**
University of Cambridge
lmtl2@cam.ac.uk

Dr Sarah **Lee**
Amallis Consulting
sarahlee@amallisconsulting.com

Dr David **Lewis**
Cancer Research UK - Beatson Institute
d.lewis@beatson.gla.ac.uk

Dr Andrew **Lonergan**
Aspect Imaging
alonergan@aspectimaging.com

Mr Patricio **Luzuriaga**
Trasis
luzuriaga@trasis.com

Dr Sven **Macholl**
Invicro
smacholl@invicro.com

Mrs Justyna **Maczynska**
The Institute of Cancer Research
justyna.maczynska@icr.ac.uk

Dr Gaurav **Malviya**
Cancer Research UK - Beatson Institute
g.malviya@beatson.gla.ac.uk

Dr Francis **Man**
King's College London
francis.man@kcl.ac.uk

Miss Daniela **Manuela Ciobota**
The Institute of Cancer Research
daniela.ciobota@icr.ac.uk

Miss Camila **Marcolan**
University College London
camila.marcolan@ucl.ac.uk

Dr Jacqui **Marshall**
The Francis Crick Institute
jacqui.marshall@crick.ac.uk

Miss Niamh **McCallum**
University of Liverpool
sgnmccal@student.liverpool.ac.uk

Mr Aishwarya **Mishra**
King's College London
aishwarya.mishra@kcl.ac.uk

Dr Filipa **Mota**
King's College London
k1514539@kcl.ac.uk

Dr André **Müller**
Life Molecular Imaging
a.mueller@life-mi.com

Dr Edward **O'Neill**
University of Oxford
edward.oneill@oncology.ox.ac.uk

Mr Bradley **Osborne**
Imperial College London
b.osborne18@imperial.ac.uk

Miss Katarzyna **Osytek**
King's College London
katarzyna.osytek@kcl.ac.uk

Prof Wim **Oyen**
The Institute of Cancer Research
wim.oyen@icr.ac.uk

Dr Anna **Pacelli**
University of Oxford
anna.pacelli@oncology.ox.ac.uk

Dr Stephen **Paisey**
Cardiff University
paiseysj@cf.ac.uk

Mr Max **Palmer**
maxpalmer@hotmail.co.uk

Dr Stephen **Patrick**
University College London
peter.patrick@ucl.ac.uk

Dr Victoria **Pell**
King's College London
victoria.pell@kcl.ac.uk

Dr Raul **Pereira**
University College London
raul.pereira@ucl.ac.uk

Miss Noemi **Perujo Holland**
University of Hull
noemi.perujoh@gmail.com

Miss Truc **Pham**
King's College London
truc.pham@kcl.ac.uk

Malcom **Plant**
Elysia-Raytest
malcom.plant@elysia-raytest.com

Mr Jarrad **Plater**
University of Hull
j.plater@2010.hull.ac.uk

Dr Florian **Raes**
The Institute of Cancer Research
florian.raes@icr.ac.uk

Dr Colin **Ratcliffe**
The Francis Crick Institute
colin.ratcliffe@crick.ac.uk

Miss Isaline **Renard**
University of Hull
i.renard@2016.hull.ac.uk

Mr Alex **Rigby**
King's College London
alex.rigby@kcl.ac.uk

Dr Charlotte **Rivas**
King's College London
charlotte.rivas@kcl.ac.uk

Dr David **Roberts**
University of Hull
d.roberts@hull.ac.uk

Prof Sean **Ryan**
University of Hertfordshire
s.g.ryan@herts.ac.uk

Dr Kerstin **Sander**
University College London
k.sander@ucl.ac.uk

Dr Gilberto **Serrano de Almeida**
Imperial College London
g.serrano-de-almeida@imperial.ac.uk

Dr Jack **Sharkey**
University of Liverpool
jsharkey@liv.ac.uk

Dr Bernard **Siow**
The Francis Crick Institute
bernard.siow@crick.ac.uk

Dr Graham **Smith**
The Institute of Cancer Research
graham.smith@icr.ac.uk

Dr Thomas **Snoeks**
The Francis Crick Institute
thomas.snoeks@crick.ac.uk

Dr Jane **Sosabowski**
Barts Cancer Institute
j.k.sosabowski@qmul.ac.uk

Dr Richard **Southworth**
King's College London
richard.southworth@kcl.ac.uk

Dr Graeme **Stasiuk**
University of Hull
g.stasiuk@hull.ac.uk

Mr Peter **Strapps**
PerkinElmer
peter.strapps@perkinelmer.com

Dr Daniel **Stuckey**
University College London
d.stuckey@ucl.ac.uk

Dr Kavitha **Sunassee**
King's College London
kavitha.sunassee@kcl.ac.uk

Miss Meena **Tanapirakgul**
King's College London
meena.tanapirakgul@kcl.ac.uk

Prof Bertrand **Tavitian**
Université Paris Descarte - INSERM
bertrand.tavitian@inserm.fr

Dr Samantha **Terry**
King's College London
samantha.terry@kcl.ac.uk

Mr Stephen **Turnock**
The Institute of Cancer Research
stephen.turnock@icr.ac.uk

Mr David **Turton**
The Institute of Cancer Research
daveturton100@gmail.com

Mr Niek **Van Overberghe**
Molecubes
niek.vanoverberghe@molecubes.com

Mr Ewout **Van Steenkiste**
Molecubes
ewout.vansteenkiste@molecubes.com

Dr Elise **Verger**
King's College London
elise.verger@kcl.ac.uk

Dr Marta **Vicente-Rodriguez**
King's College London
marta.vicente_rodriguez@kcl.ac.uk

Mr Charles **Vriamont**
Trasis
vriamont@trasis.com

Miss Ning **Wang**
Imperial College London
n.wang16@imperial.ac.uk

Mr Edward **Waters**
King's College London
edward.waters@kcl.ac.uk

Mr Andrew **Williams**
Southern Scientific Limited
andrew.williams@southernscientific.co.uk

Mr Henry **Wilson**
Aspect Imaging
hwilson@aspectimaging.com

Mr Thomas **Wilson**
University of Oxford
thomas.wilson@some.ox.ac.uk

Mrs Mary-Ann **Xavier**
University of Oxford
mary-ann.xavier@oncology.ox.ac.uk

Dr Ran **Yan**
King's College London
ran.yan@kcl.ac.uk

Ms Jennifer **Young**
Barts Cancer Institute
jennifer.young@qmul.ac.uk

Dr Zilin **Yu**
King's College London
zilin.yu@kcl.ac.uk

Dr May **Zaw Thin**
The Francis Crick Institute
m.zaw-thin@ucl.ac.uk

ACKNOWLEDGEMENTS

The organisation of the Third PNI symposium would not have been possible without the – financial and non-financial – support of organisations, societies and companies that endorse and/or sponsor the meeting, which is highly appreciated!

Due to the generous funding from companies attached to the PNI field we have been able to organise a meeting for approximately 200 attendees, whilst keeping charges at a minimum. Prizes for the poster and poster pitch competition are kindly provided by the European Society for Molecular Imaging (ESMI) and the World Molecular Imaging Society (WMIS), respectively.

We are particularly grateful for the partnership with ESMI, which is almost becoming a tradition. The scientific organisation has been endorsing the PNI since the first meeting in 2013.

Special thanks go to all the volunteers helping out at the day of the meeting.

The PNI Committee

SPONSORS


TRASIS


MILabs
Making Molecular Imaging Clear

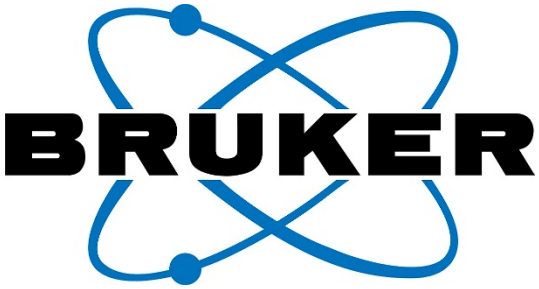
BRUKER


southern
scientific
EXPERIENCE & EXPERTISE


LabLogic


iel.


bartec
Mediso


Invicro
A Konica Minolta Company


aspectimaging


ELYSIA RAYTEST


PerkinElmer
For the Better